Assessment of LS-DYNA and Underwater Shock Analysis (USA) Tools for Modeling Far-Field Underwater Explosion Effects on Ships

Bradley Klenow

A thesis submitted to the Faculty of

Virginia Polytechnic Institute and State University

in partial fulfillment of the requirements for the degree of

MASTER OF SCIENCE

in

Ocean Engineering

Dr. Alan J. Brown, Chairman
Dr. Owen Hughes
Dr. Rakesh Kapania

April 21, 2006
Blacksburg, Virginia

Keywords: Underwater explosion, LS-DYNA, USA, shock capture, non-reflecting boundaries

Assessment of LS-DYNA and Underwater Shock Analysis (USA) Tools for Application to Far-Field Underwater Explosion Effects on Ships

Bradley Klenow

Abstract

This thesis investigates the use of the numerical modeling tools LS-DYNA and USA in modeling general far-field underwater explosions (UNDEX) by modeling a three-dimensional box barge that is subjected to a far-field underwater explosion. Past UNDEX models using these tools have not been validated by experiment and most are limited to very specific problems because of the simplifying assumptions they make. USA is a boundary element code that requires only the structural model of the box barge. LS-DYNA is a dynamic finite element code and requires both the structural model and the surrounding fluid model, which is modeled with acoustic pressure elements.

Analysis of the box barge problem results finds that the program USA is a valid tool for modeling the initial shock response of surface ships when cavitation effects are not considered. LS-DYNA models are found to be very dependent on the accuracy of the fluid mesh. The accuracy of the fluid mesh is determined by the ability of the mesh to adequately capture the peak pressure and discontinuity of the shock wave. The peak pressure captured by the model also determines the accuracy of the cavitation region captured in the fluid model. Assumptions made in the formulation of the fluid model causes potential inaccurate fluid-structure interaction and boundary condition problems cause further inaccuracies in the box barge model. These findings provide a base of knowledge for the current capabilities of UNDEX modeling in USA and LS-DYNA from which they can be improved in future work.

Acknowledgements

I would like to thank Dr. Alan Brown for his guidance and support on this project as well as the members of my committee, Dr. Owen Hughes and Dr. Rakesh Kapania. I would also like to thank the current and past members of the Virginia Tech Survivability Research Group, especially Ashley Nisewonger, Jinwon Park, Keith Webster, Jason Cordell, and Dr. John Sajdak for their input in this work.

Personally I would like to acknowledge my parents for all their inspiration, support, and love throughout my life. I would like to thank Dr. Patrick Kwon of Michigan State University for providing my first experience in graduate research, which has given me the confidence to succeed in my current research. Finally, I would like to thank my girlfriend Laura for all her love, all her belief in me, and for always being there.

TABLE OF CONTENTS

TABLE OF FIGURES

LIST OF TABLES

CHAPTER 1 INTRODUCTION

1.1 Motivation and Background

The underwater explosion (UNDEX) and subsequent ship interaction problem has many unique characteristics all of which are governed by complex physics [1]. The complexity of the problem makes it extremely difficult to generate analytical solutions for the UNDEX problem except for the most simple of cases. While solutions to simplified problems provide a solid foundation for understanding the nature of UNDEX problems they do not predict more complex explosion and structure interactions encountered in real ship design problems.

Because of this complexity, predicting the effect of an UNDEX on real ships has been limited to using very basic numerical methods. Some examples of these basic methods include using empirical relations obtained by experiment to predict UNDEX properties, the Shock Factor concept [1], and studying the ship response by applying a pressure load while neglecting the surrounding fluid. None of these methods have the capability to accurately model the entire UNDEX problem because they make many assumptions that limit their application to specific UNDEX characteristics or cases. However, with advances in computing technology and the progression of numerical methods, such as the finite element method, it has become possible to create more accurate and complete UNDEX models. With these models it may now be possible to predict UNDEX phenomena with sufficient accuracy for design applications.

1.1.1 Ship Survivability

The U.S. Navy defines survivability as, the capacity of the total ship system to avoid and withstand damage and maintain and/or recover mission integrity [2]. In a

mathematical sense, ship survivability is the relation between the probabilities of three events occurring when a threat is encountered.

First is susceptibility or the probability of a hit (probability of a threat succeeding). This variable accounts for the ability of a threat to hit the ship, and also the ship's ability to avoid the threat. Second is the probability of kill or loss of mission capacity given a hit, this is called vulnerability. Third is the probability of recovering mission capacity given a specific kill or loss, this is called recovery. Mission capacity reflects the operations on the ship that must be function in order for the ship to continue its mission. These functions include such things as, ship control and propulsion, command and control, navigation, communications, surface, air and underwater surveillance, essential maintenance of aircraft and ordnance, weapons stowage, control, launch, guidance, combat payload transport, and casualty and damage control. For this thesis ship survivability is limited to the vulnerability problem, meaning the ship only need to survive a hit.

1.1.2 Threats

Threats encompass the different weapons and scenarios that have the ability to compromise the mission capacity of a ship. There are three main types of threats associated with naval ships, air explosions (AIREX), underwater explosions (UNDEX), and penetrating weapons. A threat scenario is the event of a weapon engaging a ship at a specific proximity to the ship. Each type of threat has different characteristics that must be accounted for in a survivability model depending on a given threat scenario.

Air blast threats include any weapon that explodes in air in close proximity to the ship or in contact with the ship. In this type of threat, effects such as fragmentation must be considered due to the proximity of the threat to the ship.

Underwater explosion threats can occur in both near and far proximity. UNDEX threats can also contact the ship in which case fragmentation must be accounted for. The location of the explosion relative to the ship is of importance for underwater threat type because this can have a large impact on the severity of the threat. Figure 1.1 shows how an under keel torpedo detonation threat can be one of the most severe UNDEX threats. The main types of weapons that pose an UNDEX threat are torpedoes and mines. Such threats are the focus of this thesis.

Figure 1.1 Example of an under keel UNDEX detonation

Penetrating weapons are weapons that have warheads designed to penetrate the ship structure either above or below the waterline. In this type of threat burst from the warhead, fragmentation, heat, and fire are the main characteristics. Weapons that pose penetrating threats are armored piercing weapons such as ASMC or torpedoes.

1.1.3 Need

The need for an UNDEX damage model is evident in that no method of testing every ship design for its survivability in any threat scenario exists. Currently the U.S. Navy uses a set of guidelines and standards in conjunction with shock trial tests to determine the survivability characteristics of a ship.

Shock trial tests (Figures 1. 2 and 1.3) are performed by detonating explosive charges at various locations around the ship and recording the ship response. While shock trials give valuable information on ship response to specific UNDEX threat scenarios, there are several factors that limit the usefulness of the shock trial in the design process of a ship. First, shock trials are extremely expensive and require extensive planning [3].

Figure 1.2 USS Mobile Bay shock trial

Figure 1.3 Aircraft carrier shock trial

Secondly, because of cost limitations only the lead ship in a new class or a ship that deviates considerably from other ships in the same class undergoes shock trials [3]. Shock trials are post-design tests. They can not be used early in design before the actual ship is built. Other limitations are the safety/environmental issues associated with shock trials. There is a safety risk to the crew of the ship, an environmental risk to marine life, and a risk of damaging the ship beyond repair or even sinking it. Because of these safety/environmental issues shock trials are limited in the size/type of explosions that can be tested. Therefore shock trials only test risk-free UNDEX threat scenarios for the ship, they cannot be used to determine the survivability limits of a ship in a true combat situation [3].

A solution to the limitations of shock trials is to use mathematical models of UNDEX scenarios to approximate the explosion and structural response. Such models would allow designers to conduct virtual ship shock trials to test the survivability of alternative designs for a new ship, selecting the best design from the model results.

1.2 Underwater Explosions

1.2.1 Types

There are two classes or types of underwater explosions. In the first, the explosive charge detonates close to the ship hull. This is called a near-field underwater explosion. In the second, the charge is further away from the ship hull. This is called a far-field underwater explosion. The distance at which a problem becomes far-field is defined by the ship response.

In most cases, a charge that detonates close to the ship's hull causes the hull to rupture or causes large scale plastic deformation. A charge detonated close to the ship may also cause further damage to the ship from the fragmentation of the charge housing [4]. As the charge is detonated further away from the hull, a point is reached where the hull no longer ruptures, but only plastic deformation occurs. Further increasing the charge distance reaches a point where only elastic deformation occurs. This is a far-field explosion. Traditionally the ship is assumed to be the ship is assumed to be loaded as a whole, and the response is global [4,5]. However, in this thesis these assumptions are not made.

A ship response to an UNDEX includes the response due to the shock wave and response due to the gas bubble effects [5]. Far-field underwater explosions may be further divided into two subcategories: 1) explosions where gas bubble effects have no significant influence on the ship loading [6] and 2) explosions where bubble pulses affect the ship loading but the bubble itself does not interact with the structure [1].

In this thesis only far-field explosions of type 1 are considered. For a far field underwater explosion of type 1 the following assumptions are made: 1) the presence of the ship structure has no influence on its loading [1], 2) the distance of the explosion is far enough away from the ship that neither the shock wave or bubble effects can rupture the hull, 3) a far field explosion of type 1 occurs far enough away from the ship that the bubble pulses damp out before reaching the ship structure; so the pulses do not affect the late time response of the ship, and 4) the far-field explosion occurs deep enough that the gas bubble does migrate or the charge is close enough to the surface that the bubble vents before its first contraction.

1.2.2 Description

The general underwater explosion problem begins with an explosive charge of a certain size and material located at a depth below the free surface. The water is assumed to behave as a compressible fluid that is incapable of supporting significant tension.

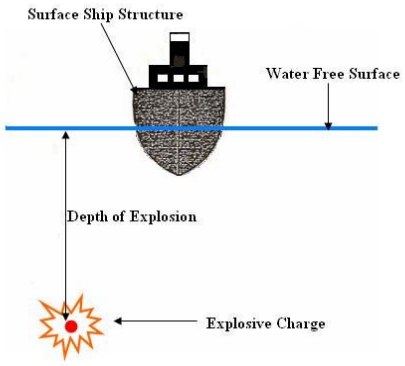

Figure 1.4 General description of underwater explosion problem [4]

The general sequence of events of an underwater explosion begins with the chemical reaction of the explosive material. This chemical reaction takes place in two parts: the initial chemical reaction and the detonation process. Prior to the start of the explosive process the explosive material is an unstable chemical substance in a gas, solid, or liquid state [7]. An initial chemical reaction, both exothermic and rapid in nature, is started by the transfer of energy (most commonly heat energy) to the explosive material [7]. The mechanism that initially transfers energy to the explosive material is called the "detonator" or "igniter". The detonator is made from a more sensitive explosive material than the primary explosive material in the charge. As the explosive material reacts and releases energy it is transformed into a more stable state. The product of the reaction is a hot gas at a very high pressure [8]. This chemical reaction is termed an explosion or explosive reaction.

If the pressure created by the initial chemical reaction is large enough, a thermo-mechanical shock wave, referred to as the "detonation wave", is created. In the detonation process, the detonation wave propagates at supersonic speed generating intense heat through the explosive material still in its original state. The intense heat sets off new explosive reactions in the unreacted material as the wave passes through, making the detonation process self-sustaining [7].

The gaseous products (the converted gas behind the detonation wave) generated by detonation process have no time to expand due to the high propagation speed of the detonation wave. As a result the gaseous products are continually heated and cannot relieve pressure through expansion. Therefore the pressures in the gas behind the detonation wave reach magnitudes in the range of 2 to 4 million psi [7, 8]. The pressure reached in the gaseous products is the "detonation pressure" or the "Chapman-Jouget" pressure. This pressure is constant, dependent on the type of explosive material used [7]. These extreme pressures are the driving force behind the rapid propagation of the detonation wave. Because of this, the chemical reactions of the detonation process can be assumed to occur instantaneously for engineering purposes [7].

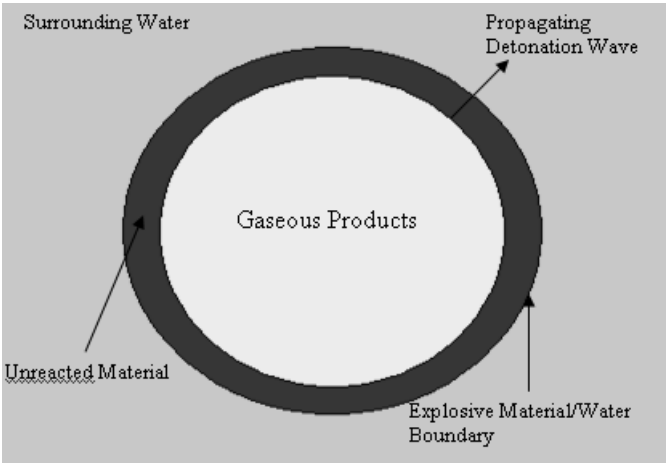

Figure 1.5 Underwater explosion during detonation process

When the detonation wave reaches the explosive material/water boundary all unreacted material has been converted to gas. The gaseous products now make up a very dense, superheated, and spherical gas bubble. At this time the detonation process of the underwater explosion is complete.

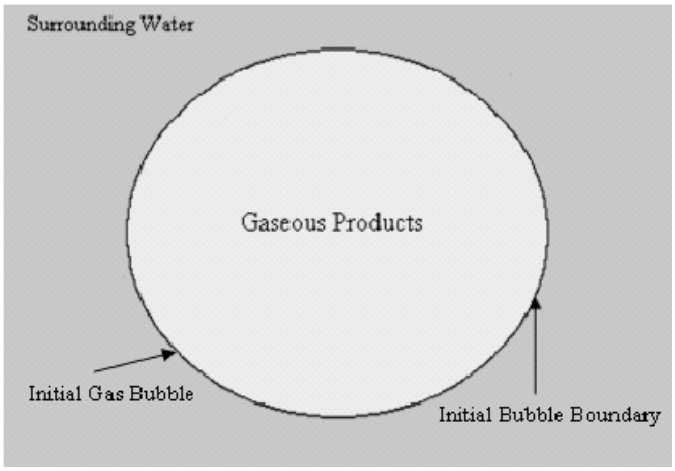

Figure 1.6 Underwater explosion at instant the detonation process is complete

The immense pressure inside the initial gas bubble is initially relieved by the generation of a large compressive pressure wave and a resulting outward flow of water. This pressure wave created by the arrival of the detonation wave at the boundary is the "shock wave".

The shock wave shape is characterized by a nearly discontinuous rise in pressure followed by a brief (a few milliseconds) exponential decay [8]. The maximum pressure reached by the shock wave is the "peak" pressure and plays an important role in calculating structural responses resulting from an underwater explosion. The shock wave propagates in water as a spherical wave, initially traveling faster than the speed of sound. As the shock wave moves further from the origin of the explosion its propagation speed falls to the speed of sound in water, where it remains constant [9]. In addition to losing

speed, the peak pressure reduces and the shape of the shock wave becomes more elongated. Figure 1.7 shows the initial shape and the shape of a shock wave as it propagates away from the explosion origin.

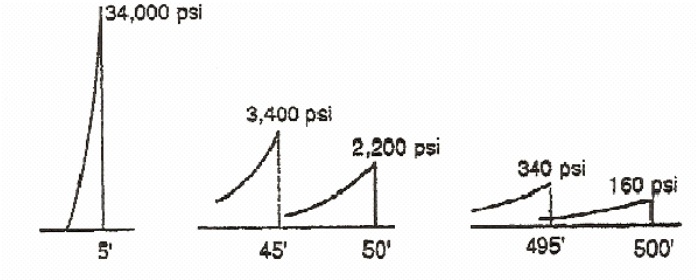

Figure 1.7 Typical shock wave profiles measured at varying distances from explosion origin [8]

As the shock wave propagates it approaches three types of boundaries: the rigid bottom boundary (seafloor), the free surface, and the fluid-structure interface. At the bottom the shock wave is reflected as a compression wave much smaller in magnitude than the original shock wave [8, 10]. If the explosion occurs in shallow water, the reflected wave from the bottom can combine with the incident shock wave and the free surface reflected wave to change the pressure field of the surrounding water significantly. However, in most near and far-field cases, the explosion is considered to occur in deep enough water that the bottom reflected wave does not interact with the other shock waves.

The first significant boundary the shock wave encounters is the fluid-structure interface of the water and the ship's hull. At this boundary the shock wave creates pressure loading on the hull that is characterized as an instantaneous rise to peak pressure followed by an exponential decay. Recall that for a far-field explosion it is traditionally assumed this load is applied to the hull as a whole. The hull response is always assumed to be elastic for a far-field explosion [9].

For all surface ships the initial pressure loading gives the hull an upward acceleration regardless of where the shock wave originates [9]. The upward acceleration continues until the hull begins to move faster than the surrounding water. When this point is reached the loading drops to zero and the water at the hull is exposed to tension [9]. Because water cannot sustain tension a cavitation region develops at the interface between the hull and water [11]. This cavitation region is termed "local" or "hull" cavitation. At the onset of local cavitation the hull has reached its maximum upward velocity, called the "kickoff" velocity, due to the shock wave loading [9].

After reaching the kickoff velocity the hull begins to slow down and the local cavitation region closes. This causes the hull to be reloaded. Reloading occurs because prior to the closure of the local cavitation region the hull is not in contact with the water. When the cavitation region closes the water impacts the hull, causing it to be reloaded [12]. The form of the reloading pressure on the hull is similar to the shock wave induced pressure, although the loads imposed on the hull from reloading are not as large as those created by the shock wave impact [9].

The second boundary that the propagating shock wave encounters is the free surface. The arrival of the shock wave above the free surface is visible in two separate phenomena. The first is an expanding ring of darkened water called the "slick". The darkness of the slick is a result of the rippled water created in the slick region by cavitation when contrasted to the surrounding water that is actually smoothed by the reflection of the shock wave. The slick lasts only a matter of milliseconds due to its rapid velocity and serves as an indication of the points the shock wave has reached on the surface [8].

Following the slick is an upheaval of white water called the "spray dome" [8]. The spray dome is created by the vertical velocity given to the water surface when the incident shock wave is reflected. Once the vertical velocity of the spray dome reaches zero it collapses, the time at which this occurs depends on the charge size and depth of the explosion [8, 10].

Beneath the free surface, the incident shock wave reflected back into the water as a tensile wave. Due to the large density difference between water and air, the pressure of the reflected wave is almost exactly the pressure of the incident shock wave. A schematic of the shock wave reflection is shown in Figure 1.8.

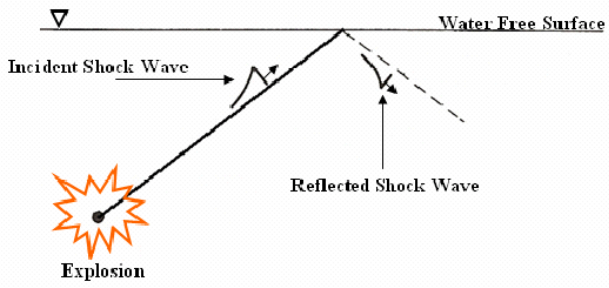

Figure 1.8 of incident shock wave at free surface [10]

The closeness of the incident and reflected wave pressures creates a "surface cutoff" effect at locations in the surrounding water where the incident and reflected shock wave meet. At these points the pressures of the shock and reflected wave cancel each other, reducing the pressure at that point to a slightly negative pressure. When surface cut off occurs at the hull, the exponentially decaying loading from the incident shock wave impact experiences a rapid drop in hydrostatic pressure [9]. The surface cutoff effect and the resulting pressure-time history of an arbitrary point P is shown in Figures 1.9 and 1.10 respectively.

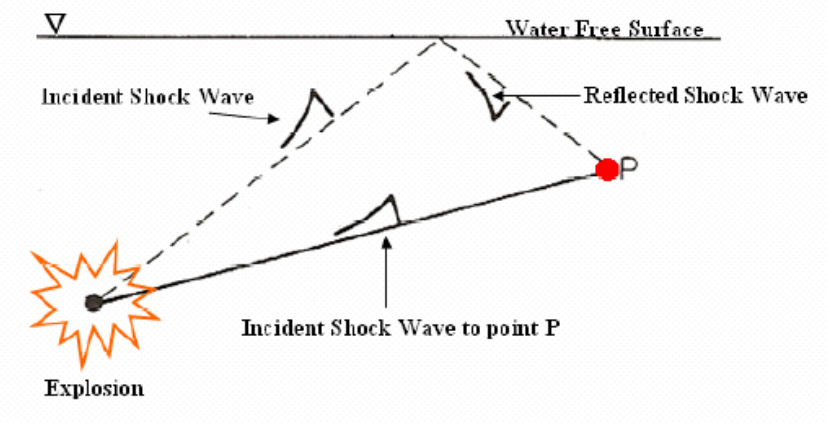

Figure 1.9 Shock wave interaction at point P due to free surface effects [10]

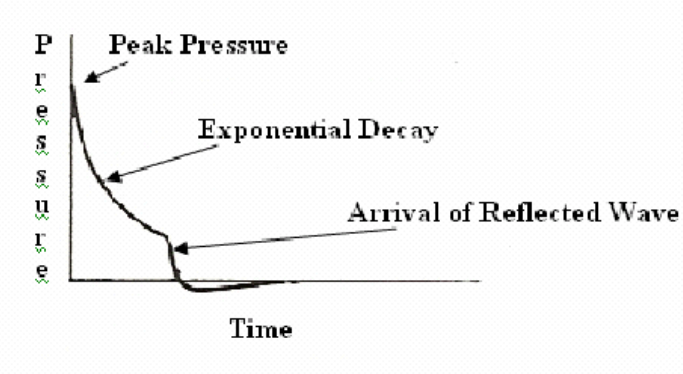

Figure 1.10 Pressure-time history due to surface cutoff of point P [10]

In addition to creating the surface cutoff effect, the reflected wave also generates a large or "bulk" cavitation region near the surface of the water. Because water cannot sustain tension and the reflected wave is a tensile wave the pressure around the water surface drops below zero and cavitation occurs [11]. The region remains cavitated until the pressure in the region returns a value that is above the vapor pressure of water.

The size of the bulk region is dependent on the location of the explosion origin and the size of explosive [11]. This region is symmetric about the vertical axis of the explosion origin and is bounded by an upper and lower boundary. Figure 1.11 shows a bulk cavitation region.

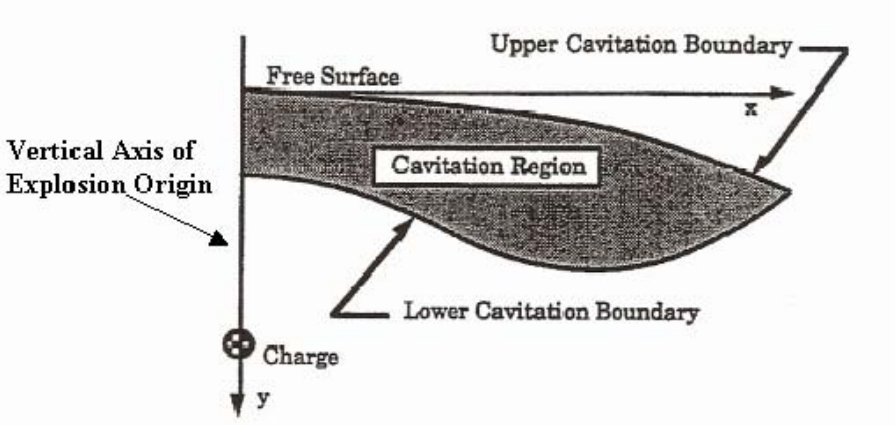

Figure 1.11 The bulk cavitation region [5]

The upper cavitation boundary is generated when the reflected wave lowers the absolute pressure to zero or below. The absolute pressure at the upper cavitation boundary is a combination of the atmospheric, hydrostatic, incident shock wave, and reflected wave pressures [11].

The lower cavitation boundary is determined by the decay rate of the reflected wave pressure. As the reflected pressure loses magnitude, it eventually reaches a magnitude that is the minimum required to cause cavitation. At this point, the lower cavitation boundary is formed. This boundary represents the line beyond which the pressure of the reflected wave is no longer large enough to reduce the absolute pressure in the water to a point where cavitation occurs.

After a certain amount of time passes the bulk cavitation region begins to close in a zipper-like manner. As it closes the water above the upper cavitation boundary crashes down on the water below the lower cavitation boundary. This causes a pressure wave, called the cavitation pulse, to radiate from the region. Much like the closing of the local cavitation region causes reloading on the ship's hull, the closing of the bulk cavitation region also causes reloading to occur. Depending on the ship's proximity to the point of

closure of the cavitation region, the impact of the water on the hull can cause pressure loads more damaging than the loads created by the initial shock wave impact [9].

The combination of the initial shock impact loading, the local cavitation reloading, and the bulk cavitation reloading account for the early time or shock response of the ship to the underwater explosion. The following paragraphs describe the explosion phenomena that account for the late time response of the ship structure. These phenomena are not accounted for in this work but are still important to understand for future work.

Recall that at the conclusion of the detonation process what remains is a very dense, superheated, and spherical gas bubble. While the release of the shock wave significantly lowers the pressure inside this gas bubble, it is still in excess of the hydrostatic pressure of the surrounding water [8]. The gas internal to the bubble seeks to return to the hydrostatic pressure of the surrounding water to restore equilibrium. These gases begin to expand reducing the internal pressure of the bubble and creating a large flow of water away from the bubble. Once the pressure of the internal gaseous products reaches hydrostatic equilibrium, the expansion of the gas bubble continues due to the inertia of the outwardly flowing water surrounding the bubble. As the inertia driven expansion continues the pressure of the gaseous products falls below hydrostatic pressure [7]. Expansion continues until the pressure differential between the hydrostatic pressure and the internal gas bubble pressure becomes large enough to cause the outward flow of water to stop [8]. At this instant the internal gas bubble pressure is at its minimum and the diameter is at its largest. Next the bubble begins to contract. As it does this, the internal gas bubble pressure increases and the diameter of the bubble gets smaller. The

bubble continues to contract until the compressibility of the gaseous products stop the contraction and force the bubble to expand again [8]. The process of expansion and contraction repeats throughout the duration of the gas bubble, making it an oscillating system. With each period, the time it takes the bubble to go through a single expansion/contraction cycle, the maximum size of the bubble decreases and the minimum size increases. This is illustrated in Figure 1.12 and is a result of energy loss during the oscillation process.

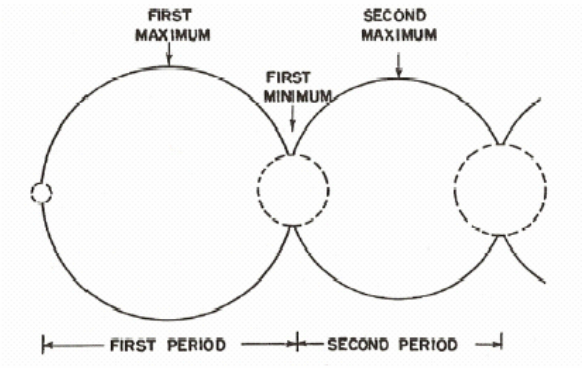

Figure 1.12 Gas bubble oscillation [8]

The oscillation of the gas bubble cause new pressure waves, called "secondary" or "bubble" pulses, to be radiated outward from the bubble. The manner in which the bubble pulses are created is very similar to the manner in which the shock wave is created. Bubble pulses are emitted when the pressure internal to the bubble is greatest which occurs at the bubble minimums [8, 9]. The velocity of the bubble pulses also propagate at the speed of sound in water [10].

Unlike the shock wave, bubble pulses do not display a discontinuous rise in pressure followed by an exponential decay. If the bubble is assumed to remain stationary at the origin of the explosion, the general shape of a bubble pulse is a gradual rise to the

peak pressure that is concave in form followed by a concave shaped decay to hydrostatic pressure. This general shape is shown in Figure 1.13. The peak pressure of the first bubble pulse is between 10% and 20% of the peak of the shock and the magnitude of the peak pressure lowers for each subsequent bubble pulse [8, 9].

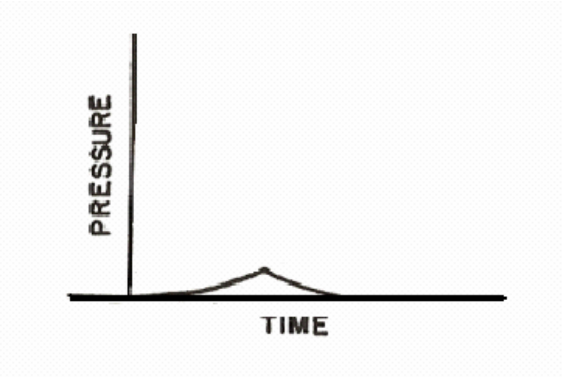

Figure 1.13 Typical bubble pulse shape assuming no bubble migration [8]

Occurring concurrently with the oscillation of the gas bubble and pulse generation is the migration of the bubble towards the surface of the water. The bubble migration is created by the buoyancy of the gaseous products internal to the bubble and is heavily influenced by the oscillation of the bubble. At larger gas bubble sizes the inertia of the outward flowing water balances out a majority of the buoyancy force causing the bubble to rise minimally. When the gas bubble is close to or at minimum size the inertia of the outwardly flowing water is greatly reduced. This allows the buoyancy force of the gaseous products to have a greater effect on the net upward force acting on the gas bubble accounting for the much higher rate of ascent of the bubble at its smallest sizes. The migration phenomenon is represented in Figure 1.14 [9].

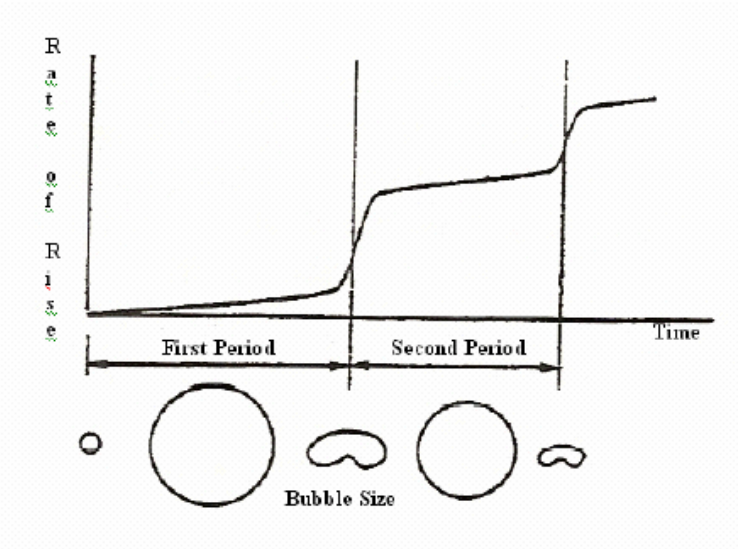

Figure 1.14 Bubble migration compared to bubble size [9]

Earlier the shape of a bubble pulse was defined with the assumption that the bubble did not migrate. However the migration of the bubble has a significant effect on the shape of the bubble and the bubble pulse. When the bubble has a large vertical velocity, as it does around its minimums, the pressure of the bubble pulse is significantly reduced. This causes the bubble pulse to assume a more triangular shape as shown in Figure 1.15. The triangular shape is a result of the impulse of the bubble pulse being unaffected by the motion of the bubble. Therefore as the peak pressure of the pulse reduces, the pulse develops a much more gradual rise and decay keeping the area under the pressure-time curve (impulse) the same as in the higher pressure bubble pulse curve.

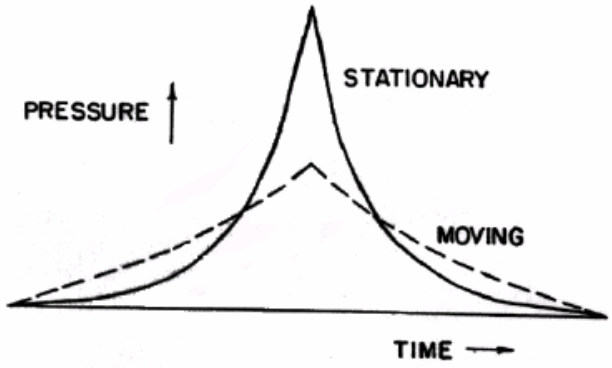

Figure 1.15 Comparison of bubble pulse shape with and without migration [8]

If the explosion occurs at the bottom boundary (sea floor), the bubble form changes into a hemispherical bubble. The hemispherical bubble initially sits on the bottom eventually breaking away due to buoyancy. After breaking away, the hemispherical bubble oscillates and migrates in the same manner as the spherical gas bubble [10].

The bubble pulses are the second phenomena of an underwater explosion to reach the ship's hull. Because the bubble pulses are so much weaker than the shock wave only the first bubble pulse considered in most cases. Though this is the strongest bubble pulse it does not always create a damaging response. The response it generates in the ship is largely dependent on the wave's frequency, phase, and the proximity of the bubble to the hull [9].

The bubble pulse contributes to the shock wave damage depending on its phase when it strikes the hull. No additional local cavitation occurs from the bubble pulse loading so the loading due to the bubble pulse is due only to initial impact.

If the bubble pulse is generated at a close proximity to the hull then it can rupture the hull as almost all of its energy impacts the hull. If the explosion occurs far enough

away from the hull, the bubble pulses will damp out and have no effect on the ship's response.

When the frequency of the shock response and bubble pulse response matches the resonant frequency of the ship, whipping occurs. The whipping motion of the ship can break the ship's hull girder or cause other types of severe structural damage [9].

The last underwater explosion phenomenon to reach the free surface is the gas bubble. As the bubble approaches the free surface and the ship, it experiences an attraction force to the ship and a repulsion force from the free surface [8, 10]. If the bubble migrates such that it is close to the hull at the time it reaches the free surface than two types of loading can occur.

The first type of gas bubble loading is created by the outwardly flowing water around the bubble contacting the hull of the ship. Pressures on the hull in this case are quite high and the duration of the loading period is much longer than the loading period of the shock wave. These loads are capable of creating significant damage to the hull in localized areas, in some cases greater than the shock wave induced damage to the hull.

The second type of gas bubble loading occurs when the bubble actually collapses onto the hull of the ship. This occurs as the bubble contracts in contact with the hull, creating a pressure differential that results in both the collapsing bubble and a high-speed water jet [9]. The impact of the water jet can be sufficiently forceful to puncture the hull. In other cases the water jet causes an initial pressure loading like that of the shock wave and gives the hull a secondary kickoff velocity.

The ship response created by the bubble pulse and gas bubble loading make up the late time response of the ship. In circumstances where the water jet impacts the hull it

is estimated that 60% of the total damage may result from the late time response and only 40% from the early time (shock wave impact) response [10].

If the bubble is close to the surface during its initial motion and at a sufficient distance away from the hull then upon arrival at the free surface it vents into the atmosphere in the form of a "plume". The plume is a comprised of white water mixed with the explosive gas products. This mixture is thrown vertically into the air and once its maximum height is reached it crashes back down to the water surface. A typical plume is shown Figure 1.16. Both the slick and what remains of the dome are also visible.

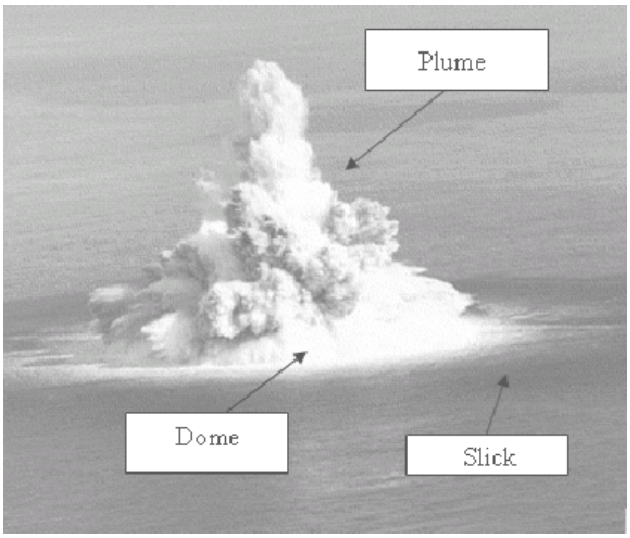

Figure 1.16 Plume, spray dome, and slick

1.2.3 Similitude

Analytical equations describing the physics of underwater explosions (UNDEX) outlined in the previous section can be very complex. The method of similitude offers a quick and simple way to calculate approximate characteristics of an underwater explosion. Similitude relations yield information on properties such as pressure, impulse, and energy associated with each of the three major events of an underwater explosion [8]: 1) the shock wave, 2) the gas bubble, and 3) the secondary pressure pulses.

Developed mainly in the 1940s, the similitude equations use experimentally-determined constants and a set of generic equations in three variables, the charge weight, explosion depth, and a point of interest in the explosive field to estimate shock and bubble characteristics. The method assumes that if the variables of two separate explosions are different by some ratio, the characteristics of the explosions are the same at two corresponding points of interest scaled by the same ratio [8]. This is referred to by Cole as the "principle of similarity".

While the similitude equations give a good understanding of the general physics of underwater explosions they are limited because they are experimentally based. Therefore they only apply to a certain range of the variables of charge weight, explosion depth, and point of interest location [13]. In addition to these limitations a number of assumptions, some which will be discussed in following sections, are required. The assumptions made in the similitude equations are that there are no effects from boundary surfaces, or the explosion takes place in "freewater" [13], and no migration of the gas bubble takes place [14]. In the case of the far-field problem, where both a free surface and structure are present, the similitude equations become invalid when the shock wave reaches these boundaries.

When considering the far field problem only the similitude equations that estimate shock wave properties are of interest. The main three relations are presented below in Equations 1.1, 1.2, 1.3 and give the peak pressure, time constant and pressure-time history for the shockwave. Each equation has a set of constants (Table 1.1) associated with it that are determined by fitting the equation to experimental data. The constants are derived using a specific unit system (here metric units are used) but are treated as unit-

less when input into the equations without units. The final units of the solution are assumed based on the equation. For example, units of Pa are assumed for the peak pressure approximation.

$$P_{peak} := K \cdot \left(\frac{W^{\frac{1}{3}}}{R} \right)^{\alpha} \tag{1.1}$$

$$\tau := (W)^{\left(\frac{1}{3}\right)} \cdot K \cdot \left[\frac{(W)^{\left(\frac{1}{3}\right)}}{R} \right]^{\alpha} \tag{1.2}$$

$$P(t) = P_{peak} e^{-t/\tau} \tag{1.3}$$

Table 1.1 Constants used in Equations 1.1, 1.2, 1.4 and 1.5 [13]

Equation	**K**	**α**
Peak Pressure (1)	52.4	1.13
Time Constant (2)	0.084	-0.23
Impulse (4)	5.75	0.89
Flux Density (5)	84.4	2.04

Equation 1.1 is known as the peak pressure approximation. It has been experimentally verified for numerous UNDEX cases and is generally accepted as accurate prediction of the peak pressure of the shock wave [15]. The pressure-time history is created by assuming an exponential decay from the peak pressure to hydrostatic pressure. While this assumption matches the general form of a shock wave, it is known that the exponential decay assumption is only valid for a period of $t-t_{peak}$ less than twice the time constant [15]. The validity range for an example UNDEX case is shown in Figure 1.17.

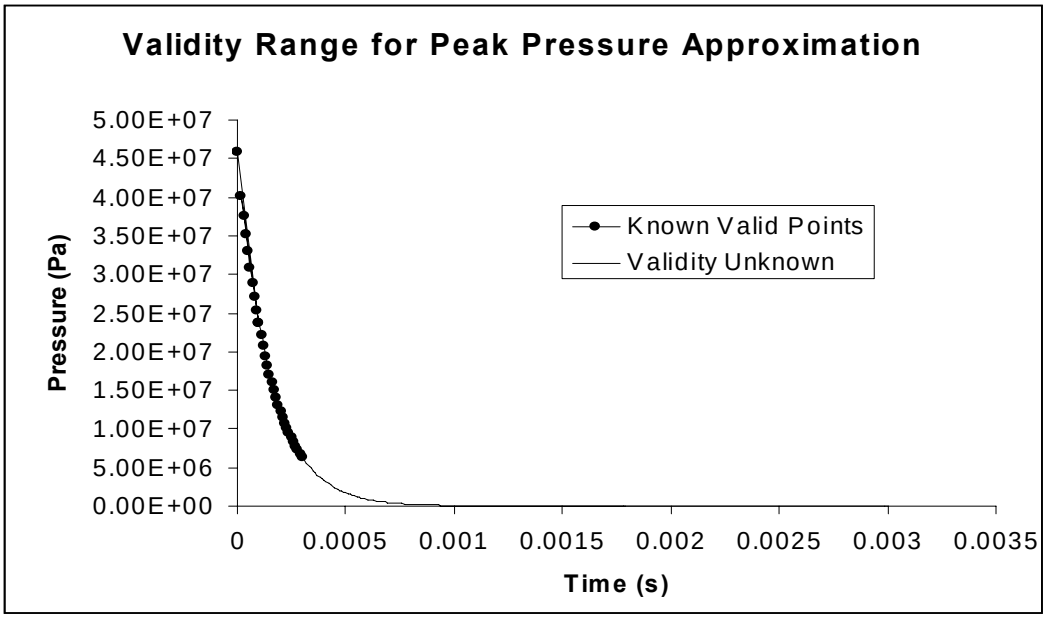

Figure 1.17 Pressure-Time history for an example UNDEX case showing the valid range of the peak pressure approximation

Two other shock wave parameters, impulse and flux density, can be calculated using similitude. These relationships are given in Equations 1.4 and 1.5 respectively.

$$I := \left(\frac{W}{kg}\right)^{\frac{1}{3}} \cdot K_I \cdot \left[\frac{\left(\frac{W}{kg}\right)^{\left(\frac{1}{3}\right)}}{\frac{R}{m}}\right]^{\alpha_I} \cdot Pa \cdot s \cdot 10^3 \tag{1.4}$$

$$E := \left(\frac{W}{kg}\right)^{\frac{1}{3}} \cdot K_E \cdot \left[\frac{\left(\frac{W}{kg}\right)^{\left(\frac{1}{3}\right)}}{\frac{R}{m}}\right]^{\alpha_E} \cdot m \cdot Pa \cdot 10^3 \tag{1.5}$$

The validity range for the similitude equations (Table 1.2) places restrictions on the type of UNDEX events to which they can be applied. Table 1.2 shows that for Equations 1.1, 1.2, 1.4, and 1.5 if the calculated peak pressure of the shock wave at the point of interest

is greater than 138 MPa, then that result can not be considered accurate. This places a restriction on charge size and location when modeling the shock wave using the similitude method.

Table 1.2 Validity range for shock wave similitude equations [13]

Parameter	Variable	Validity Range
Peak Pressure (P_{peak})	P_{peak}	3.4-138 MPa
Peak Pressure Decay	$t-t_{peak}$	$<2\tau$
Decay Time Constant (τ)	P_{peak}	3.4-138 MPa
Shock Wave Impulse (I)	P_{peak}	3.4-138 MPa
Shock Wave Energy Flux (E)	P_{peak}	3.4-138 MPa

Similitude methods are good predictors of specific phenomena of UNDEX but they are limited to specific cases, make to many simplifying assumptions, and can not provide any information on structural response. Therefore they can not be used to create a general far-field UNDEX model.

Analytical models for UNDEX problems are also limited to very simple problems. The Taylor plate problem [11] solves the response of an air backed flat plate subjected to only a shock loading. The Bleich-Sandler problem is very similar only it considers local cavitation in its solution. Because these analytical and similitude methods are so limited in terms of the structures they use, the UNDEX phenomena they account for, and the assumptions they require, there is a need to consider more complex numerical models of the UNDEX problem.

1.3 Modeling Literature Survey

1.3.1 The Finite Element Method - Hydrocodes

Most techniques used to model UNDEX problems use the finite element method either in whole or in part.. In cases where the finite element method is used to model the fluid domain of the UNDEX problem, hydrocodes are used. Hydrocodes simulate the response of fluids and solids under highly dynamic conditions where shock wave propagation is a dominant parameter [16] and multi-materials may be involved. Compared with other standard computational fluid dynamics (CFD) codes, hydrocodes solve the more fundamental equations of fluid mechanics [16]. By solving these equations, hydrocodes make fewer simplifying assumptions than standard CFD codes [5,16].

In application to the far-field UNDEX problem, hydrocodes are used to simulate detonation, shock wave propagation, and fluid-structure interaction. Hydrocodes can be divided into two categories, Eulerian and Lagrangian.

1.3.2 Eulerian Hydrocodes

Eulerian hydrocodes use a mesh that is fixed in space meaning after each time step any distortion that occurs in the mesh is restored by an advection or "remapping" phase [16]. By using a fixed mesh, problems that arise from mesh distortion are avoided, however there is less detailed information available for each element in the mesh. This results from the lack of history and the smearing of information as mass moves thorough the fixed Eulerian grid [17]. Smearing may also cause the Eulerian mesh to calculate the peak pressure of the shock wave at a lower value than the real value [5]. The Eulerian

method is more computationally expensive than other hydrocode methods as the mass flux through each element must be computed in the advection phase of each time step.

Pangilinan, *et. al* [18] used the Eulerian hydrocode CTH to model pressure-time histories resulting from PETN detonation in water and Chisum [19] used a multi-material Eulerian mesh in MSC/DYTRAN to model a deep (178.6 m below the surface) water TNT explosion.

1.3.3 Lagrangian Hydrocodes

In Lagrangian hydrocodes the mesh remains fixed to the material, which allows the mesh to distort as the material does. While the Lagrangian mesh method is quicker than the Eulerian mesh method because no advection phase is needed, it may cause difficulties associated with large mesh distortions. When mesh distortions become too large in the Lagrangian method, the calculation breaks down [17].

Mair, *et. al* [5] used a purely Lagrangian approach in the hydrocode DYNA3D to model an explosion near a curved plate and found that the mesh eventually broke down in the late-time part of the problem, validating the major limitation of the purely Lagrangian method.

1.3.4 Coupled Eulerian/Lagrangian Methods

In coupled Eulerian/Lagrangian methods a Eulerian mesh is used to model the fluid domain and a Lagrangian mesh is used for the structural domain. A coupling procedure is performed on the interface between the domains to calculate the interaction between the fluid and structure. Shittke, *et. al* [6] used the coupled hydrocode DYSMAS/ELC to model the structural response of a catamaran hull section to a far-field underwater explosion.

The fluid-structure interaction is calculated in the coupling module of DYSMAS, DYSMAS/C. In the coupling module the structure defines a time-varying boundary condition for the fluid through which mass and energy are exchanged. Hydrodynamic loads created by the arrival of the shock wave are transferred into pressure forces on the structure [6]. The influence on the structural response on the fluid is calculated by the momentum change in the fluid due to the displacements of the structure. [20].

The Schittke, *et. al* model seemed to be successful in capturing the shock loading on the hull section and the effects of cavitation by assuming that the shock wave could be treated as a plane wave but was not validated by any experimental data. It was concluded the model was not able to accurately capture the peak pressure of the shock wave but was able to capture the impulse of the shock wave. A limitation of the DYSMAS/ELC method arises from the plane front shock wave assumption made to model the fluid using a 2D grid. Recall that UNDEX problems where the charge is relatively close to the structure but close enough to the surface that the bubble vents before interacting with the structure still fall into the category of far-field. In such a problem the shock wave cannot be assumed to be planar when it reaches the structure and therefore this limits the DYSMAS/ELC method described above to traditional far-field problems where the charge a significant distance away from the structure.

1.3.5 Other Numerical Methods - USA

Another approach to solving the UNDEX problem is to use a boundary element method. The Doubly Asymptotic Approximation (DAA) is a boundary element method used in the Underwater Shock Analysis program (USA). The significant advantage of the DAA method is that the governing equations of the fluid-structure interaction are

expressed in terms of the wet surface variables only. Therefore the fluid surrounding the structure does not need to be modeled allowing for much faster computation times [21, 22].

In 1992 Fox modeled a submerged cylindrical shell subjected to a far-field UNDEX. This model was classified as far-field type 1 because the initial charge location was such that the gas bubble vented to the surface before interacting with the cylinder [23]. The cylindrical shell was modeled without a surrounding fluid and because of the depth cavitation was not accounted for in the analysis. The results of the USA model were compared to experimental data of the same UNDEX problem to show that the USA model compared well qualitatively with the experimental results.

Beiter [24] and Wood [11] modeled "ship-like" box structures on the surface subjected to far-field UNDEX. As in the cylindrical shell model, the fluid surrounding the structure was not modeled and cavitation was not included in the analysis. No comparisons to experimental data or verification of method were made but the results were concluded to be reasonable.

1.3.6 Other Numerical Methods - SPH

Smoothed particle hydrodynamics or SPH is a numerical method with potential application for shock wave modeling. The SPH method is an explicit numerical method that is Lagrangian in nature [25]. The goal of the SPH method is to obtain a numerical solution to the initial-boundary value problem defined by the partial differential equations that govern the system [17]. Unlike standard Lagrangian finite-difference methods which use grids to approximate spatial derivatives, the SPH method applies interpolation theory to a random group of particles that represent the state of the system [17]. Finite element

based methods for spatial derivatives assume that particles initially surrounding each other maintain their connection. The SPH method makes no such assumptions; there is no connectivity or spatial relationships between particles in the SPH method [17]. This means that particles in the SPH method are not interacting mass elements but rather interpolation points that move freely in space and carry all computational information [17, 25]. Because no grid is needed in the SPH method it is termed a "meshless" technique.

Liu *et. al*, [25] successfully applied the SPH method to model detonation and shock wave propagation in a simple UNDEX problem. Swegel and Attaway [17] used coupling between PRONTO and SPH to model a flat circular plate subjected to an underwater explosion. Their results showed that the PRONTO/SPH method accurately models shock loading and early time effects on the plate but fails to accurately model late time phenomena. The inaccuracy of the late time model is due to the large influence of numerical parameters such as artificial viscosity on the problem [17]. A downfall of the SPH method is its heavy reliance on numerical parameters that are mathematically based rather than physics based to produce accurate results. For example, assume the UNDEX problem is formulated correctly. In finite element work only two variables, element size and number of nodes can affect the results. In SPH there are many more variables that can affect the results.

1.3.7 Coupled Finite Element Methods – LS-DYNA/USA

The LS-DYNA and USA can be couples in the far-field UNDEX problem to simulate the structural response. The finite element code LS-DYNA is used to model a small portion of the fluid domain where cavitation occurs using the cavitating acoustic finite

element (CAFE)method. LS-DYNA is also used to analyze the response of the ship structure to shock loading. USA is used to model the rest of the fluid domain by acting as a radiation boundary on the LS-DYNA fluid domain boundary [26]. Using this method allows the entire fluid domain of the far field problem to be modeled as a boundary value problem with less computation time as elements are not needed to model the entire domain.

LS-DYNA/USA was used by Wood to model an UNDEX with a ship-like box structure model. In his model a rectangular fluid mesh was created in LS-DYNA using the MAT_ACOUSTIC formulation, which allows for cavitation to be modeled [11]. The conclusion was that the results agreed with the physics of the problem [11] but no comparison to analytical or experimental results was made. Wood also found that cavitation plays a significant role in the response of a structure to a far-field underwater explosion, and concluded that at least a partial fluid model is required to accurately model surface ship UNDEX problems.

Shin modeled an actual shock trial performed on the USS Winston S. Churchill (DDG 81) [3] using LS-DYNA/USA. In this model Shin accounted for cavitation by creating a cylindrical surrounding fluid mesh in LS-DYNA. Due to the complex hull form of the DDG 81, Shin developed the concept of using a multiple-layered fluid mesh to meet the USA code stability criteria, and keep the fluid mesh perfectly orthogonal to the structural mesh. The multiple layered mesh consists of the inner liner, the inner mesh, the transitional mesh and the outer mesh. The inner liner serves as the fluid-structure interface and must mesh perfectly with the structural mesh in order for the model to behave properly [3]. The outer mesh encloses the three previous meshes and extends the

fluid mesh out to the DAA wet surface boundary. By experimenting with different meshes Shin found that the best results were obtained when the outer mesh was extended to a depth equal to that of the bulk cavitation region. Shin found that the model is very sensitive to small changes in the depth of the fluid mesh. This demonstrates that a very specific mesh is needed to obtain the most accurate results in the DDG 81 model.

After adjusting the mesh, Shin found acceptable results from the model when compared to actual shock trial data obtained for the DDG 81, thus validating his model for specific mesh configurations. However, the uniqueness of the fluid mesh needed for accuracy in Shin's model and the lack of verification of the LS_DYNA/USA methods means that no conclusions can be reached on the LS-DYNA/USA modeling method for the general UNDEX problem.

1.3.8 Spectral Element Methods – CASE

The spectral element method is a combination of traditional spectral methods, which are generally very accurate, and the finite element which is more geometrically flexible. Sprague and Geers [38] have applied the spectral element method (SEM) to the far-field UNDEX problem using the CAFE approach to modeling the fluid domain. They label this approach as the cavitating acoustic spectral element method (CASE).

Sprague and Geers have applied the CASE method to a number of far-field UNDEX problems. The first was a one dimensional mass-spring problem [38] and most recently they have applied the CASE method to a three dimensional ship like barge [74]. Results in both of problems have shown that the CASE method provides more accurate results at less computational cost than the traditional CAFE approach. However, these conclusions

are based on comparison between CASE and CAFE results. Results obtained with the CASE method have not been compared to experimental results for either problem.

1.4 Thesis Objectives

In Sections 1.2 and 1.3 past methods for modeling UNDEX problems were discussed. Based on that discussion it is concluded that past UNDEX models are not adequate for use in the creation of a general UNDEX model for use in survivability design. The similitude method, for example, is good at predicting shock wave characteristics for simple UNDEX problems, but the similitude method is limited because it is not physics based. Similitude is accurate for only a certain range of problems and no boundary interactions are included in the formulation. The numerical UNDEX models of presented in Section 1.3 gave some good results, showing that it is theoretically possible to apply numerical methods to the UNDEX problem, but most have not been validated by experiment. Furthermore, these models make too many assumptions and some are modeled in ways that limit them to very specific UNDEX problems.

Therefore, the primary objective of this thesis is to assess the capabilities and validity of numerical tools currently used to model UNDEX problems to determine their general applicability to survivability design. This is accomplished by modeling an UNDEX problem in which a simple box barge structure is subjected to a far-field Type 1 explosion using the programs USA and LS-DYNA. By studying the results of this problem and by developing a fundamental understanding of the tools (USA and LS-DYNA) used, the limitations of these programs to model far-field UNDEX problems are assessed. Finally, possible improvements in areas such as element type and boundary

conditions are suggested to improve results and expand the capability of these tools so that in the future they may be used in more general far-field UNDEX problems.

1.5 Thesis Outline

The first section of Chapter 2 begins with a discussion on the background of LS-DYNA and a look at the formulation of the finite element and the time integration scheme it uses. Next the LS-DYNA options that are used in UNDEX modeling are discussed and related to the specific UNDEX phenomena they model. Finally the coupling between LS-DYNA and USA is discussed.

The second section of Chapter 2 details the formulation of the DAA equations, which provides the mathematical foundation of USA. A brief introduction into the user options found in USA is also given.

Chapter 3 details the creation of the box barge UNDEX models and then provides results obtained using USA only and LS-DYNA only. In the next section the results of different box barge models are compared to investigate the accuracy of the results found in USA and LS-DYNA. Next the formulation of fluid elements and boundary conditions in LS-DYNA are studied to determine their applicability to the box barge UNDEX problem. Finally in Chapter 3, the global response of the box barge is investigated to determine the affect of an UNDEX on the entire ship structure.

In Chapter 4 the boundary conditions used in the LS-DYNA box barge UNDEX model are assessed to determine if the are working correctly. Then a general introduction to non-reflecting boundary conditions is given with example problems demonstrating the effectiveness of LS-DYNA non-reflecting boundaries and a non-reflecting boundary not

available in LS-DYNA. Finally, the general requirements for an effective UNDEX non-reflecting boundary condition are presented.

Chapter 5 provides concluding remarks on the findings of Chapters 2 and 3 with suggestions for future work that may solve some of the problems encountered in modeling the box barge UNDEX problem.

CHAPTER 2 ANALYSIS TOOLS

Chapter 1 showed that past UNDEX models have been limited to very specific problems or make many assumptions. In this chapter the tools LS-DYNA and USA, which have been used most successfully in UNDEX modeling are analyzed to determine their assumptions and formulations. The objective of this analysis is to provide a fundamental understanding that can be used to determine the validity of a simple UNDEX model that is presented in Chapter 3. Based on the results of the simple UNDEX model of Chapter 3 conclusions can be reached about the future use of LS-DYNA and USA in UNDEX modeling.

2.1 LS-DYNA

LS-DYNA 970 is the most recent version of the non-linear, dynamic, three-dimensional, finite element code LS-DYNA created by the Livermore Software Technology Corporation in 1989. It is essentially a modified version of an older three-dimensional finite element code, DYNA3D, created in 1979 at the Lawrence Livermore National Laboratory by J.P. Hallquist. LS-DYNA packages together many options for elements, material models, and boundary conditions some of which apply to the UNDEX problem [27].

A general LS-DYNA UNDEX finite element model as used by Shin and Wood [3,26,11] consists of a fluid domain modeled with solid elements and a structural domain modeled with shell elements (Figure 2.1). The following gives a brief background into the elements and other options used in the creation of the general LS-DYNA UNDEX model.

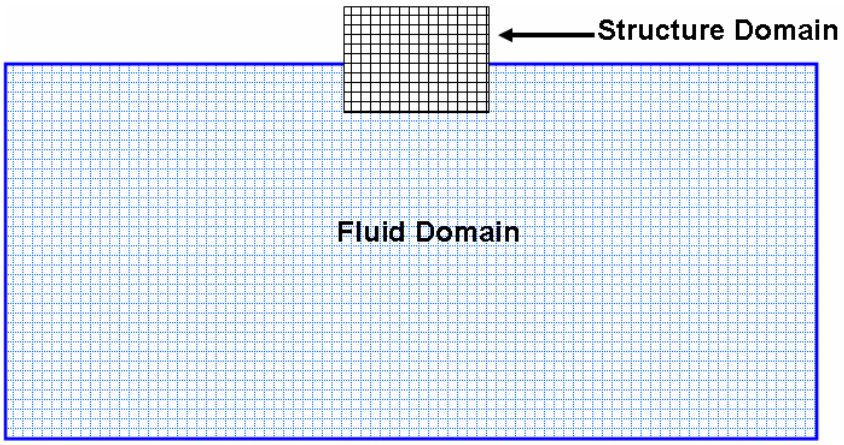

Figure 2.1 Representation of the fluid and structure domains in a general UNDEX model

2.1.1 Elements

In general LS-DYNA seeks an approximate solution to the momentum equation in Equation 2.1 using initial and boundary conditions input by the user. It approximates the solution by creating a weak formulation of the governing equation and then uses the standard Galerkin formulation or the Petrov-Galerkin formulation of the problem to obtain the finite element solution. The Petrov-Galerkin option is limited to certain elements, none of which are used in the UNDEX model.

$$\sigma_{ij,i} + \rho f_i = \rho \ddot{x}_i \tag{2.1}$$

For the fluid domain of the UNDEX model 8-node solid elements are used. These elements use first order polynomial shape functions for each node and the mass matrix for these elements is transformed into a diagonal matrix using the row-sum technique. Making the mass matrix diagonal or lumping the mass matrix can reduce computation time but the row-sum technique can also result in negative nodal masses which can cause the solution to blow up in time.

The type of solid element used for the UNDEX fluid domain is the acoustic pressure element. Acoustic pressure elements assume small fluid displacements and neglect viscosity. LS-DYNA acoustic elements track low stress pressure waves through an acoustic medium. The acoustic element requires that only one unknown, pressure, be found at each node making it a very cost effective element [27]. Further detail on the formulation of acoustic pressure elements is given in Section 3.4.2. The MAT_ACOUSTIC material model must be used when acoustic elements are selected. In this material model the user defines density, speed of sound, atmospheric pressure, gravity, and the free surface boundary of the domain. Atmospheric pressure and gravity terms are used to calculate hydrostatic pressure which is added to the element solution as in Equation 2.2. The defined free surface boundary in the material model treats reflections of the pressure wave at the boundary as an interface boundary where one material is the acoustic material and the other is air.

$$p_{final} = p_{element} + p_{atmospehre} + \rho g z_{depth} \tag{2.2}$$

The MAT_ACOUSITC model also allows the user to control a damping factor and includes an option to consider cavitation in the acoustic medium [28].

For the structure domain Belytschko-Tsay shell elements are used. Shell elements allow for a two dimensional element to be used in conjunction with a defined thickness to model a three dimensional domain. The Belyschko-Tsay element is the default shell element formulation in LS-DYNA 970 because of its computational efficiency. The efficiency of the element is obtained from its combined co-rotational and strain-velocity relation [27]. Because of this formulation Belytschko-Tsay elements are limited to

problems with small strains. The small strain assumption is valid in the far field UNDEX model because only elastic deformation of the ship structure is allowed.

The Belytschko-Tsay element works by creating a four node quadrilateral element to define the surface at the midpoint of the shell thickness, called the midsurface. A coordinate system that deforms with the element is defined for each element's midsurface. From this the co-rotational coordinate system is defined. The co-rotational strain-velocity relations are evaluated at the element quadrature point and nodal position. Velocity and angular velocity are solved at the midsurface using interpolation with bilinear shape functions for a four node quadrilateral element. Stresses resulting from the solution of the velocity-strain relations are integrated through the shell thickness to obtain the nodal forces and moments [27].

2.1.2 Time Integration

LS-DYNA uses the central difference method to perform the time integration of the model. The central difference scheme is conditionally stable with second order accuracy. Time integration in LS-DYNA is explicit meaning that the solution at the current time step can be determined from the solution at the previous time step without solving a system of simultaneous equations. Therefore the mass and damping matrices in the semi-discrete equation of motion must be diagonal [29]. The diagonal matrices are created via the row-sum technique and are subject to the complications outlined in Section 2.2.1. Accelerations are solved for by inverting the mass matrix in the semi-discrete equation of motion and then used to solve for velocity and displacement. Nodal positions are updated at each time step by adding the current nodal displacements to the nodal position

at the previous time step. Details of the time integration loop performed in LS-DYNA are shown in Figure 2.2.

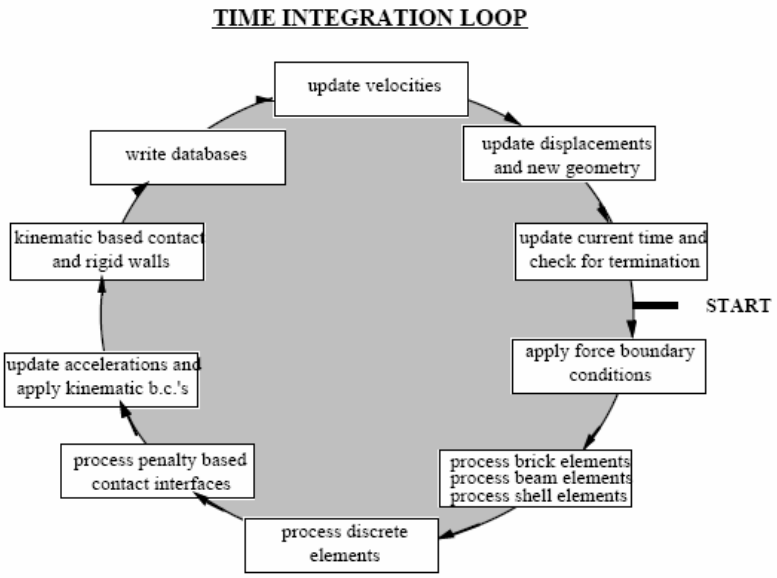

Figure 2.2 LS-DYNA time integration loop diagram [27]

Stability of the central difference method is controlled by the size of the time step used in the analysis. A maximum time step is defined for which the model will be stable for any time smaller than the maximum time step. LS-DYNA computes the maximum or critical time step for stability by finding the minimum critical time step over all of the elements in the model. For solid elements the critical time step is calculated using Equation 2.3 and 2.4 where $V_{element}$ is the element volume, $A_{element}$ is the area of the largest element side, Q is a function of the bulk viscosity factors, and c is the speed of sound in the element.

$$L_c = \frac{V_{element}}{A_{element}} \tag{2.3}$$

$$\Delta t_{critical} = \frac{L_c}{\sqrt{Q + \left(Q^2 + c^2\right)}} \tag{2.4}$$

For shell elements the critical time step is determined by the ratio of the characteristic element length to the speed of sound in the element (Equation 2.5). Several methods of determining the characteristic element length are available. These options offer the user the choice of how conservative a time step is required for the analysis. The default method given for an equal length quadrilateral element in Equation 4 was used in the UNDEX model to find the characteristic length. In the UNDEX model this calculation controls the minimum critical time step as the shell elements of the ship structure require smaller time steps than the fluid.

$$\Delta t_{critical} = \frac{L_c}{c} \tag{2.5}$$

$$L_c = \frac{A_{element}}{h_{element}} \tag{2.6}$$

2.1.3 Boundary and Initial Condition options

To model the explosion in the UNDEX model, the INITIAL_DETONATION option is used in LS-DYNA. The INITIAL_DETONATION option is used to initialize the detonation process in a modeled explosive material. This option also works uniquely with acoustic elements to initialize a shock wave within the fluid domain of the UNDEX model. The user is required to first input the location of the charge, which can be internal or external to the fluid domain. In the far field UNDEX model the charge location is always defined external to the fluid domain. Next the user must input a point on the free surface of the fluid domain, in the far field model the coordinates of a node on the free surface of the fluid is used. Then the user must input the peak pressure and time constant for the UNDEX scenario. These inputs are used to initialize the shock wave pressure

time history using the peak pressure approximation (Equation 1.3**).** The shock wave is initialized at time zero at a node that is located one element length away from the structure. Finally the user must define the standoff point, which is located on the bottom boundary of the fluid domain on the line that can be drawn between the charge location and the structure. LS-DYNA uses the standoff point to determine the acoustic mesh boundary for the fluid domain. The acoustic mesh boundary acts as a transmitting boundary that keeps the reflected shock wave from re-entering the fluid domain and contaminating the results once it has reached the domain boundary. The function and inputs of the INITIAL_DETONATION option are outlined in Figure 2.3.

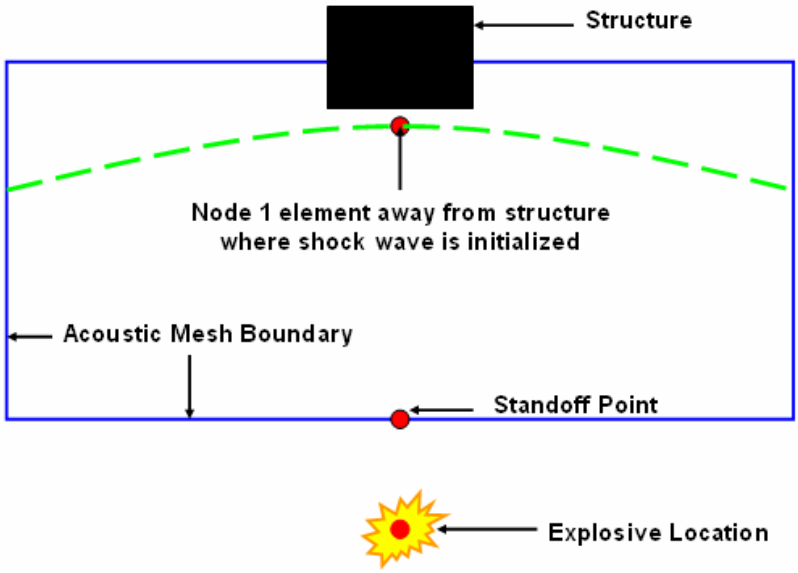

Figure 2.3 Schematic of the function and input of the LS-DYNA option INITIAL_DETONATION

2.1.4 Coupling with USA

LS-DYNA and USA coupling is achieved using the BOUNDARY_USA_SURFACE option. In this option the user defines the wet surface boundary of the ship structure in

LS-DYNA. The USA code is then applied to this wet surface boundary if no fluid is modeled or the outer fluid domain boundary if the fluid is modeled. Two items should be noted when modeling an UNDEX scenario using USA, the first is that the INITIAL_DETONATION option must still be defined in LS-DYNA. The second is that the normal vectors of the elements on the wet surface boundary must point outwards into what would be the surrounding fluid if no fluid is modeled.

2.2 USA

USA is a boundary element method code developed by the Lockhead Palo Alto Research Laboratory. It assumes the UNDEX model is a linear system and requires coupling with a finite element code to discretize the structural domain of the problem. The primary advantage of using USA is that the fluid surrounding the model does not need to be modeled, greatly reducing the computational effort for the far field UNDEX problem.

Modeling the far field UNDEX problem in USA first requires a structural model in LS-DYNA. USA then couples with LS-DYNA using a staggered solution procedure in which the structural response equations are solved in LS-DYNA and the fluid response equations are solved in USA. Coupling terms in the equations are extrapolated between the two programs to generate the final solution [11]. USA requires three input files augmat, flumas, and timint. In these input files the user specifies the charge location, the peak pressure of the explosion, the time constant, the standoff point, the location on the structure where the shock wave will first impact, whether cavitation is to be considered, and the time integration parameters.

In USA the fluid-structure interaction or coupling is modeled using the Doubly Asymptotic Approximation (DAA), which replaces the fluid domain model. The DAA formulation and procedure is described by DeRuntz [30] and is summarized in the following section.

The DAA is a system of differential equations in time that combines the Plane Wave Approximation, which is exact at high frequency (early time response), with the Virtual Mass Approximation, which is exact at low frequency (late time response) [30].

To calculate the fluid-structure interaction, USA first models detonation using the peak pressure relationship (Equation 1.3) to define the initial pressure of the shock wave. Once the shock wave reaches the structure, USA solves the interaction by equating taking dynamic response equation for a linear structure (Equation 2.7) and equating it to the excitation force of a submerged structure due to a plane wave (Equation 2.8) [21].

$$M_s\ddot{x} + C_s\dot{x} + K_s x = f \tag{2.7}$$

$$f = -GA_f\left(p_I + p_S\right) + f_D \tag{2.8}$$

Where x is the displacement vector of the structure, M_s is the structural mass matrix, C_s is the damping matrix, K_s is the stiffness matrix, and f is the excitation force vector. In Equation 2.8 p_I is the nodal pressure vector for the wet surface of the fluid elements due to the incident shock wave, p_S is the nodal pressure vector for the wet surface that is used to solve for the structural response. f_D is the force vector applied to the dry surface, A_f is the diagonal area matrix of the fluid elements, and G is the transformation matrix that is used to relate the structural and fluid node forces [31]. The matrix G is rectangular with more rows than columns as the number of degrees of freedom for the structure exceeds the degrees of freedom of the fluid. Because of this discrepancy in the degrees of

freedom, the matrix G is calculated such that only translational degrees of freedom (no rotation allowed) of the structure couple with the fluid degrees of freedom [30].

Next USA uses the DAA (Equation 2.9) to model the fluid-structure interaction in terms of the wet surface nodal pressure, p_s [21].

$$M_f \dot{p}_s + \rho c A_f p_s = \rho c M_f \dot{u}_s \tag{2.9}$$

Where u_s is the vector of scattered wave fluid particle velocities normal to the wet surface of the structure and the variables c and ρ are the speed of sound and density in the fluid. M_f is the symmetric fluid mass matrix for the wet surface. The symmetric fluid mass matrix (M_f) is generated by applying a boundary element approach to Laplace's equation for the flow generated in the surrounding fluid by the motion of the structure's wet surface. In this approach the surrounding fluid is assumed to be irrotational, inviscid, incompressible, and infinite fluid [30].

Assuming the incident wave is acoustic when it encounters the structure, the vector of scattered wave fluid particle velocities normal to the wet surface of the structure (u_s) can be expressed in terms of the structural response (Equation 2.10). Equation 2.10 implies that the normal fluid particle velocity must match the normal structural velocity on the wet surface [30].

$$G^T \dot{x} = u_I + u_s \tag{2.10}$$

Substituting Equation 2.10 into Equation 2.9 and 2.8 into 2.7 the following relations are obtained:

$$M_s \ddot{x} + C_s \dot{x} + K_s x = -G A_f \left(p_I + p_S \right) \tag{2.11}$$

$$M_f \dot{p}_s + \rho c A_f p_s = \rho c M_f \left(G^T \ddot{x} - \dot{u}_I \right) \tag{2.12}$$

Equations 2.11 and 2.12 are the interaction equations. The right-hand side of Equation 2.12 is the Plane Wave Approximation [22]. USA solves the interaction equations by applying a staggered solution procedure where M_s is assumed to be non-singular, Equation 2.11 is partitioned to find $G^T x$ which is then substituted into Equation 2.12. The resulting equation is pre-multiplied by $A_f M_f^{-1}$ to obtain Equation 2.13, the equation for scattered pressure in the fluid [25,30]. Solving Equation 2.13 gives the displacement, velocity, and acceleration of the structure [11].

$$A_f \dot{p}_s + \left(D_{f1} + D_s\right) p_s = -\rho c A_f G^T M_s^{-1}\left(C_s \dot{x} + K_s x\right) - D_s p_I - \rho c A_f \dot{u}_I \qquad (2.13)$$

$$D_{f1} = \rho c A_f M_f^{-1} A_f$$

$$D_s = \rho c A_f G^T M_s^{-1} G A_f$$

The DAA, and therefore USA, is limited in its application. It is not theoretically formulated to handle multiple structures, concave structures, or explosions near the free surface [23]. Because the DAA cannot account for large displacement hydrodynamic flow it assumes the incident shock wave is an acoustic wave [23, 30]. Therefore, DAA is only valid for UNDEX problems where the charge is significantly removed from the structure such that the shock wave has dissipated enough to be treated as a plane acoustic wave. Another limitation is that although the DAA approaches an exact solution at both late and early time, it can significantly deviate from the exact solution at times where neither late time nor early time effects dominate the response [23].

Because the DAA can only be used for problems where the fluid domain remains linear it can not be used to model problems in which cavitation must be considered. USA does include the option of using the Cavitating Fluid Analyzer (CFA) [31, 32], but the accuracy of these results is heavily dependent on the modeled UNDEX scenario [1].

Therefore as discussed in Section 1.3.7 the common method to include cavitation in the far field UNDEX model is to model a portion of the fluid domain in LS-DYNA and apply USA to the outer boundary of the fluid domain to act as a radiation boundary condition. However there is some question as to whether the DAA formulation used on LS-DYNA/USA can be applied to fluid points in this fashion as it was originally derived to be applied to structural points. This will be discussed in detail in Section 3.4.4.

Given the fundamental overview of LS-DYNA and USA in Chapter 2, there are still many questions about the details of their implementation in a far-field UNDEX problem. Chapter 3 investigates this implementation by modeling a simple far-filed UNDEX problem similar to the model created by Wood [11]. The results are compared to previous models to check their validity. The results are then weighed against the assumptions made in the fundamental formulation of LS-DYNA and USA to determine their applicability to general UNDEX problems.

CHAPTER 3 MODELING FAR-FIELD UNDERWATER EXPLOSIONS USING LS-DYNA AND USA

In Chapter 3 a far-field UNDEX model is created in USA and LS-DYNA to determine the UNDEX modeling capabilities of the programs. The model is similar to previous LS-DYNA/USA models [11] so that model can be validated by comparing results. Once the model is validated, the results are analyzed using the fundamental understanding of USA and LS-DYNA developed in Chapter 2. This analysis is used to determine what UNDEX phenomena are important to account for, how well the results represent a real UNDEX problem, and the limitations of the programs. By determining the current capabilities of the programs USA and LS-DYNA, an attempt can be made to improve these programs and UDNEDX modeling in general on a fundamental level.

3.1 Box Barge Problem

The far-field UNDEX problem modeled created in this thesis is a box barge ship structure subjected to a 20 lb. TNT explosion. The charge is placed 18 meters below the keel at amidships of the box barge (Figure 3.1). It is assumed that the explosion is a type 1 far field explosion, therefore all bubble effects are neglected and the box barge response is assumed to be elastic.

A finite element model of this UNDEX scenario was created using LS-DYNA in accordance with the general procedure for UNDEX modeling in LS-DYNA suggested by Shin and others [3,11,26]. This requires a one-to-one nodal contact at the fluid-structure interface, the fluid domain is assumed to be an acoustic medium, and the fluid mesh must be deep enough to contain the bulk cavitation region. Analysis was done with and without including cavitation to study the impact it has on the UNDEX problem. Also several

fluid meshes were generated and compared to see which mesh gave the best results and to make sure the mesh did not dominate the solution. The different meshes were also used to analyze the effect mesh geometry has on the behavior boundary conditions in the box barge model.

Because no analytical solution or experimental data is available to validate the finite element results the box barge problem was also modeled in USA as a check for the LS-DYNA results. The LS-DYNA to USA comparison does not validate the results. It only shows that two methods give similar results and therefore capture the same physics.

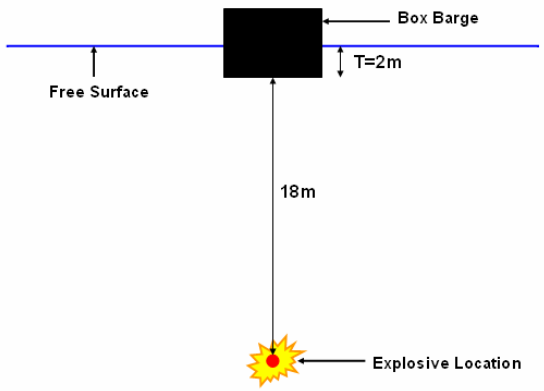

Figure 3.1 Schematic of box barge problem setup

3.1.1 Box Barge Structural Model

The box barge structural model is shown in Figures 3.2 and 3.3. It is 9 meters in length with a constant beam and depth of 5 meters. It consists of the bottom, inner bottom, longitudinal girder, two traverse frames, a deck, sides, stern and bow. An internal view, showing the layout of the box barge structure is shown in Figure 3.4. The box barge was modeled with the elastic material model MAT_ELASTIC using mild steel (Table 3.2).

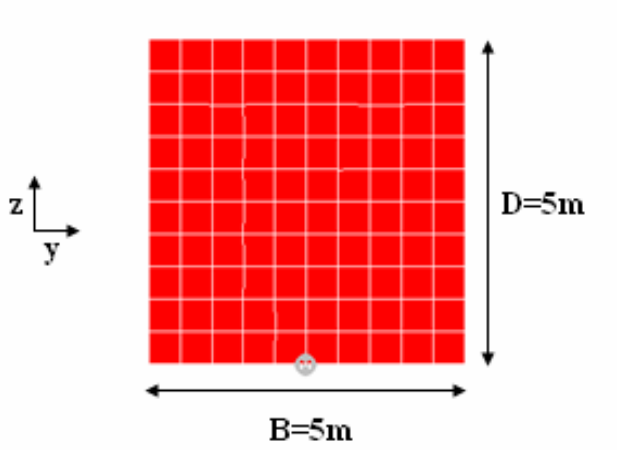

Figure 3.2 Front view of box barge showing beam and depth (50cm mesh)

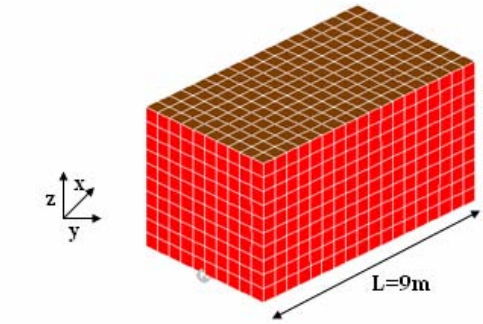

Figure 3.3 Isometric view of box barge showing length (50cm mesh)

Table 3.1 Box barge geometry

Length	9 m
Beam	5 m
Depth	5 m
Draft (light ship)	1.044 m
Displacement (light ship)	48174 kg

Table 3.2 Mild steel properties used for box barge model

Density	7780 kg/m^3
Young's Modulus	1.9x10^{11} Pa
Poisson's Ratio	0.281

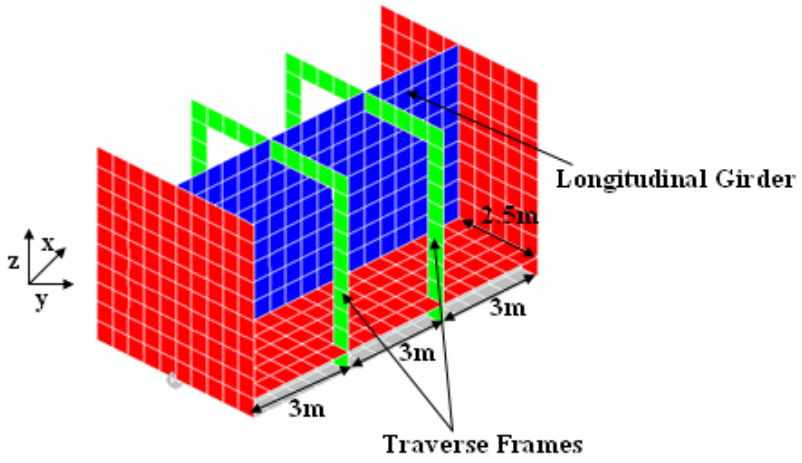

Figure 3.4 Internal view showing layout of traverse frames and longitudinal girder (50cm mesh)

The light ship draft of the box barge is 1.044 meters but to make modeling the waterline easier three equally distributed mass nodes were added to the bottom of the box barge to make the draft 2 meters. The distribution of the mass nodes is shown in Figure 3.5.

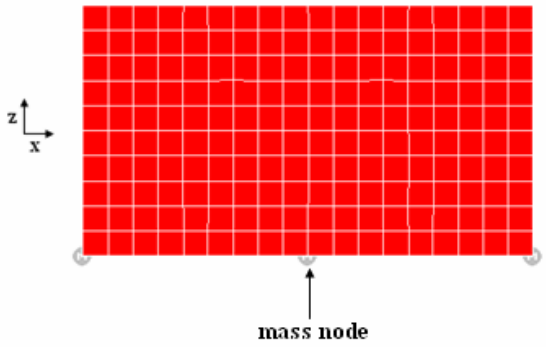

Figure 3.5 Side view of box barge showing distribution of the mass nodes (50cm mesh)

In the box barge problem the structural mesh size is controlled by the fluid mesh size to maintain one-to-one nodal contact at the fluid-structure interface. Therefore

three box barge meshes were created. A coarse mesh of 50cm elements, a medium mesh of 25cm elements, and a fine mesh of 15cm elements.

For the initial investigation of the box barge problem, vertical velocity responses for four locations on the box barge where recorded. Only vertical velocity responses were looked at because a ship always has a vertical velocity response no matter where the charge is located [4]. These locations are shown in Figures 3.6, 3.7 and 3.8. The first is located on the keel (centerline) of the bottom hull (node 386 in figures) while the second is on the bottom hull off of the keel (node 573 in figures). The third is located on the traverse frame (node 4110 in Figure 3.8) and the fourth node is located on the side of the hull (node 5724 in figures). For the velocity response only the vertical velocity is considered because it dominates the box barge response for the modeled UNDEX scenario. Furthermore it allows for the kick-off velocity (see section 1.2.2) to be studied.

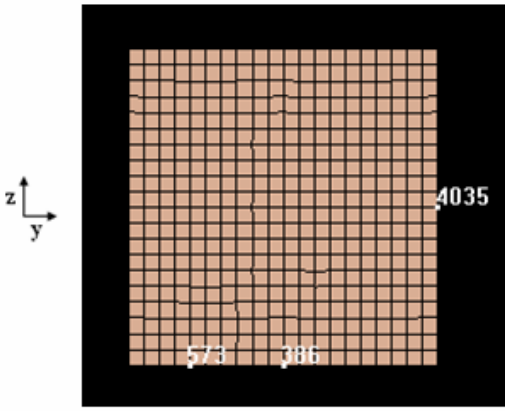

Figure 3.6 Front view of box barge showing velocity result locations (25cm mesh)

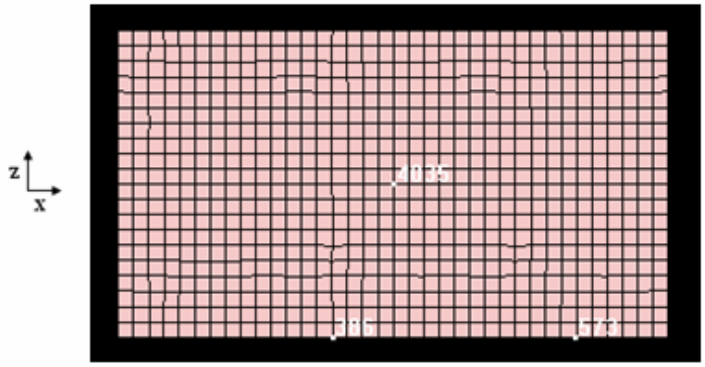

Figure 3.7 Side view of box barge showing velocity result locations (25cm mesh)

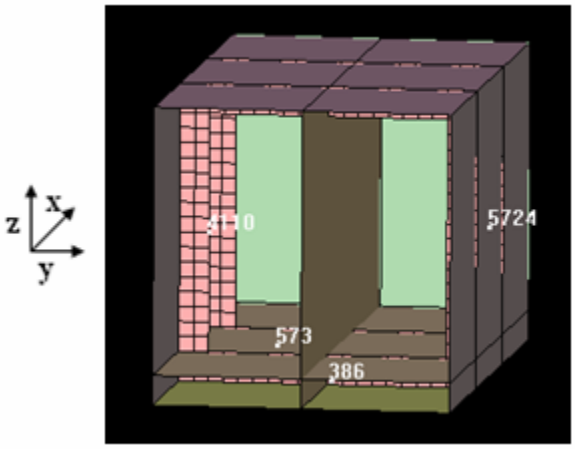

Figure 3.8 Internal view of box barge showing velocity result locations (25cm mesh)

3.1.2 Box Barge Fluid Model

The fluid model for the box barge problem is created in a similar fashion to the one created by Wood in his analysis of a similar problem [11]. It is modeled assuming inviscid flow, small fluid displacements, and that the fluid nodes remain attached to the structural nodes at the fluid structure-interface. Standard salt water properties, ρ=1025 kg/m^3 and c=1514 m/s, are used for the fluid in the model. The dimensions, given in Figure 3.10, of the main fluid model are 15m x 15m x 7 m. For the x and y dimensions it is assumed that it is adequate to have the fluid mesh extend from the ship to a distance equal to the beam of the ship. As shown in previous models [31],

the depth of the fluid mesh should not be less than the maximum depth of the bulk cavitation zone, so the fluid mesh is extended to 5 meters below the keel of the box barge in the fluid model.

Modeling the fluid in the UNDEX problem presents a unique challenge. The fluid surrounding a ship in a large body of water is an infinite domain, but because of computational limitations the fluid domain in the finite element model must be modeled as a finite domain. Therefore it is necessary to apply specially formulated boundary conditions such as the transmitting boundary used by the INITIAL_DETONATION option in LS-DYNA to the fluid domain in order to make the fluid model behave as an infinite domain.

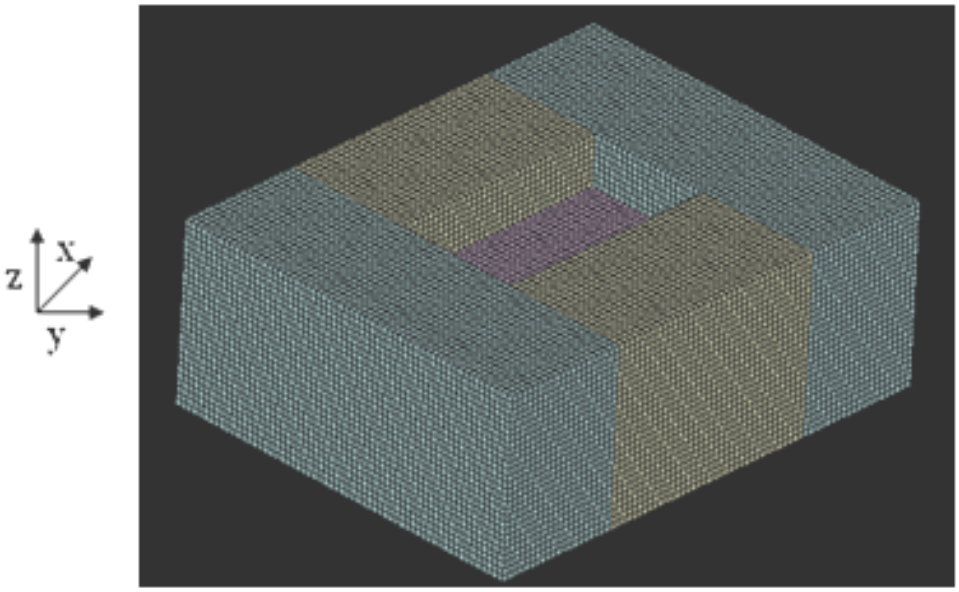

Figure 3.9 Isometric view of the main fluid mesh used in the box barge problem

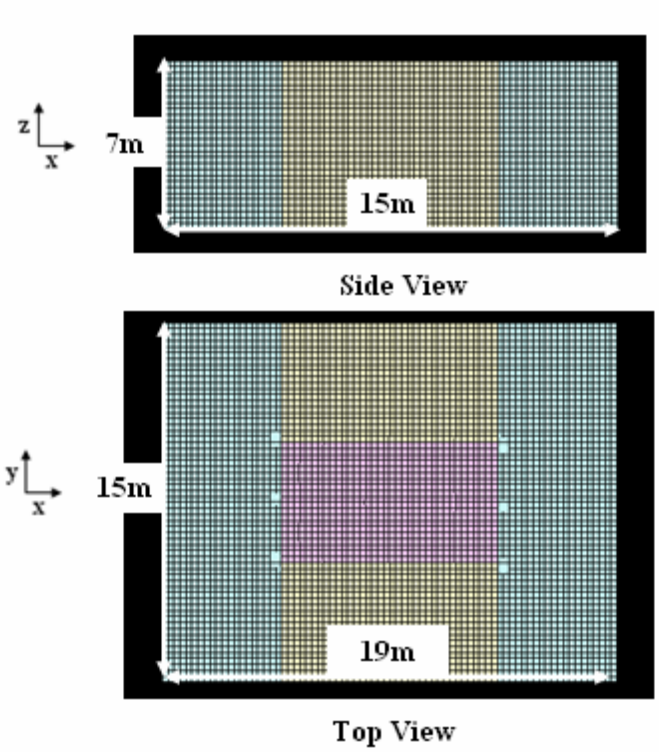

Figure 3.10 Side and top view showing dimensions of the 25 cm fluid mesh

To analyze the affects of the fluid model on the results of the box barge UNDEX simulation four different fluid meshes were created. The first two fluid meshes are a coarse mesh of 50cm elements, and a medium mesh of 25cm elements. These two meshes use the dimensions of the main fluid model described above. The third fluid model is a fine mesh that uses 15cm elements. Because of computer limitations, the x and y dimensions of the fine mesh fluid domain were reduced as shown in Figure 3.11.

The final fluid mesh created was a cylindrical fluid mesh. The cylindrical mesh is not uniform so the fluid-structure interface uses 25cm elements to maintain a one-to-one nodal contact with the 25cm box barge model. The element size increases as the boundary of the fluid model is approached. The dimensions and element sizes of the cylindrical mesh are shown in Figures 3.12 and 3.13.

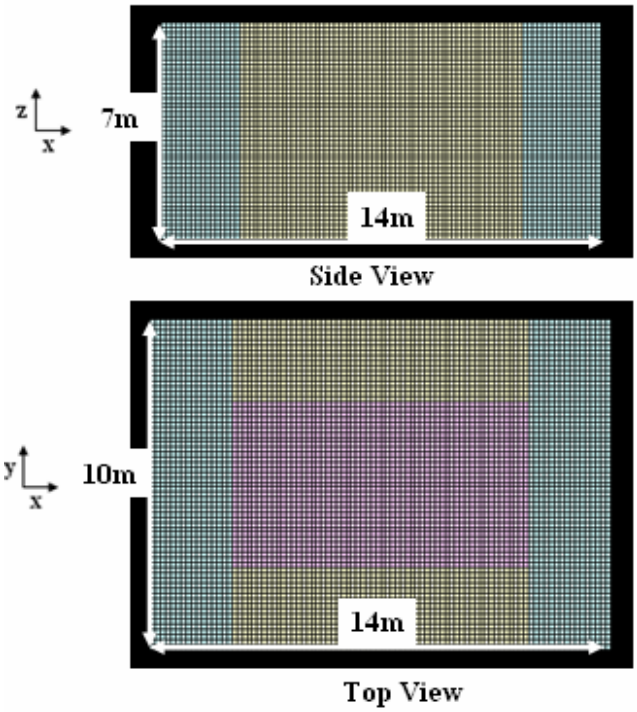

Figure 3.11 Side and top view showing dimensions of the 15 cm fluid mesh

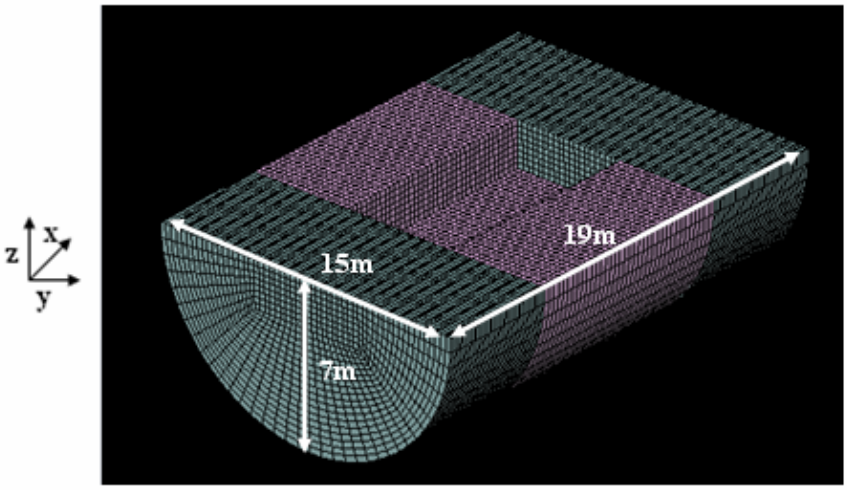

Figure 3.12 Isometric view of the cylindrical fluid mesh showing dimensions

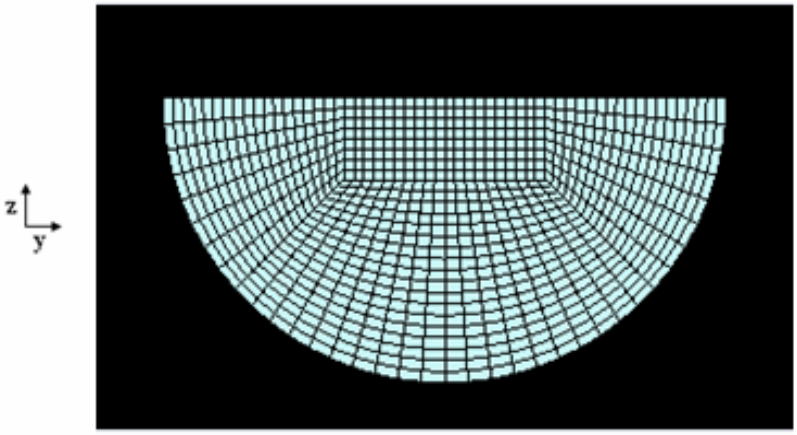

Figure 3.13 Front view of cylindrical fluid mesh showing element sizes

Table 3.3 Number of total elements in the box barge model for each fluid mesh type

Mesh Size	Elements
50 cm	16595
25 cm	135731
15 cm	264097
Cylindrical	86915

For the initial investigation of the box barge problem, results from three elements in the fluid mesh, one at the free surface (Point A), one at the middle of the fluid (Point B), and one at the fluid-structure interface (Point C), were chosen for each fluid mesh. The locations of the three elements are shown in Figures 3.14 - 3.17. At each of these elements a pressure-time history is obtained and analyzed to determine if the fluid model is returning reasonable results.

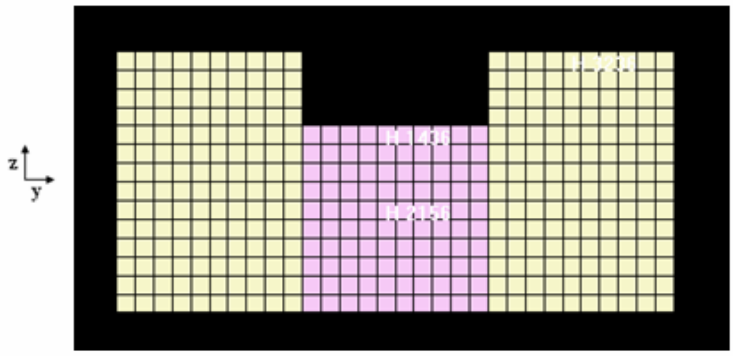

Figure 3.14 Pressure-time history element locations for 50cm mesh

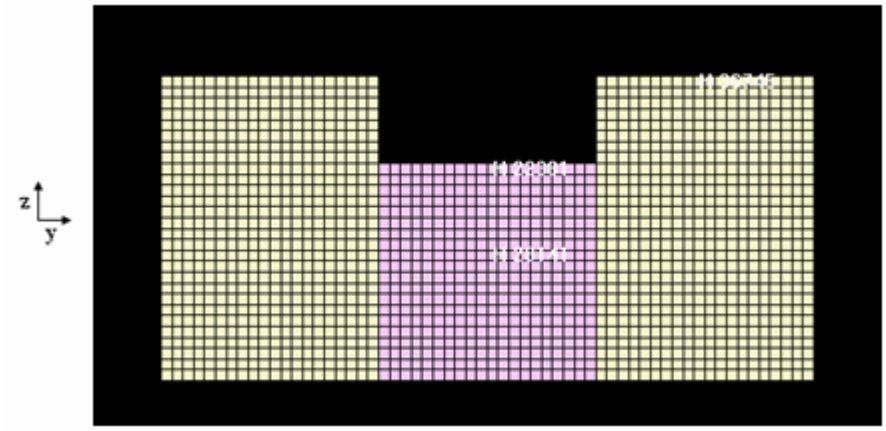

Figure 3.15 Pressure-time history element locations for 25cm mesh

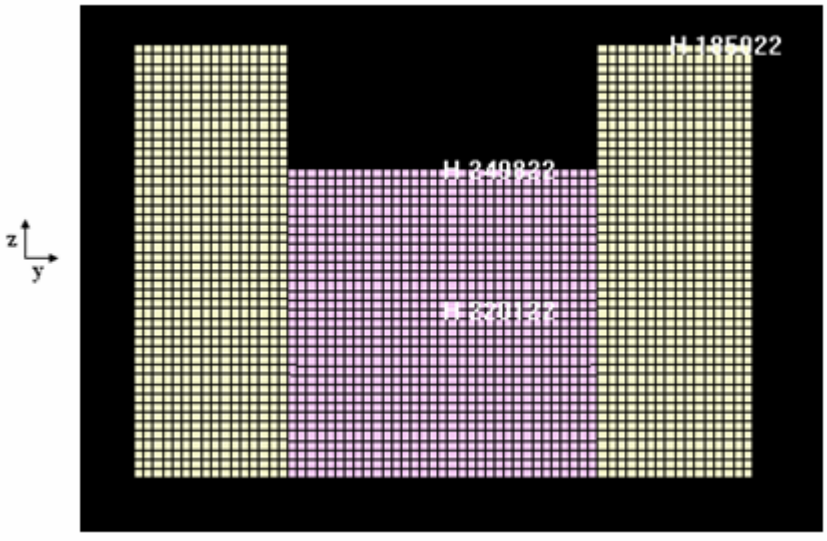

Figure 3.16 Pressure-time history element locations for 15cm mesh

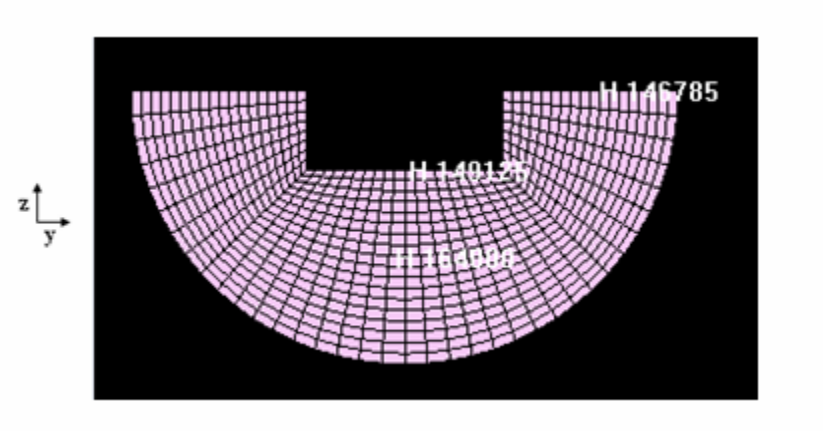

Figure 3.17 Pressure-time history element locations for cylindrical mesh

3.2 Box Barge Model Using USA

The box barge model results using USA applied to the wet surface (area below the waterline) of the box barge are given in Figures 3.18 – 3.21. The models take 5 minutes to process in USA and then an additional 2 minutes to run in LS-DYNA. Only the vertical velocity response of the structure is given as pressure-time histories in the surrounding fluid on the structure is not tracked in USA. The locations on the box barge where the vertical velocities are measured are shown in the small figure above Figure 3.18. On the bottom hull (Figures 3.18 and 3.19) results show there is a sharp rise in velocity until the maximum velocity is reached, which is about 3 m/s for the box barge model. Note that in the USA model cavitation is not accounted for so the maximum velocity is not the true kick-off velocity. On the hull there are a few initial oscillations after the maximum velocity is reached but the results eventually begin to damp out. Two factors cause the difference between the on and off keel results. One factor is the longitudinal girder, which causes a stiffer velocity response along the keel. The other factor is the on keel location is closer to the point where the shock wave impacts the hull. Therefore the response at this point is more severe, meaning it is characterized by a sharp

acceleration followed by a sharp deceleration. The frame and side hull velocities (Figures 3.20 and 3.21) have a more oscillatory response than the bottom hull and a lower peak velocity than the bottom hull. This is reasonable because the bottom hull of the box barge absorbs energy from the impact of the shock wave before transferring energy to the structure.

Nothing can be said for the true accuracy of these results because there is no experimental or analytical data to compare to. However, comparison to previous work shows that they follow similar trends found in similar problems using USA [11] and to results obtained from actual shock trials [3].

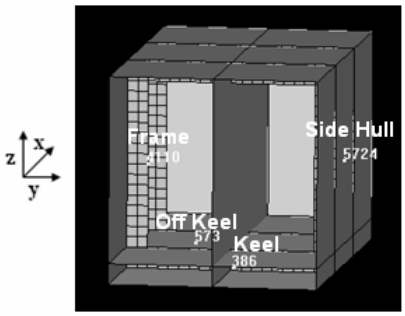

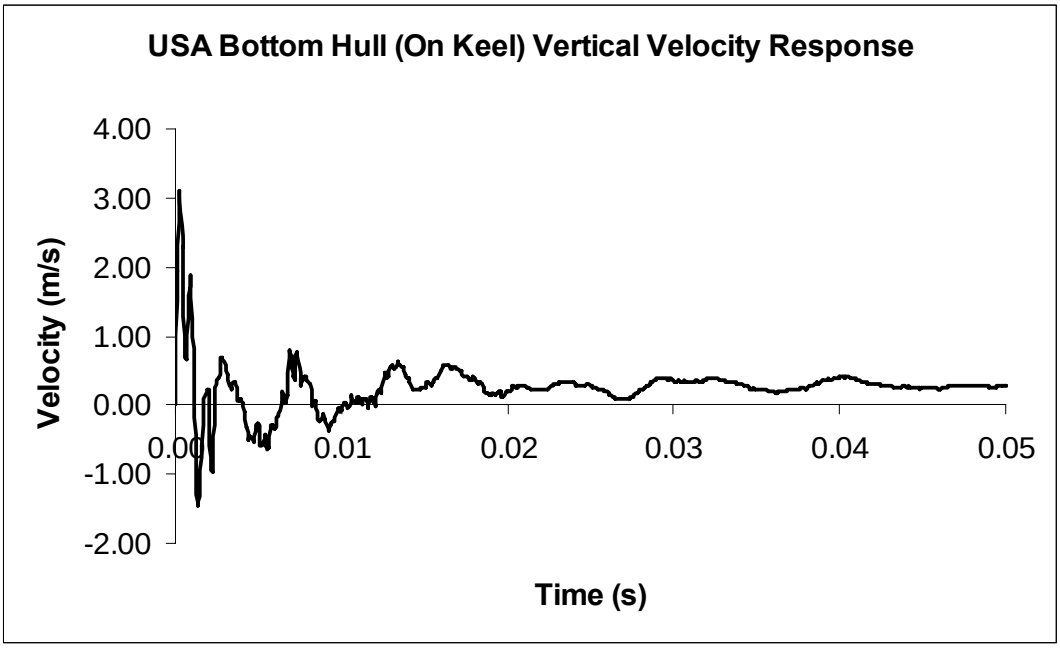

Figure 3.18 USA result for vertical velocity on the keel

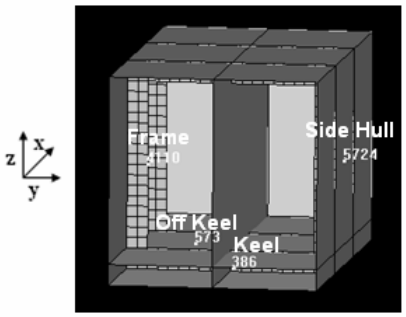

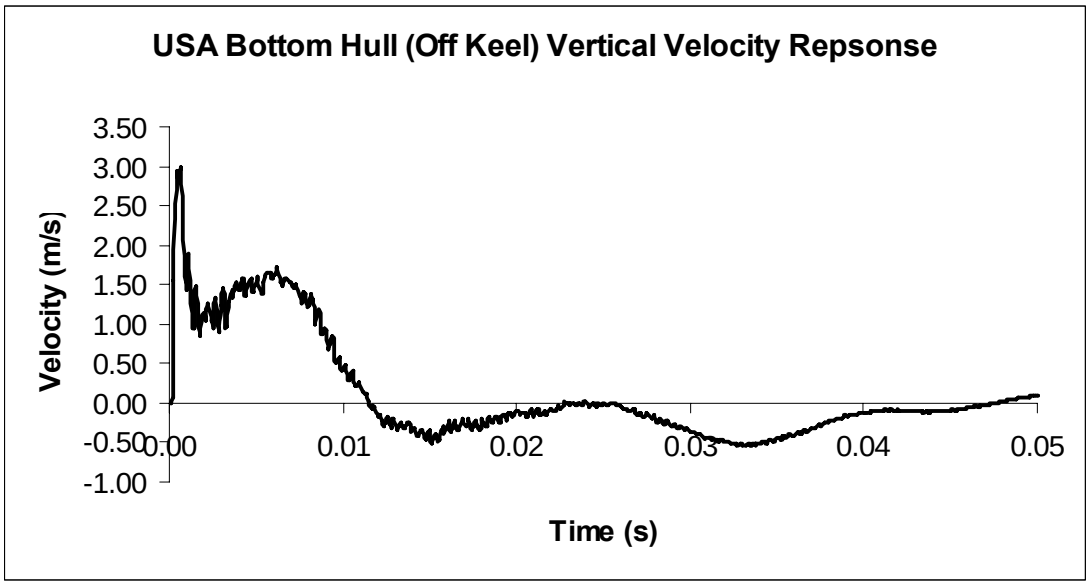

Figure 3.19 USA result for vertical velocity off the keel

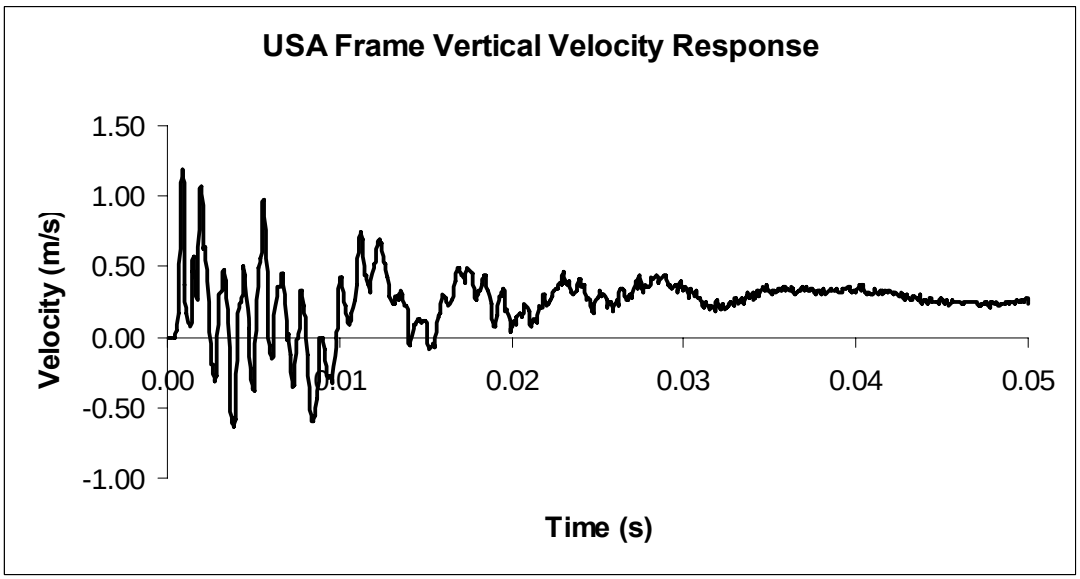

Figure 3.20 USA result for vertical velocity on the frame

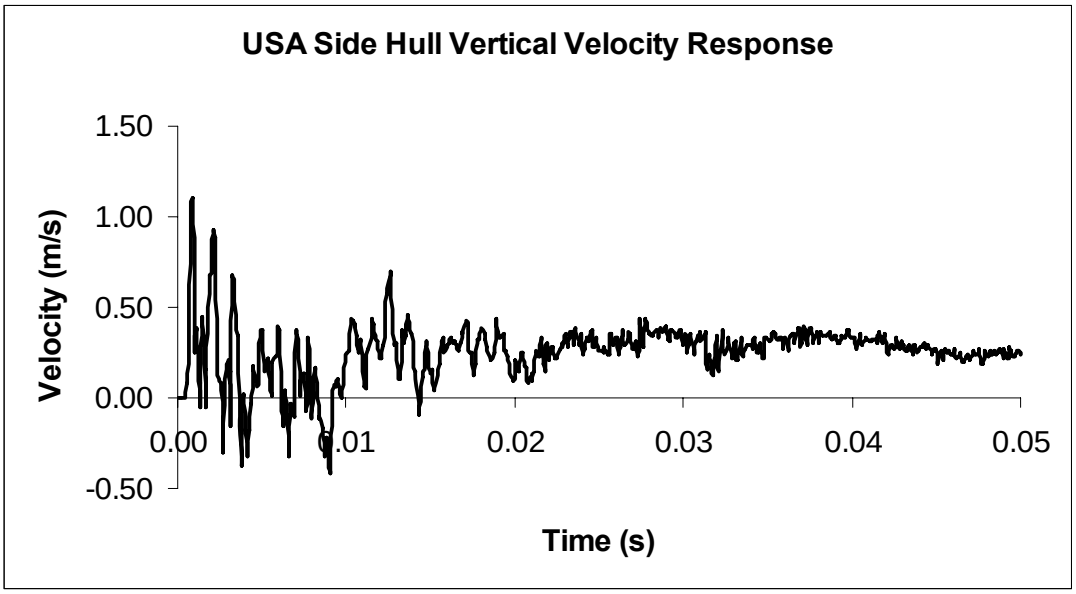

Figure 3.21 USA result for vertical velocity on the side hull

3.3 Box Barge Model Using Only LS-DYNA

Next, the box barge model was run in LS-DYNA with and without cavitation using the four fluid meshes described in Section 3.1.2. Average run times for each fluid mesh are given in Table 3.4. Considering cavitation did not cause longer run times for the models.

Table 3.4 LS-DYNA run times for box barge problem

Mesh	Run Time (min.sec)
50 cm	1.07
25 cm	11.50
15 cm	30.00
Cylindrical	7.54

The results for the nodes located on and off the keel on the bottom hull are given in Figures 3.22 - 3.29. For the 50cm no cavitation case the on keel (Figure 3.22) point has a lower kick-off velocity than in the USA model. As the element size decreases the

kick-off velocity at this point increases and the results oscillate less. Other than these two differences the general response remains similar for all element sizes.

When cavitation is considered on the keel the initial response prior to the kick-off velocity is the same as in the no cavitation case for all element sizes. It is not until after the kick-off velocity is reached that the effects of considering cavitation are seen. The results show cavitation causes a more gradual slope down from the kick-off velocity. This is especially true for the 15cm mesh (Figure 3.28). In all mesh cases with cavitation the velocity does not fall below zero as much as in the no cavitation case and the results damp out more at later times.

The off the keel point on the bottom hull results behave differently from the on keel results, especially in the 50cm, 25cm, and cylindrical models. For the no cavitation 50cm, 25cm, and cylindrical models results are somewhat similar to the USA results but for the 15cm case the results are very different. The difference in results seen between the meshes is a sign that the finite element mesh has a large affect on the results of the simulation. This is not to say that the mesh should not affect the results, small changes in accuracy are expected. But a change in finite element mesh should not change the general characteristics of the results.

When cavitation is considered in the models, the off the keel results change drastically. As seen in the on keel results, the kick-off velocities do not change when cavitation is considered but there is a more gradual return to zero velocity. Unlike the on keel results, cavitation causes a greater negative velocity at the off keel point to occur.

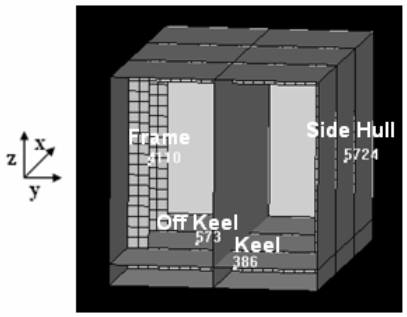

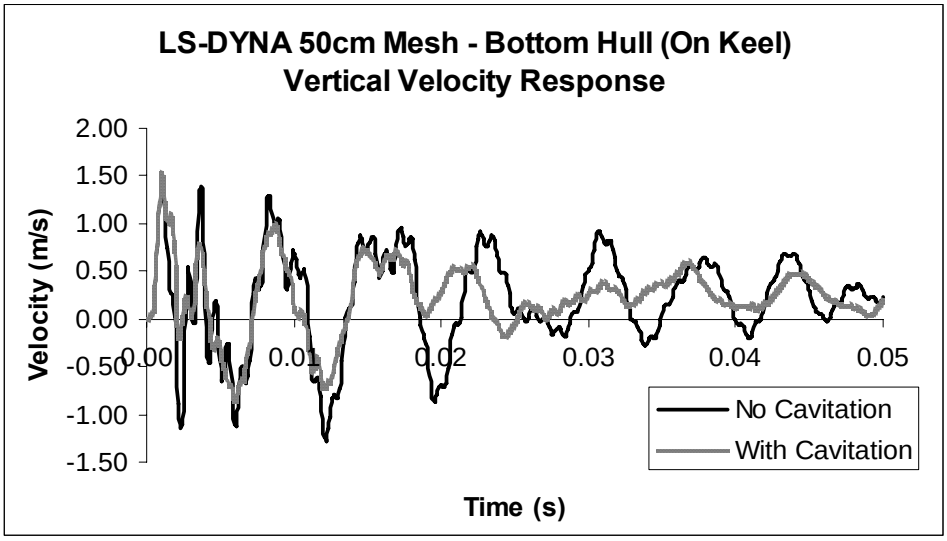

Figure 3.22 50cm mesh LS-DYNA result for vertical velocity on the keel

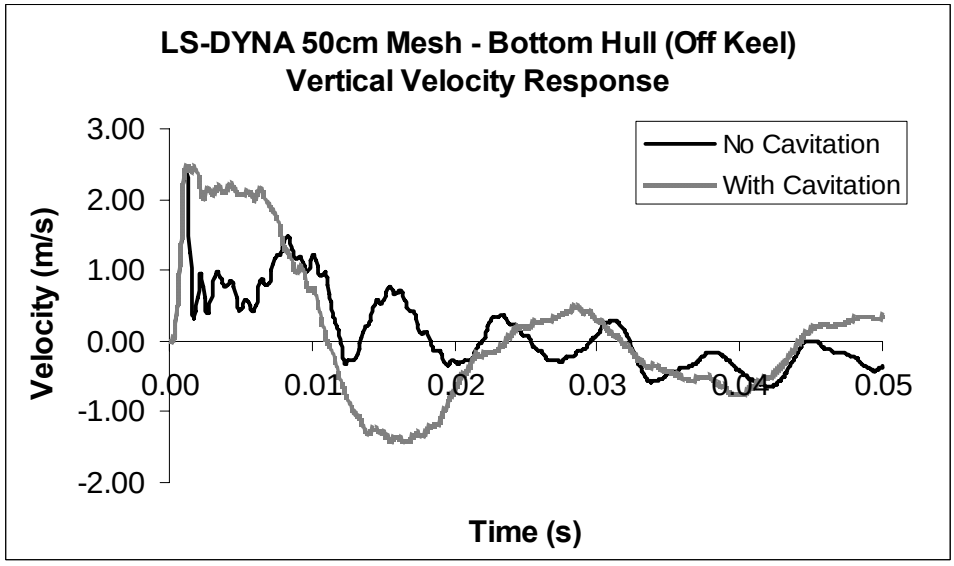

Figure 3.23 50cm mesh LS-DYNA result for vertical velocity off the keel

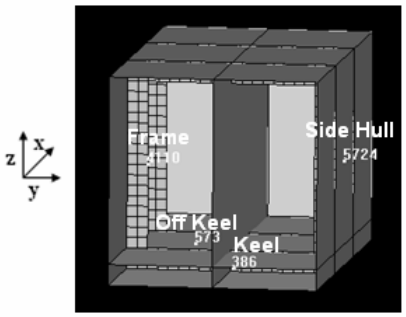

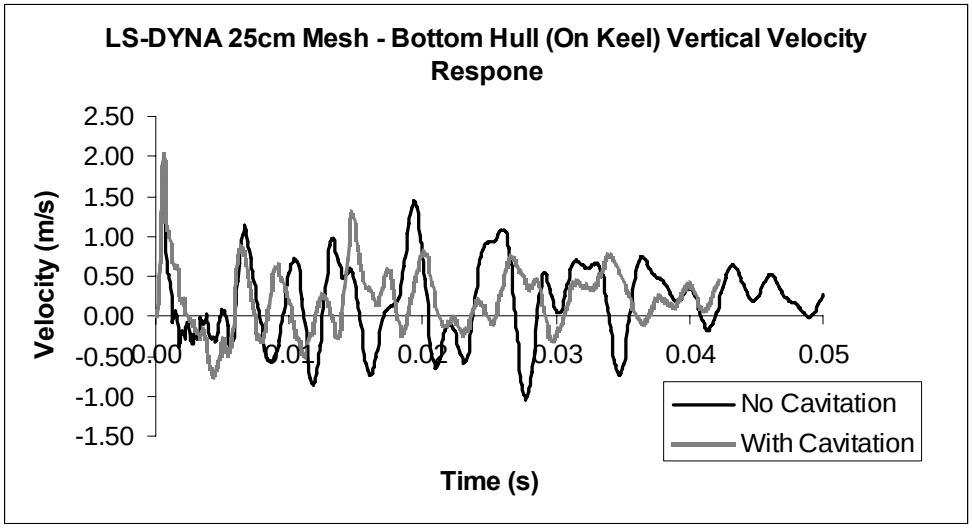

Figure 3.24 25cm mesh LS-DYNA result for vertical velocity on the keel

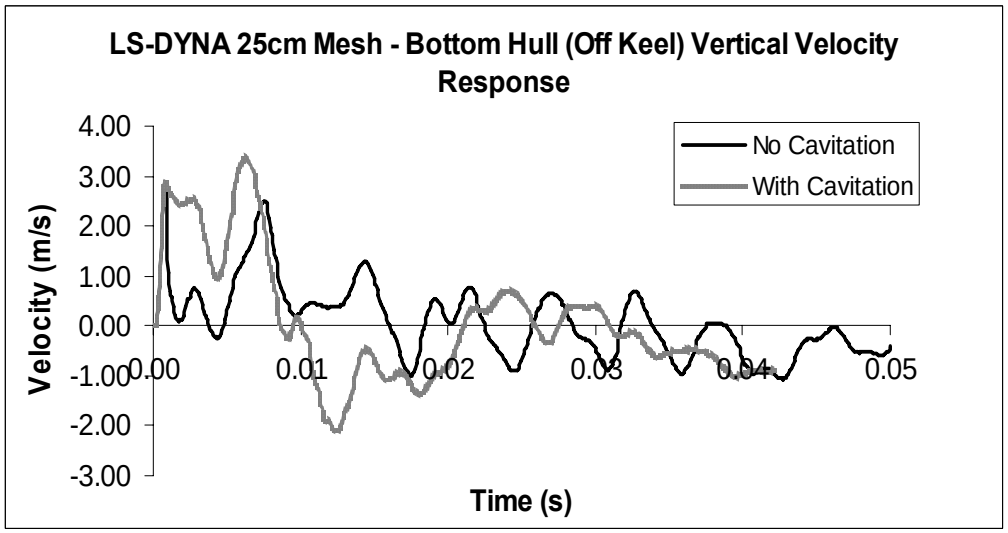

Figure 3.25 25cm mesh LS-DYNA result for vertical velocity off the keel

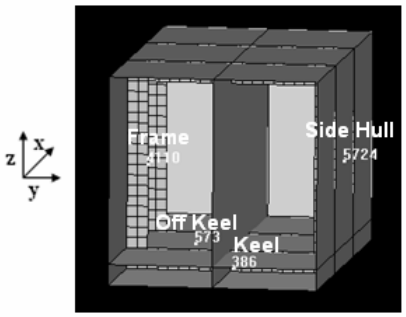

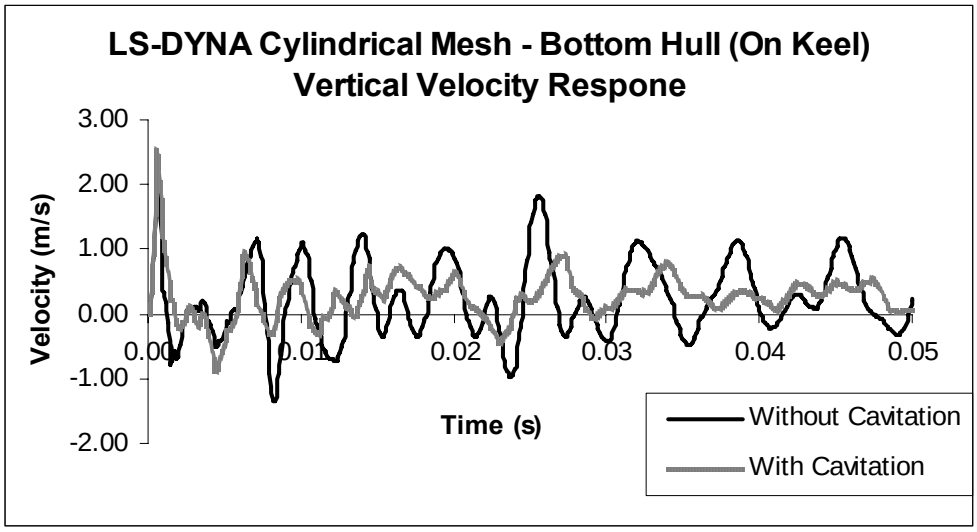

Figure 3.26 Cylindrical mesh LS-DYNA result for vertical velocity on the keel

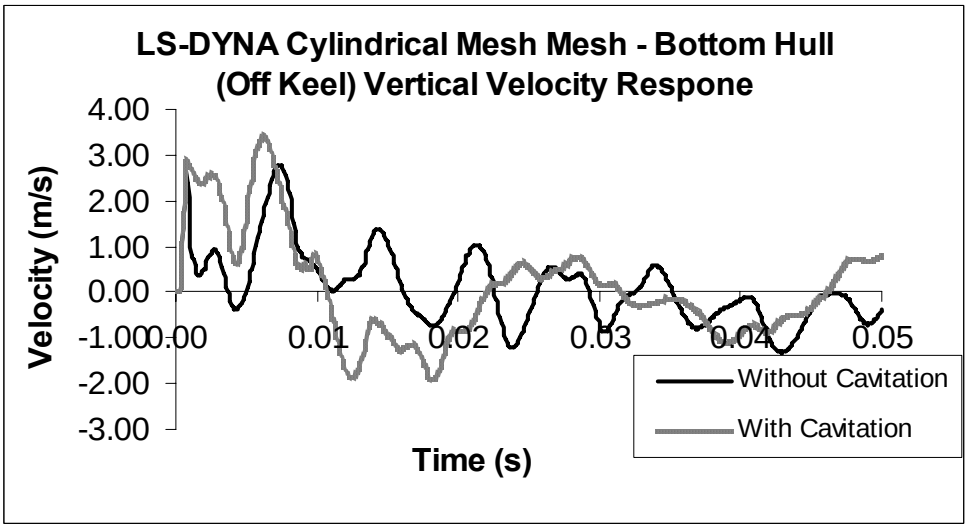

Figure 3.27 Cylindrical mesh LS-DYNA result for vertical velocity off the keel

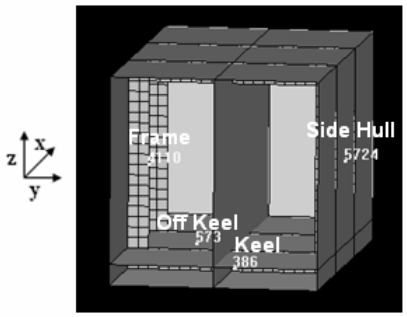

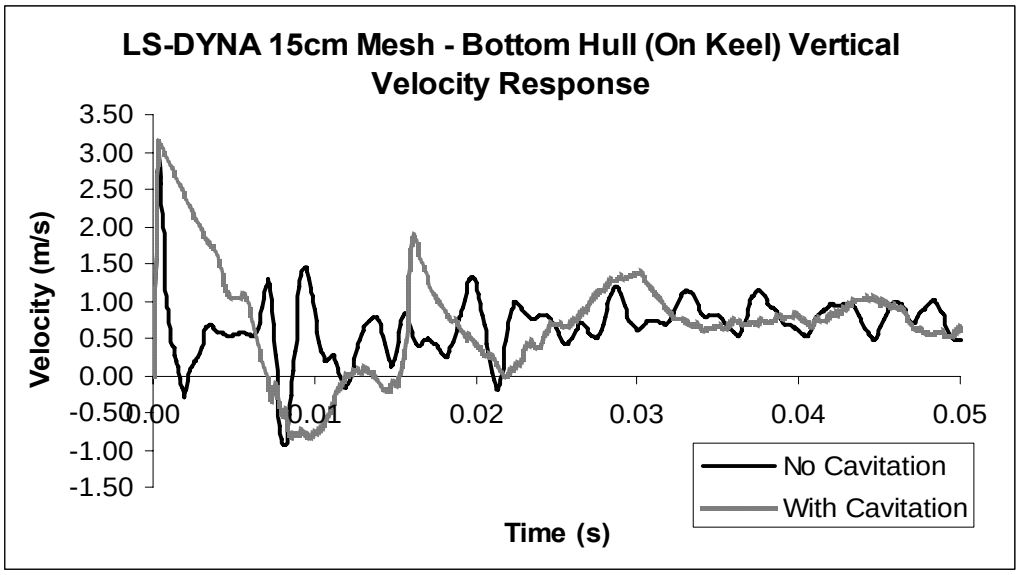

Figure 3.28 15cm mesh LS-DYNA result for vertical velocity on the keel

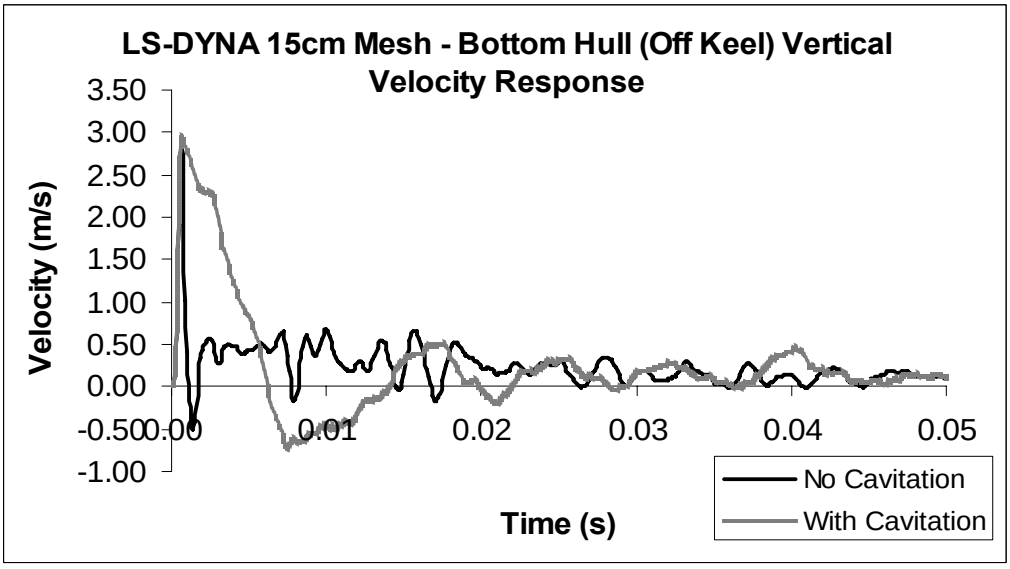

Figure 3.29 15cm mesh LS-DYNA result for vertical velocity off the keel

The velocity results for the side hull and frame locations are given in Figures 3.30 – 3.37. These results generally show smaller velocities and much more oscillatory responses than the bottom hull results. The 50cm, 25cm, and cylindrical cases have very similar velocity magnitudes and frequencies at the side hull and frame. In all of these cases including cavitation does not have a large effect on the results. The largest cavitation effect in the 50cm, 25cm, and cylindrical models is that the frame velocity magnitudes in the 50cm model are lower and oscillate at a lower frequency at later times in the response (Figure 3.30).

The 15cm mesh has significantly lower velocity magnitudes at the frame and side hull than the 50cm, 25cm, and cylindrical cases. Figure 3.36 shows that the 15cm side hull results also oscillate at a much higher frequency. Unlike the 50cm, 25cm, and cylindrical models, when cavitation is included in the 15cm model the response at the frame (Figure 3.32) oscillates at a lower frequency and with larger amplitudes at later times. The general response of the side hull is not affected significantly by cavitation a, as in the 50cm, 25cm, and cylindrical models. The negative velocities early in the response when cavitation is considered are not as large. A comparison of the results for the different mesh sizes as well as a discussion on cavitation effects in the models is given in Section 3.4.1.

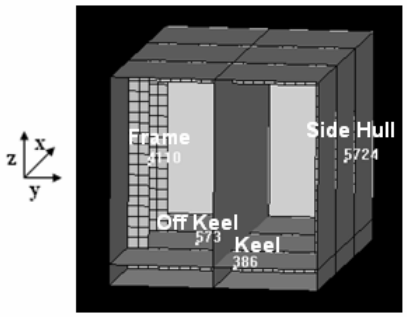

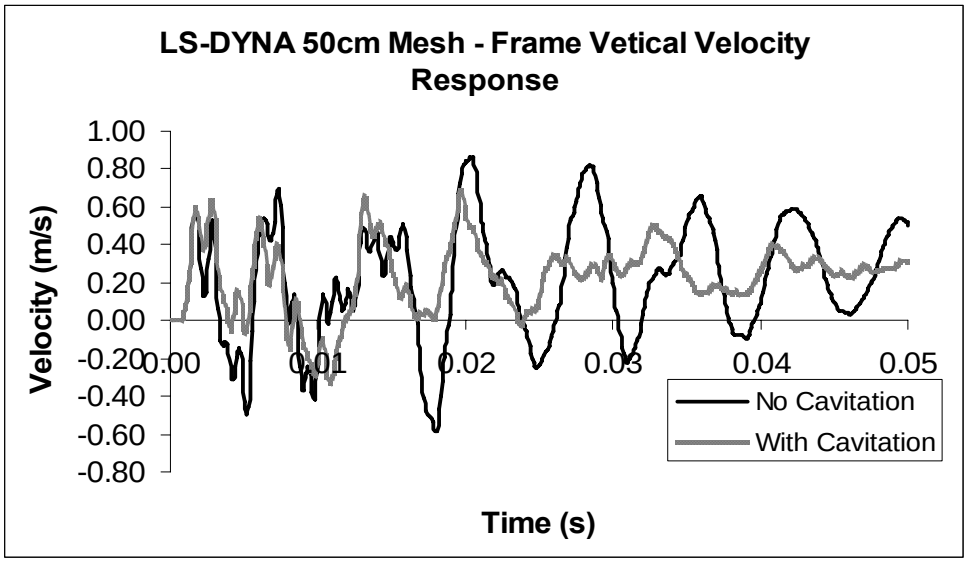

Figure 3.30 50cm mesh LS-DYNA result for vertical velocity on the frame

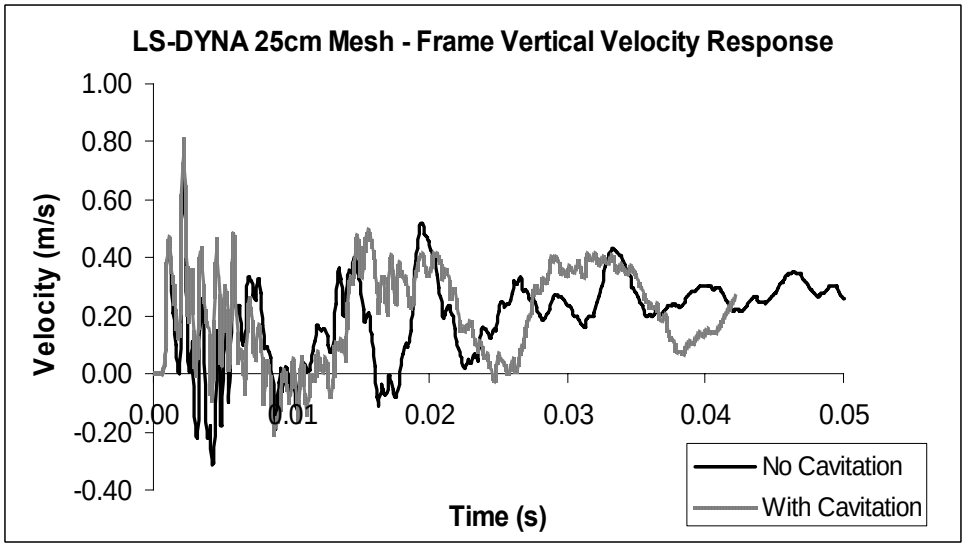

Figure 3.31 25cm mesh LS-DYNA result for vertical velocity on the frame

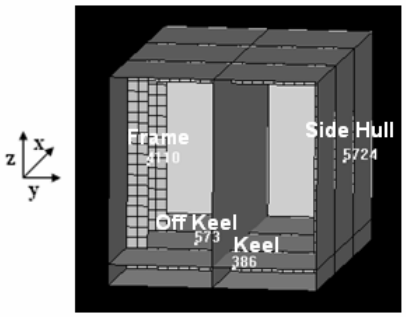

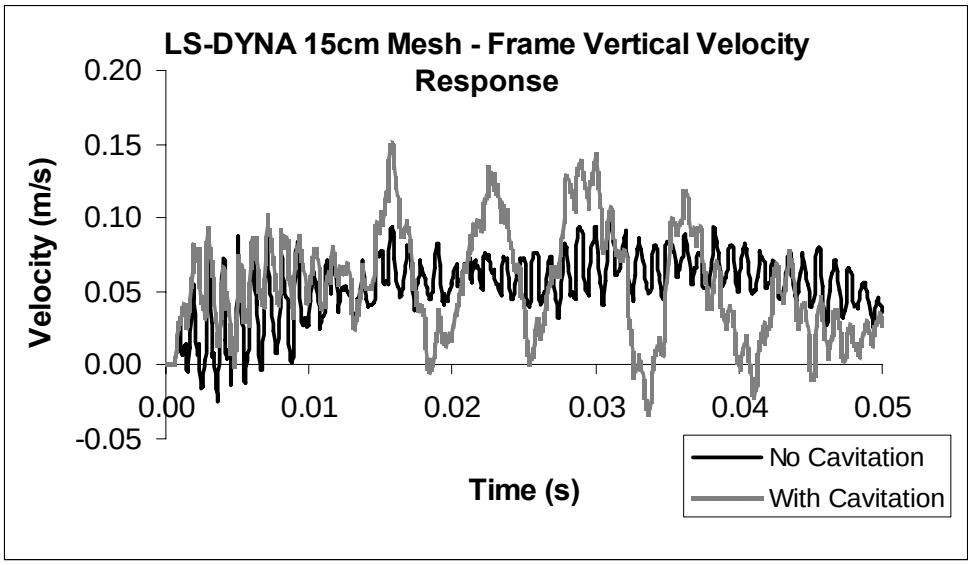

Figure 3.32 15cm mesh LS-DYNA result for vertical velocity on the frame

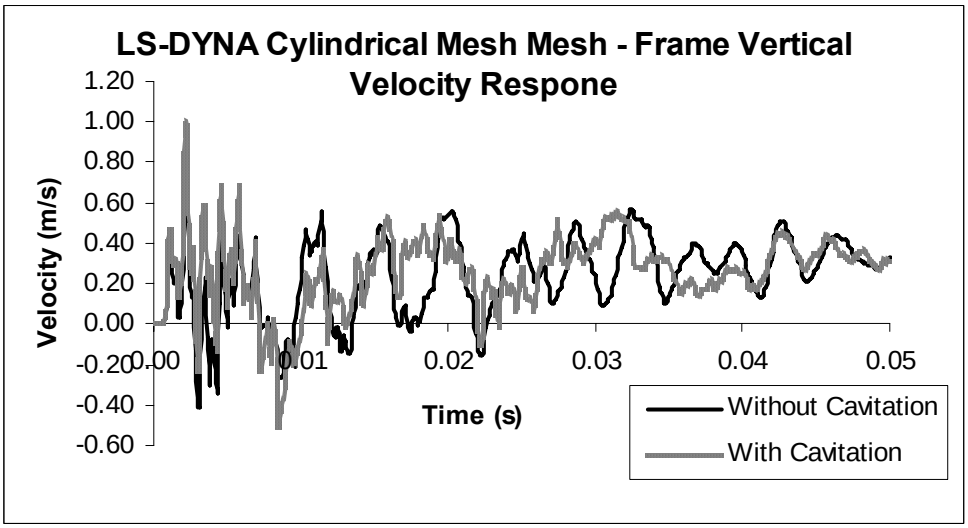

Figure 3.33 Cylindrical mesh LS-DYNA result for vertical velocity on the frame

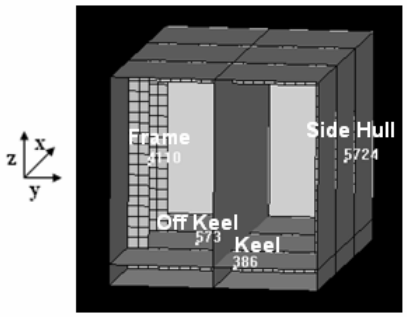

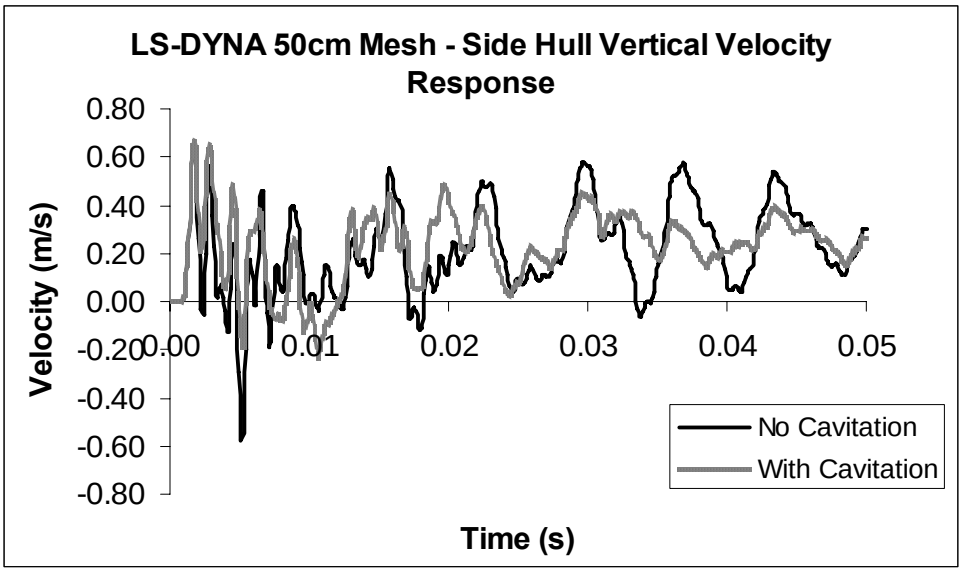

Figure 3.34 50cm mesh LS-DYNA result for vertical velocity on the side hull

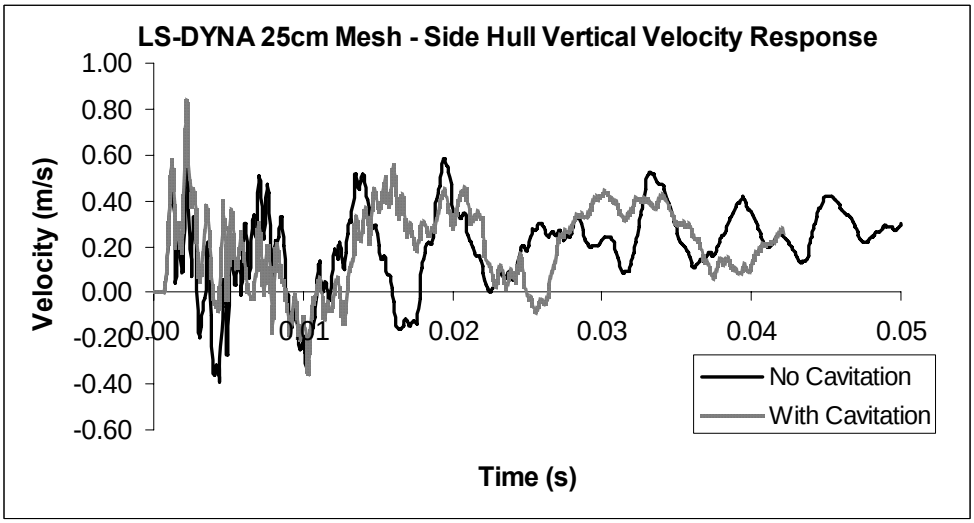

Figure 3.35 25cm mesh LS-DYNA result for vertical velocity on the side hull

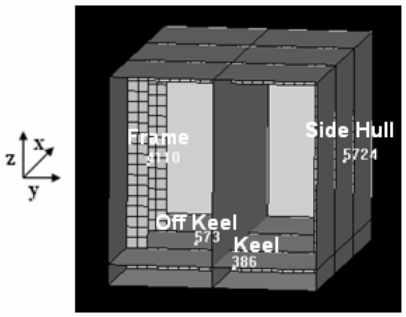

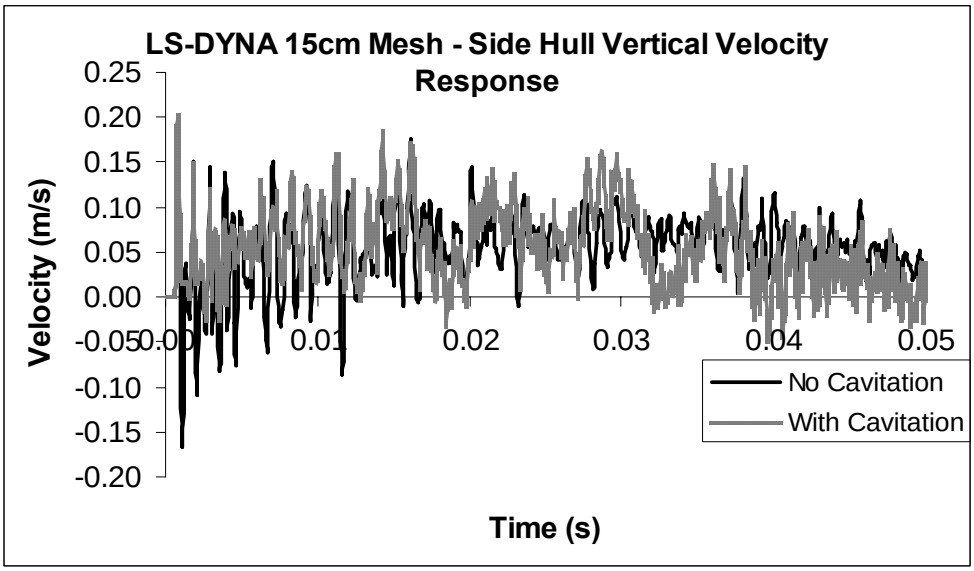

Figure 3.36 15cm mesh LS-DYNA result for vertical velocity on the side hull

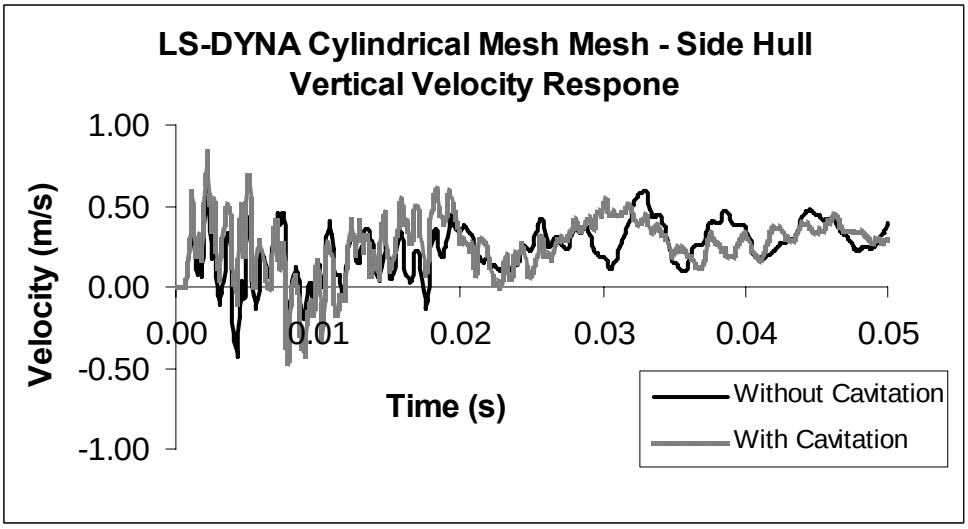

Figure 3.37 Cylindrical mesh LS-DYNA result for vertical velocity on the side hull

Next, the pressure-time histories in the fluid mesh at the three points described in Section 3.1.2 are assessed. At the free-surface of each fluid mesh the pressure-time history should show a shock wave reflecting properly from the free surface in cases where cavitation is not considered. At the middle of the fluid mesh the pressure-time history is checked for signs of the bulk cavitation and for signs of reflected waves re-entering the model as a result of poor boundary conditions. The element pressure-time history at the fluid-structure interface is checked and compared against the peak pressure approximation (Equation 1.3) to determine if the shock wave is captured correctly as it arrives at the hull.

The free-surface pressure-time histories for each fluid mesh are given in Figures 3.37-3.41. To determine if the free-surface properly reflects the shock wave it can be assumed that the shock wave behaves as a plane wave at the free surface of the model. Because the fluid is modeled as an acoustic medium, this reflection problem can be treated as a reflection between two acoustic mediums. The basic laws of reflections show that when an incident compression wave reflects at a water-air boundary, 99% of the incident wave amplitude is reflected back into the water as a tension wave. Therefore the free-surface pressure-time histories should show a reflected tension wave of almost equal magnitude of the incident shock wave when cavitation is not considered.

The results show that for the cases without cavitation correctly there is a reflected wave, and for the cases where cavitation is considered the reflected wave is cutoff. This behavior is consistent with the expected behavior of the cavitation model.

The free-surface results also show that the fluid model does not capture the discontinuity of the shock wave and there are some oscillations as the pressure damps to

hydrostatic. The peak pressure of the incoming shock wave as predicted by the peak pressure approximation is 4.07 MPa, but this value does not account for the presence of the structure so can not be used to determine the accuracy of the free surface pressure results. The discontinuity gets sharper as the mesh is refined but the peak pressure at the surface is unchanged by the mesh size in the 50cm, 25cm, 15cm and cylindrical cases.

The fluid mesh the pressure-time history results show that a pike in pressure precedes the bulk cavitation region occurring at the middle of the fluid mesh. This is represented in Figures 3.41-3.45 as the small area of zero pressure between 0.002 and 0.01 seconds. Similar results were seen in the middle of the fluid in Wood's box like ship UNDEX mode [11]. After the cavitation occurs small oscillations in pressure are seen as the fluid damps to hydrostatic pressure. The mesh size did not have a large impact on the results in the middle of the fluid.

In the cases where cavitation is not considered the results show a reflected wave passes through the middle of the fluid at the same time cavitation should occurs After the reflected wave passes a large spike in pressure occurs in the 50cm, 25cm, and cylindrical cases at 0.01 seconds. The pressure spike should not occur and seems to cause the results to oscillate heavily unlike the free-surface results which damped to hydrostatic pressure. The conclusion reached is that the pressure spike and oscillations are caused by energy that re-enters the model from the bottom boundary of the fluid mesh due to a break down of the fluid boundary condition in LS-DYNA. More information on fluid boundary conditions in LS-DYNA is given in Section 3.3.4 and Chapter 4.

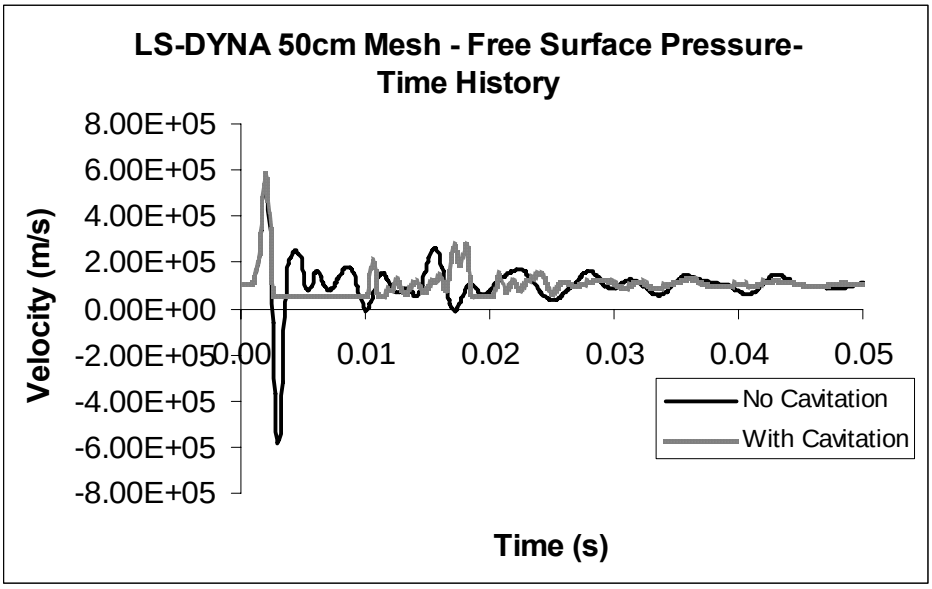

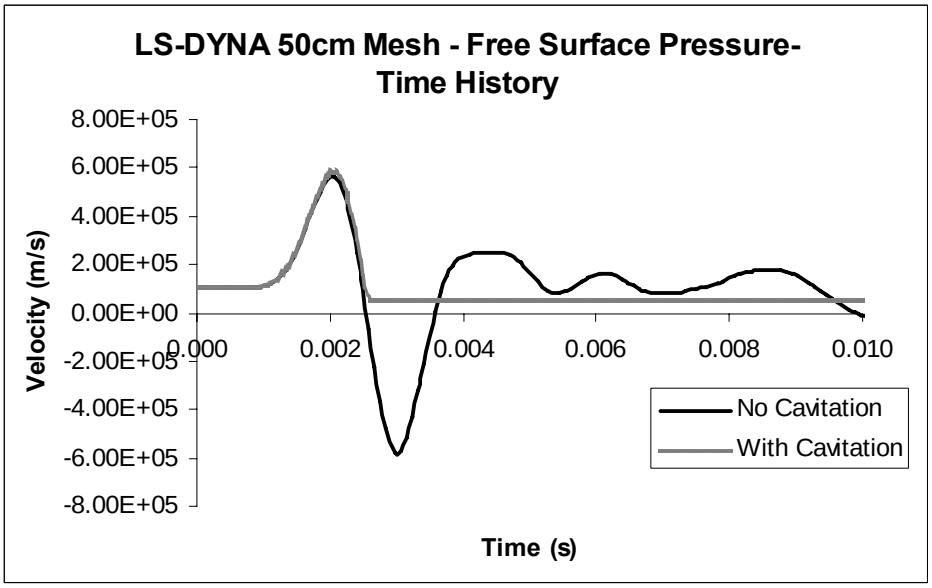

Figure 3.38 50cm mesh LS-DYNA free-surface pressure-time history on two time scales

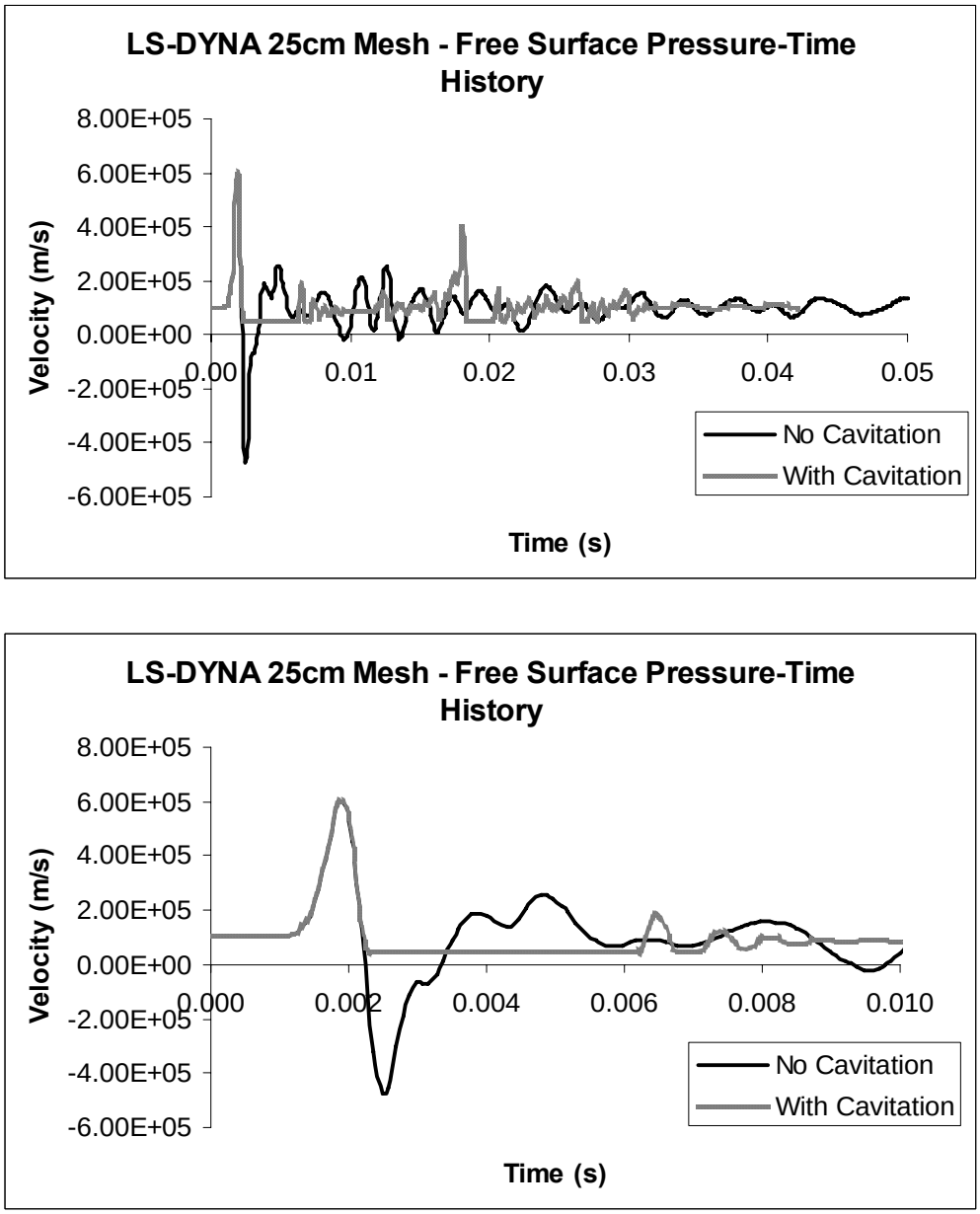

Figure 3.39 25cm mesh LS-DYNA free-surface pressure-time history on two time scales

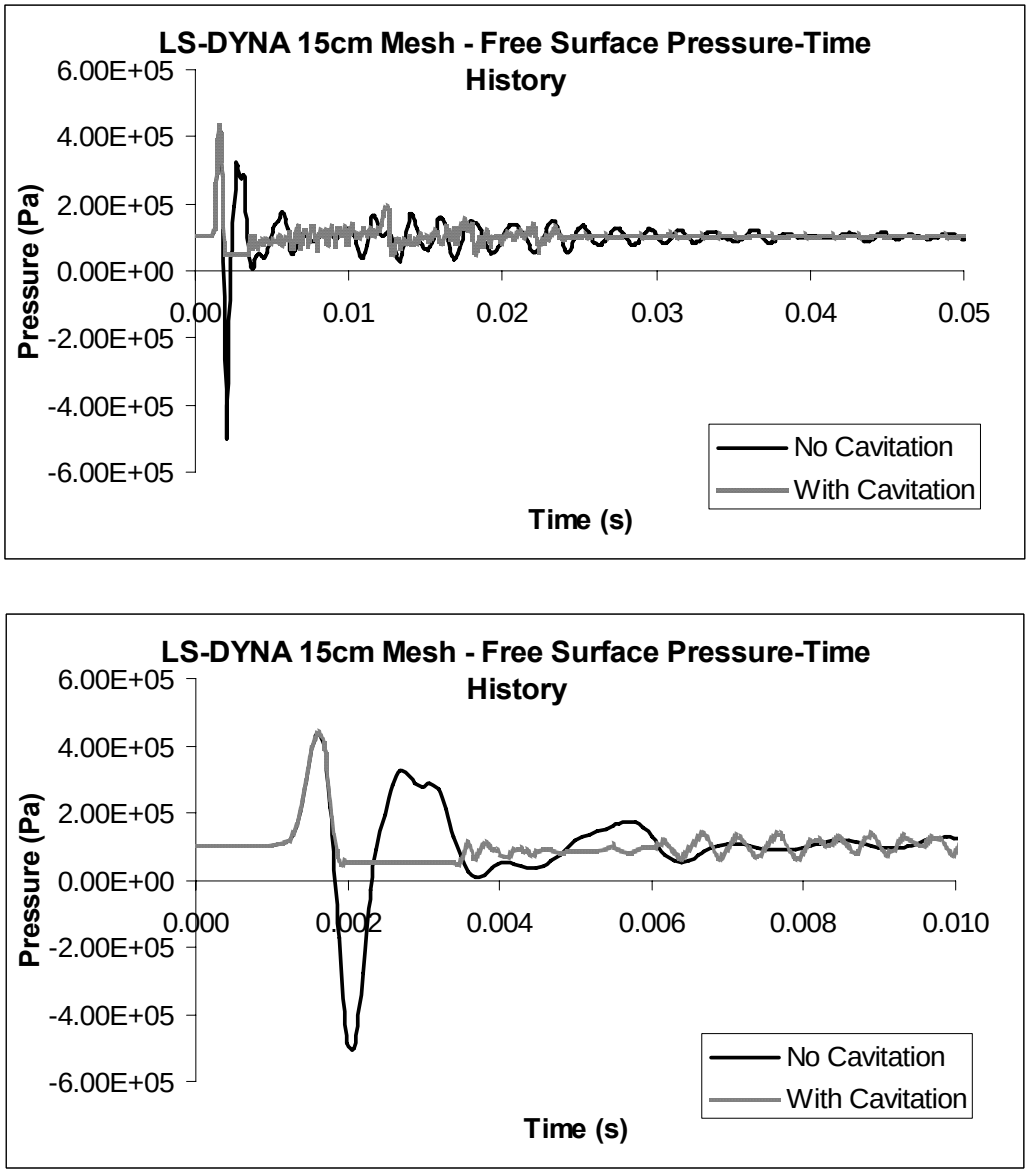

Figure 3.40 15cm mesh LS-DYNA free-surface pressure-time history on two time scales

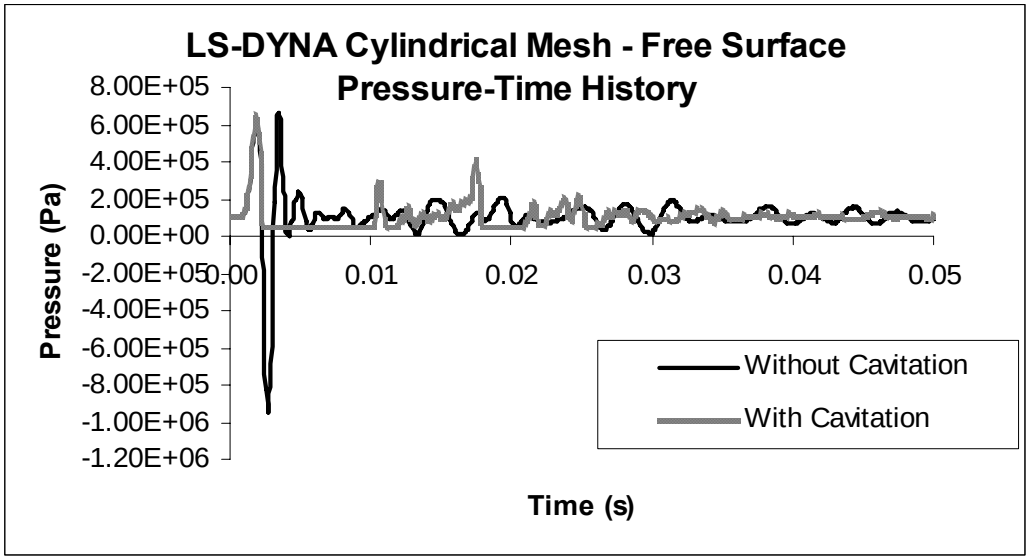

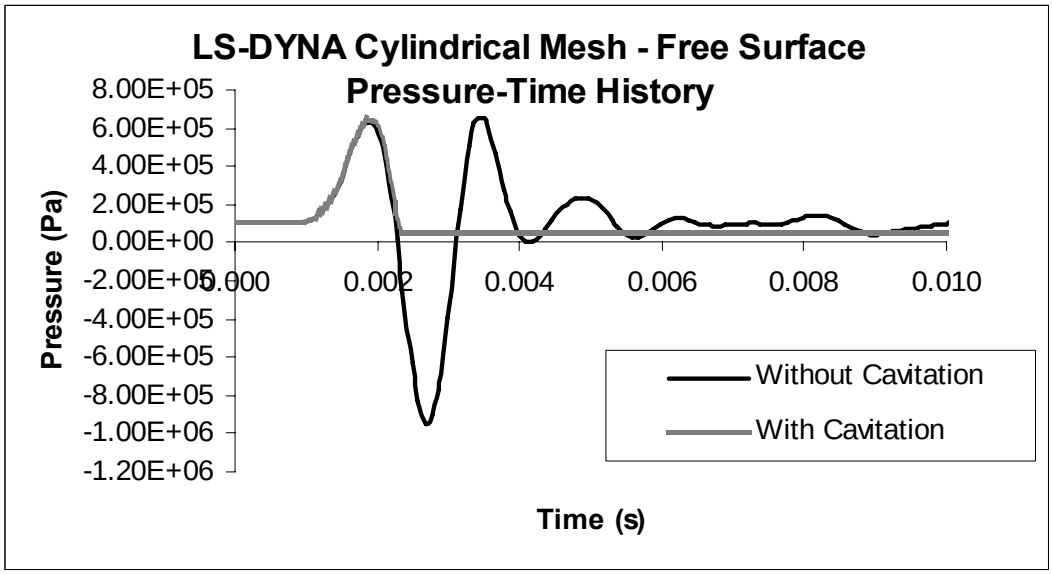

Figure 3.41 Cylindrical mesh LS-DYNA free-surface pressure-time history on two time scales

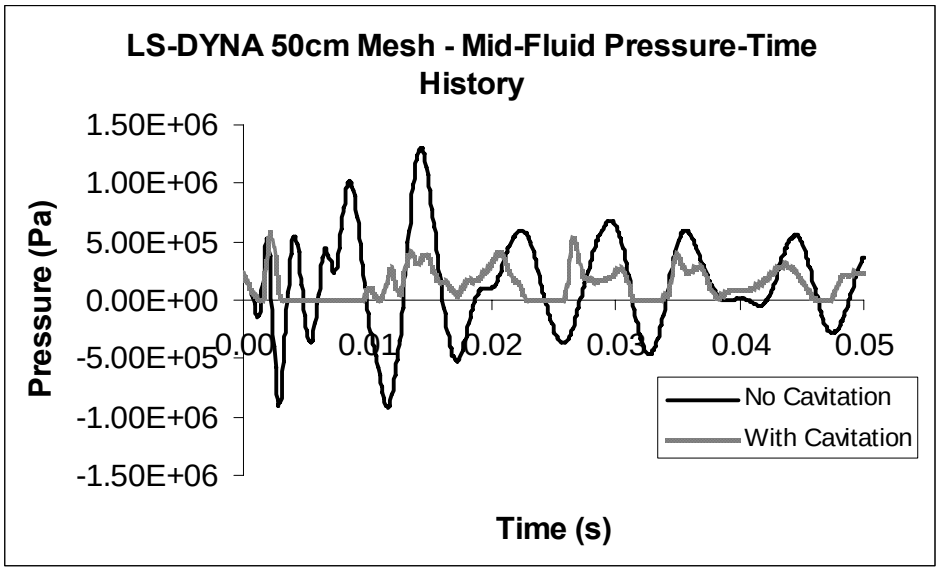

Figure 3.42 50cm mesh LS-DYNA middle fluid pressure-time history

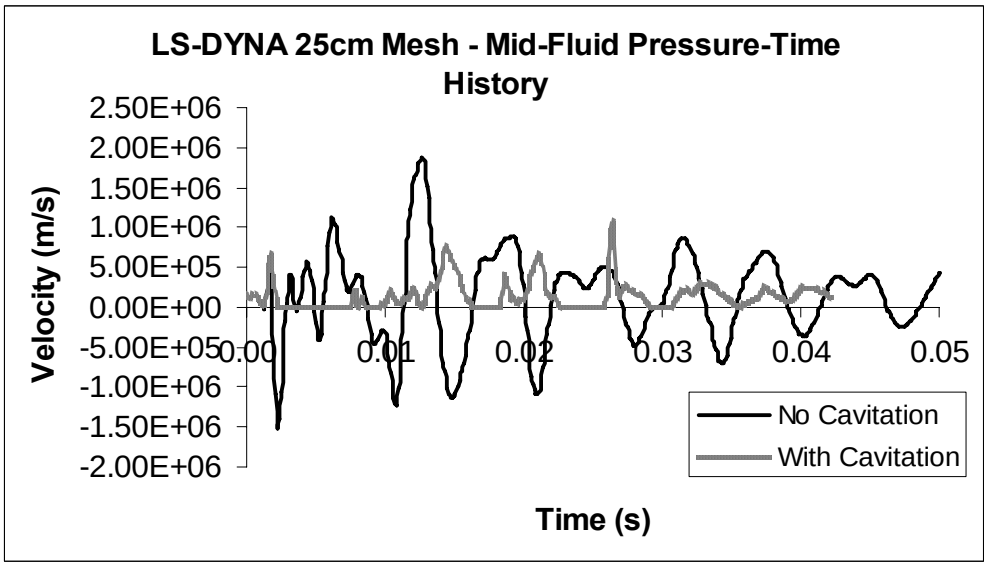

Figure 3.43 25cm mesh LS-DYNA middle fluid pressure-time history

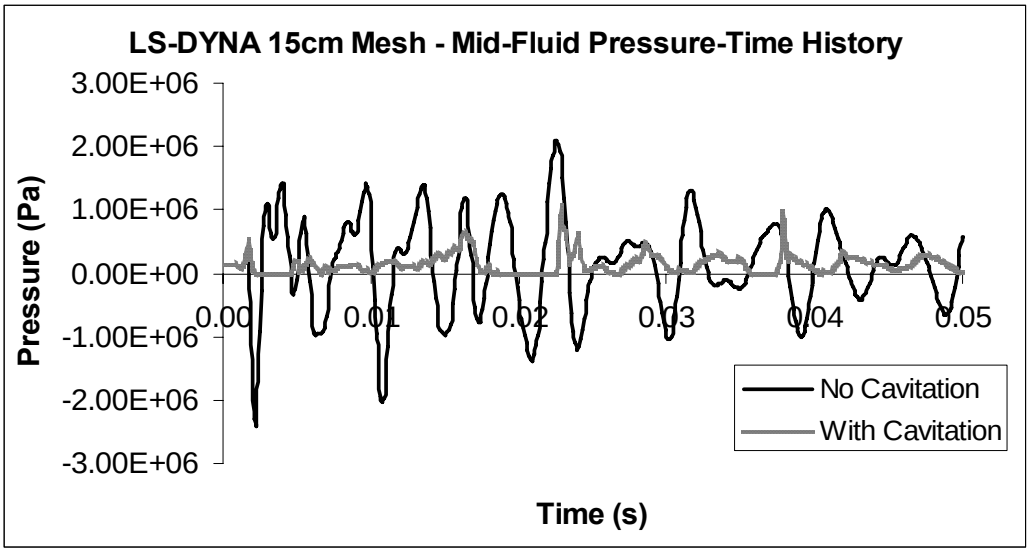

Figure 3.44 15cm mesh LS-DYNA middle fluid pressure-time history

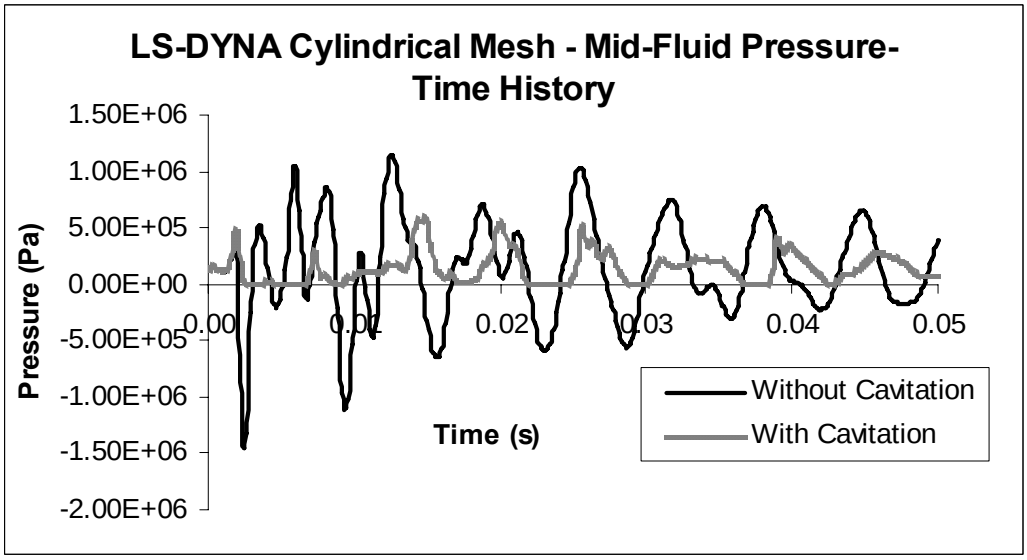

Figure 3.45 Cylindrical mesh LS-DYNA middle fluid pressure-time history

The most important early time result from the fluid model is the ability of the model to capture the shock wave. The shock wave dominates the early time response of the box barge and also determines the accuracy of the bulk cavitation region model. Because the shock wave in LS-DYNA is initialized one element away from the structure the results for the fluid element on fluid-structure interface are used to determine if the shock wave is captured accurately. Results for the fluid-structure interface pressure-time

history are given in Figures 3.45-3.43. For each fluid mesh the results follow the expected general trends. In the cases where cavitation is neglected the results show the incident peak pressure followed by the reflected wave returning into the fluid after reaching the structure. When cavitation is neglected a spike in negative pressure is seen for all meshes around 0.005 seconds. This spike in pressure is the reflection of the shock wave from the bottom boundary of the fluid model which is supposed to be absorbed by the transmitting boundary LS-DYNA applies there. The failure of the transmitting boundary to absorb the shock wave is discussed further in Section 3.4.4.

In the cases where cavitation is considered the results show the bulk cavitation region occurring beneath the box barge bottom between 1ms and 8ms. Following the bulk cavitation region is a small peak in pressure as the box barge is re-loaded by the fluid. The reflections seen in the models where cavitation is neglected are not seen because of two possibilities. One is that the tension wave is not propagated to the boundary due to the presence of the cavitation region. The second is that the tension wave is reflected at the boundary but still has enough magnitude to cause cavitation to occur, meaning the reflection wave is not seen in the results because it is in the cavitation region where pressure is zero.

When compared to the peak pressure approximation the results show that the size of the fluid mesh determines both the sharpness of the discontinuity and the accuracy of the peak pressure captured by the fluid model.

The 50cm case gives poor results with cavitation and without considering cavitation. The shape of the shock wave is almost parabolic and the amplitude of the peak pressure is less than the theoretical value. When the mesh size is reduced to 25cm

the shape of the shock wave becomes less parabolic but the peak pressure is still much lower than the peak pressure approximation predicts. The cylindrical results match closely with the 25cm results because they share the same element size at this location. The 15cm results show that the shape of the shock wave is greatly improved and the peak pressure found in LS-DYNA is almost the same as the peak pressure approximation. However, the model still has difficulty capturing the discontinuous front of the shock wave as seen in Figure 3.49.

Figures 3.51-3.57 show images of the propagation and reflection of the shock wave for the 25cm model with and without cavitation. Figure 3.52 shows the shock wave impacting the box barge with and without cavitation. At 2ms, Figure 3.53, the first difference between the fluid mesh with cavitation and without cavitation is observed in the form of negative pressures seen only in results without cavitation. In both cases the slick can be seen on the free-surface. The bulk cavitation region can be seen in Figure 3.54. Without cavitation a green ring of negative pressure is visible on the surface. When cavitation is considered this area is displayed as zero pressure, a dark blue ring, which means cavitation is occurring. Once 4ms is reached in Figure 3.55, the cavitation region has closed and the pressure begins to damp out. For the results without cavitation a reflected tension wave is seen moving towards the bottom boundary. Figures 3.56 and 3.57 show the fluid mesh damping out to hydrostatic pressure.

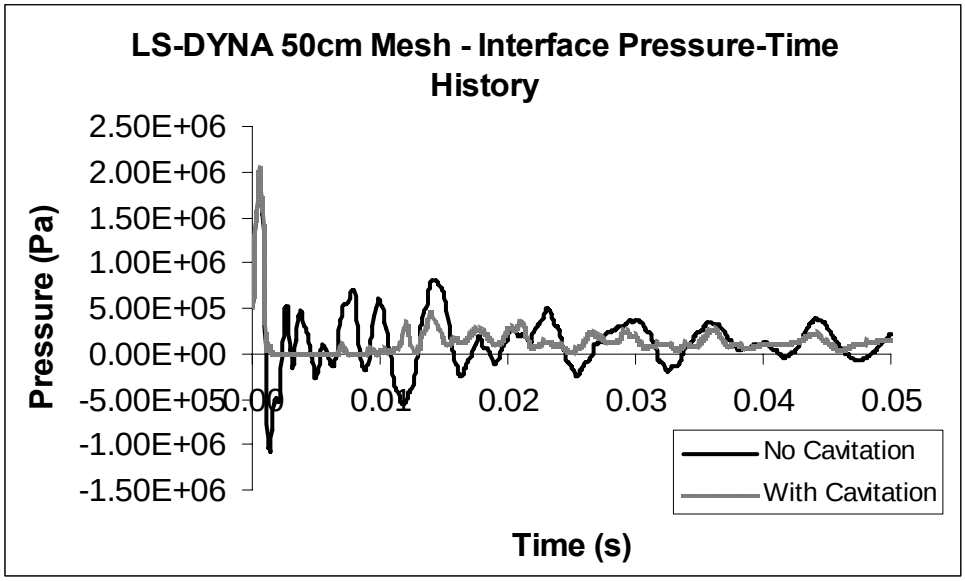

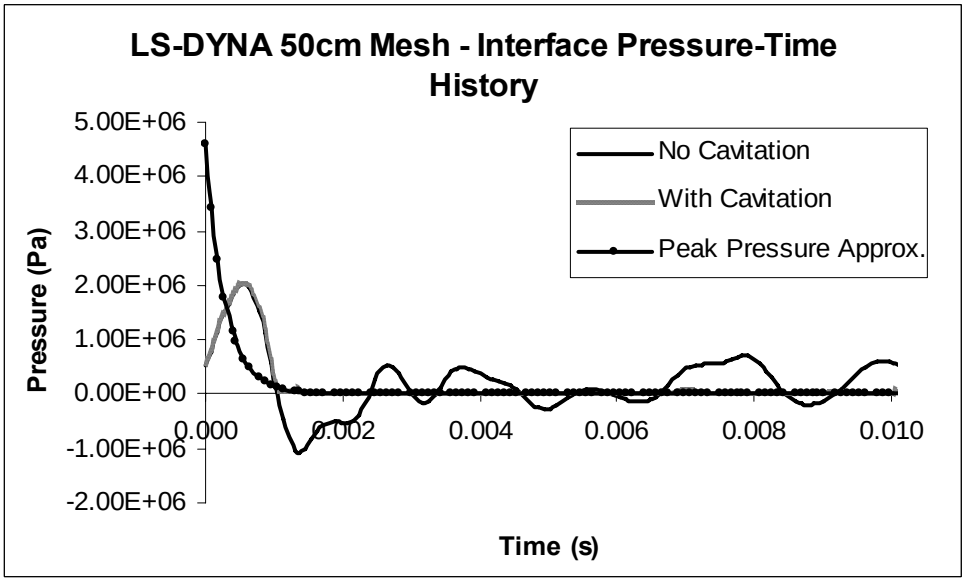

Figure 3.46 50cm mesh LS-DYNA fluid-structure interface pressure-time history on two time scales

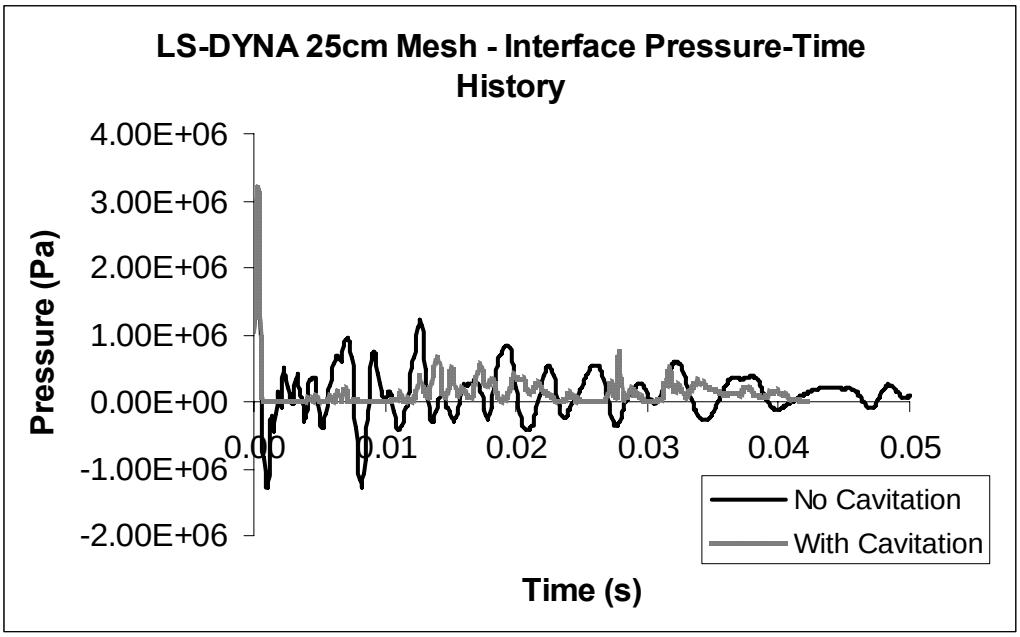

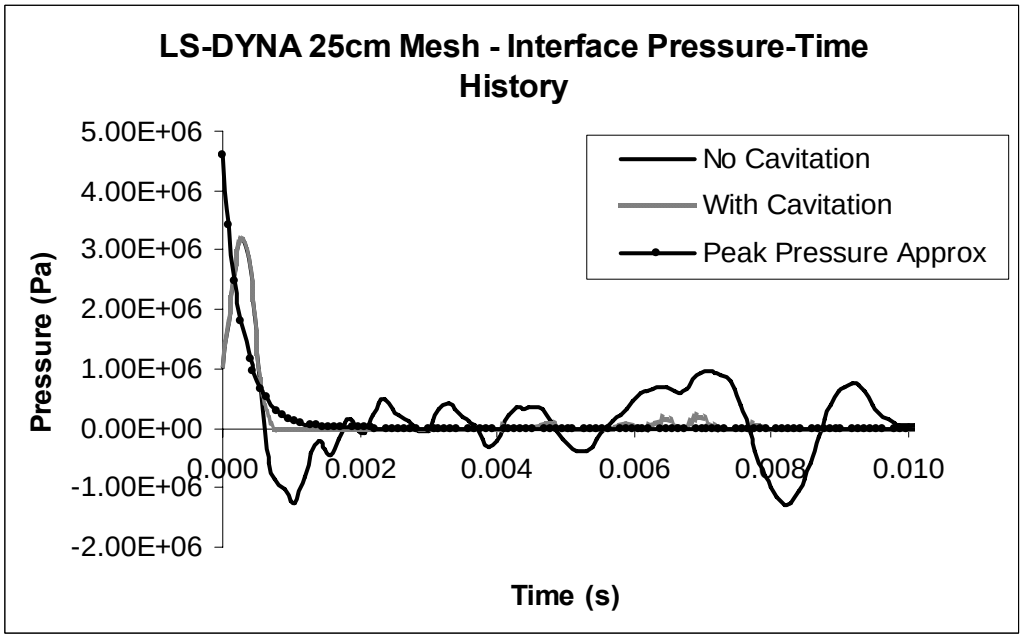

Figure 3.47 25cm mesh LS-DYNA fluid-structure interface pressure-time history on two time scales

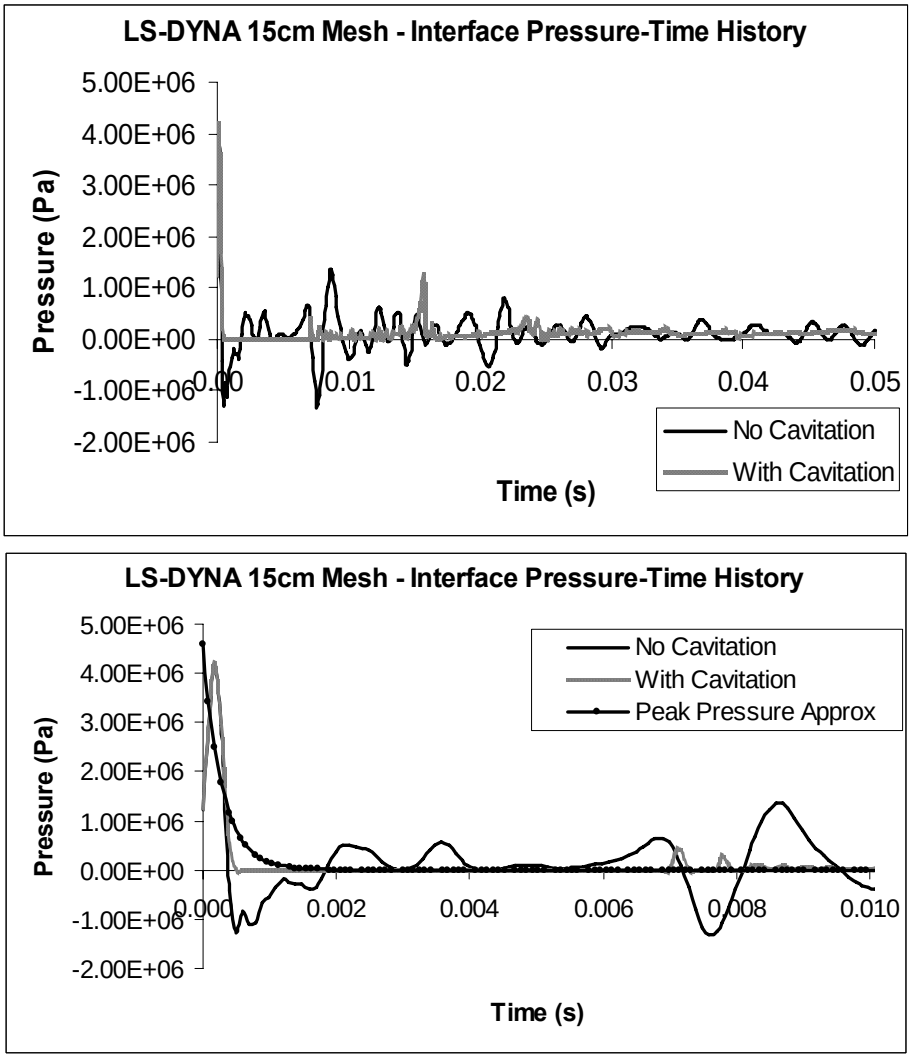

Figure 3.48 15cm mesh LS-DYNA fluid-structure interface pressure-time history on two time scales

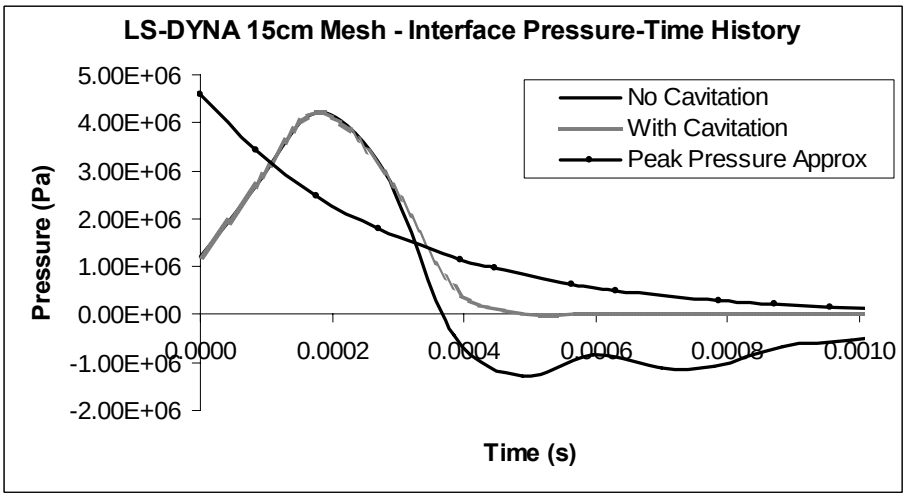

Figure 3.49 15cm mesh fluid-structure interface pressure-time history from 0 to 1ms

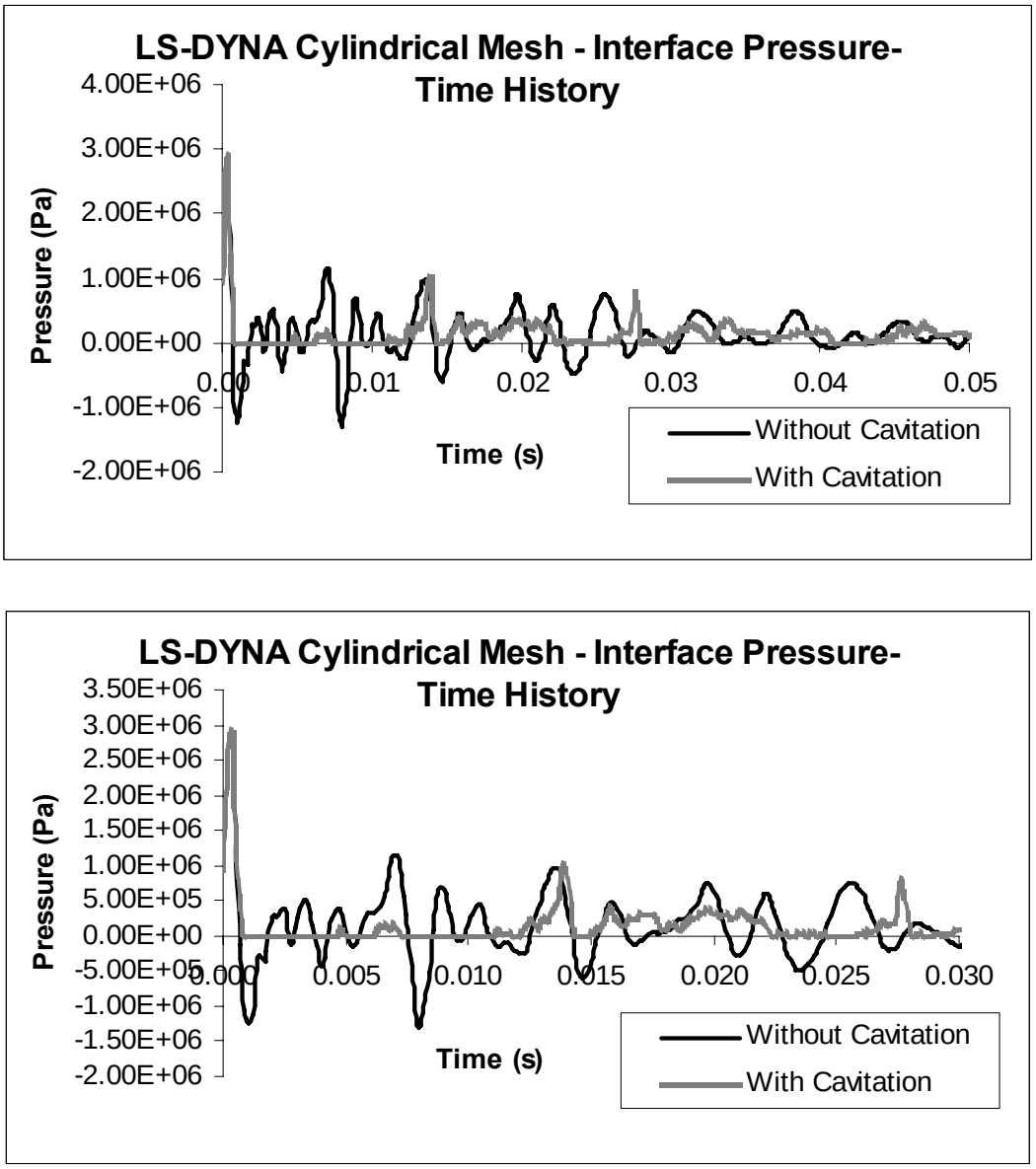

Figure 3.50 Cylindrical mesh LS-DYNA fluid-structure interface pressure-time history on two time scales

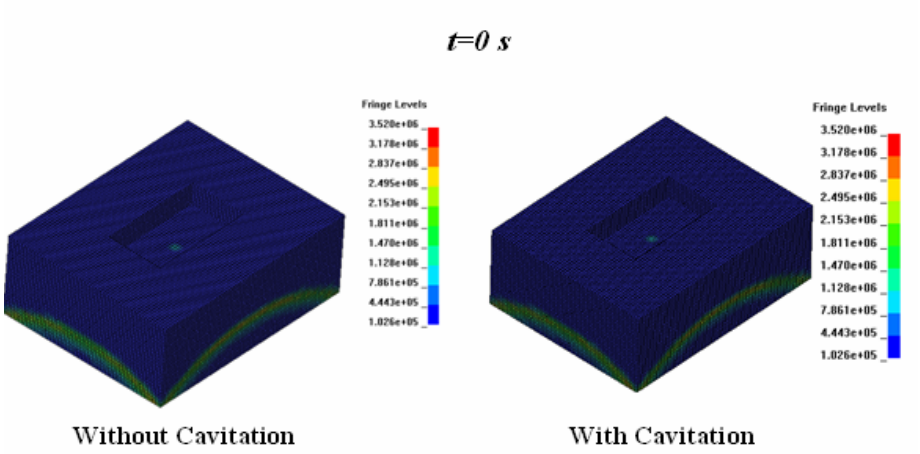

Figure 3.51 Comparison of pressure in 25cm fluid mesh at initial time

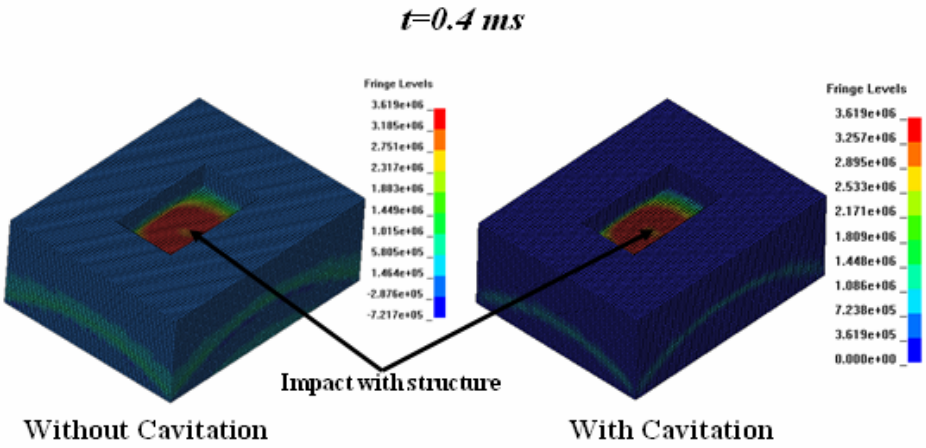

Figure 3.52 Comparison of pressure in 25cm fluid mesh at 0.4ms

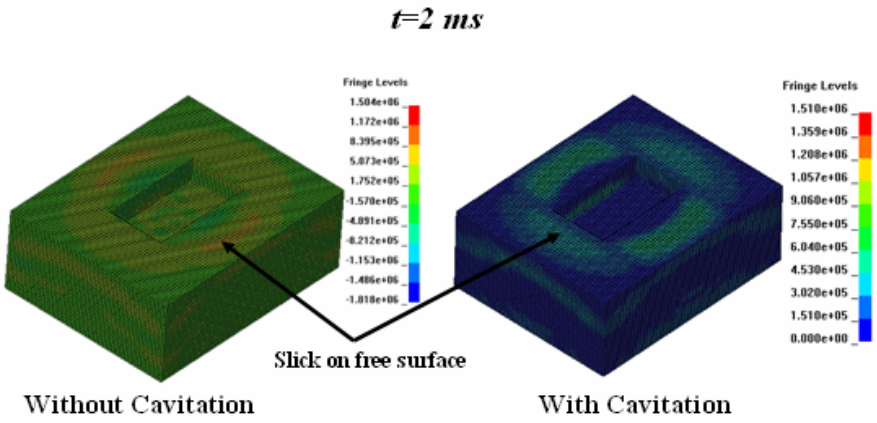

Figure 3.53 Comparison of pressure in 25cm fluid mesh at 2ms

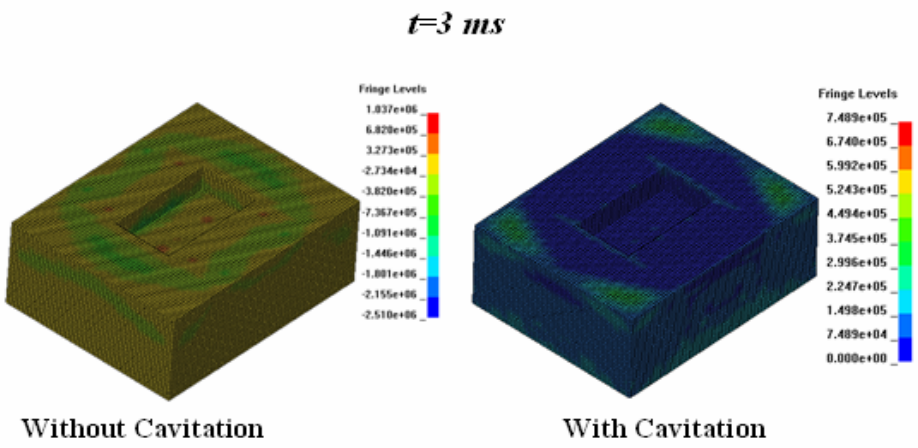

Figure 3.54 Comparison of pressure in 25cm fluid mesh at 3ms

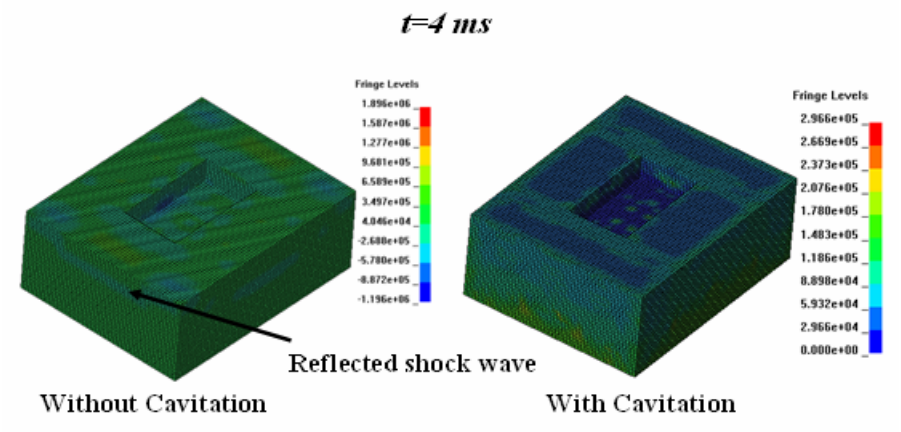

Figure 3.55 Comparison of pressure in 25cm fluid mesh at 4ms

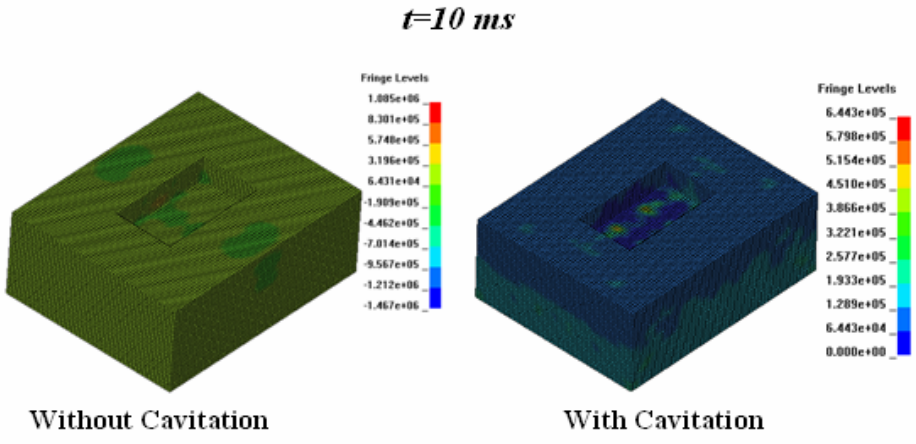

Figure 3.56 Comparison of pressure in 25cm fluid mesh at 10ms

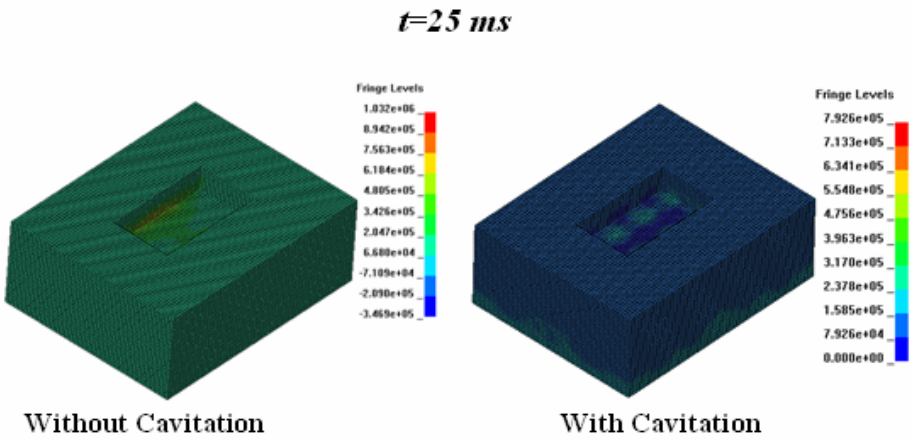

Figure 3.57 Comparison of pressure in 25cm fluid mesh at 25ms

3.4 Comparison of Results and Assessment

In the following sections the results presented in Section 3.2 and 3.3 are compared and their validity assessed. Because no comparisons to experimental data or analytical solutions can be made for the box barge problem, the results are assessed by comparing the results against knowledge of the physics of underwater explosions and results from similar work. The assumptions made in the mathematical model and finite element model of the box barge are also examined to determine their affect on the quality of the results.

3.4.1 Comparison

First the cylindrical model results are compared to the 25cm model results. The 25cm model is used for comparison because in the cylindrical model the structure and fluid-structure interface elements are the same as in the 25cm model. Figures 3.58 - 3.62 compare the structural responses of the two models. These results show that using a cylindrical mesh does not change the response of the box barge significantly. In fact,

assuming USA gives an accurate kick-off velocity, the cylindrical mesh gives a more accurate kick-off velocity for the keel, Figure 3.58, than the rectangular mesh.

In the fluid, the cylindrical mesh also gives very similar results to the 25cm mesh. Based on these results it is concluded that if needed, a cylindrical mesh can be used to model a surrounding fluid in an UNDEX model. For the comparisons made in this section it is assumed that the 25cm and cylindrical fluid mesh give the same results.

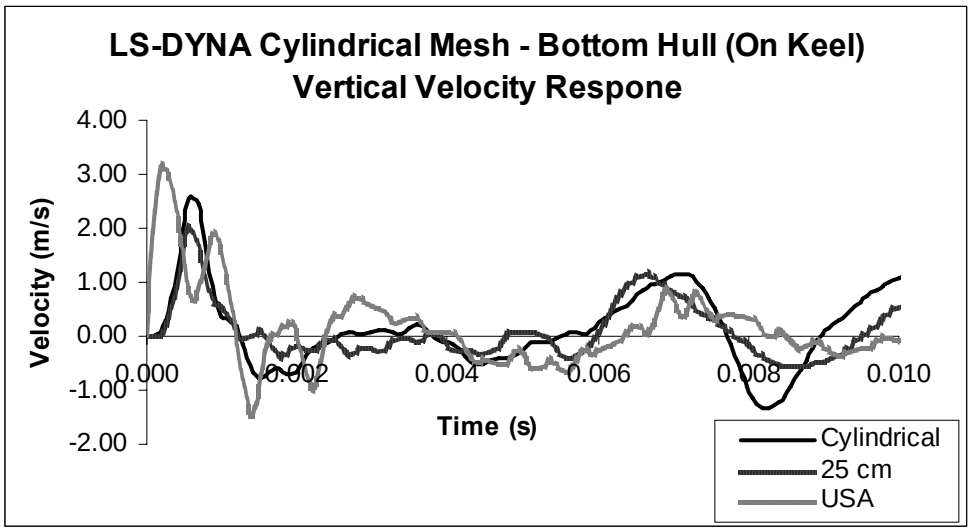

Figure 3.58 Comparison of cylindrical and 25cm model velocity results on the keel of the box barge

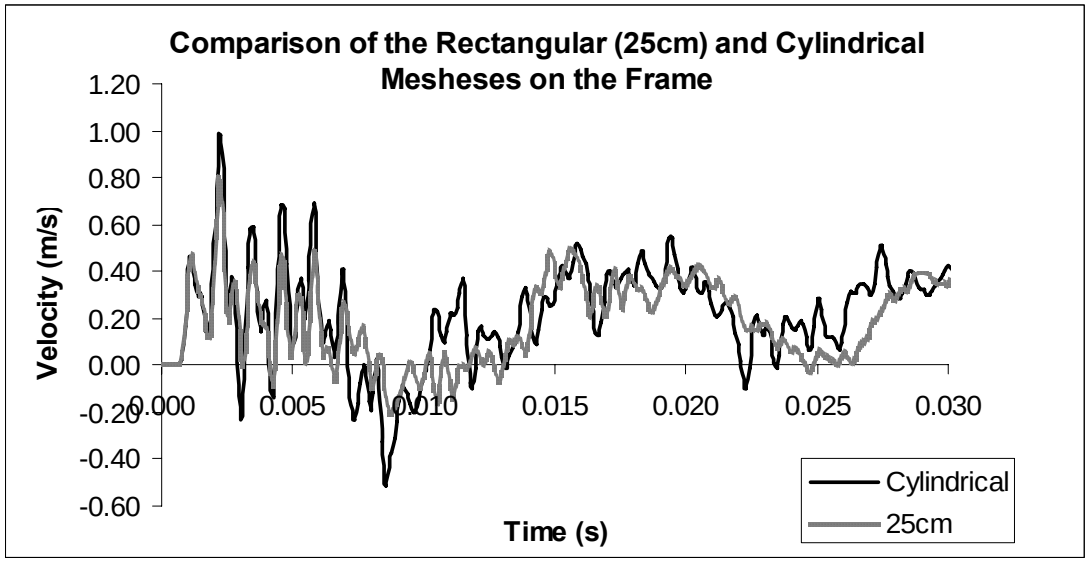

Figure 3.59 Comparison of cylindrical and 25cm model velocity results on the frame of the box barge

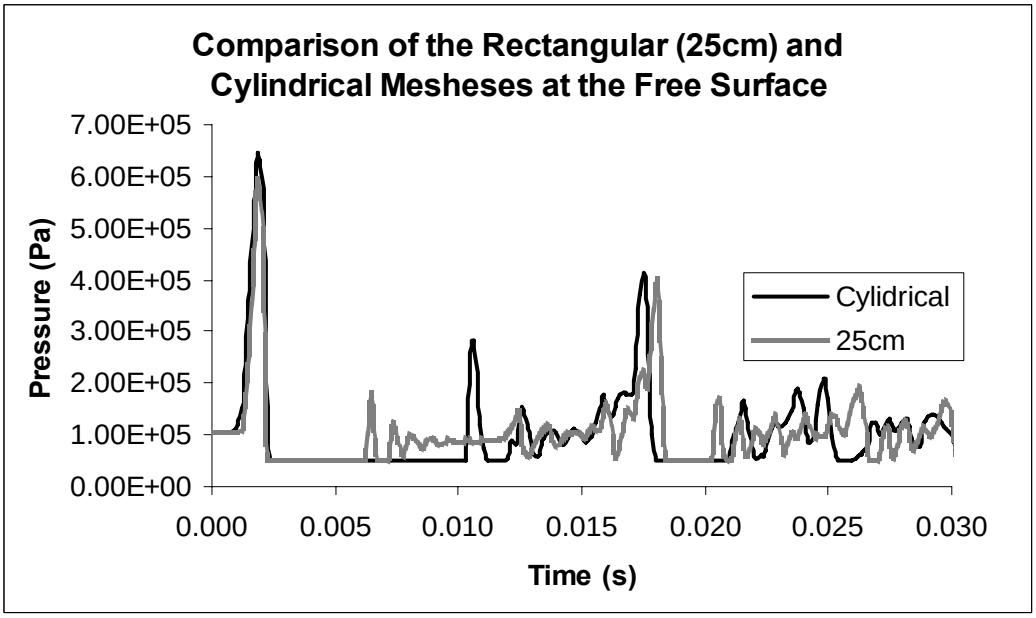

Figure 3.60 Comparison of cylindrical and 25cm model pressure-time history at the free surface of the fluid

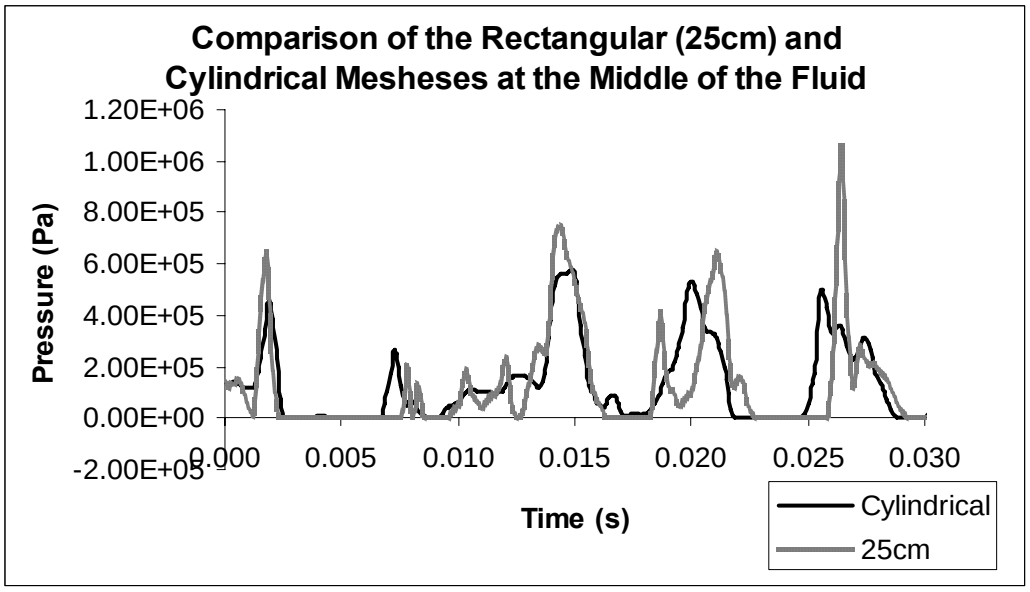

Figure 3.61 Comparison of cylindrical and 25cm model pressure-time history at the middle of the fluid

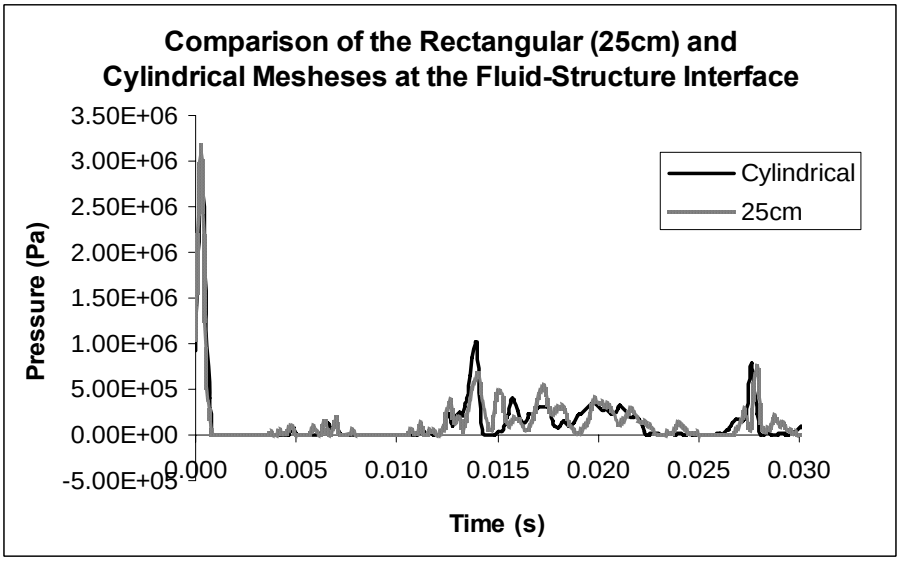

Figure 3.62 Comparison of cylindrical and 25cm model pressure-time history at the fluid-structure interface

Next, the LS-DYNA results are compared to the USA results to determine which LS-DYNA model gives the most accurate results. USA is assumed to provide accurate results for the box barge response without cavitation because it is based on a proven method for fluid-structure interaction models, the DAA. Comparing the USA and LS-

DYNA (without cavitation) in Figures 3.63-3.64 shows that in general USA and LS-DYNA are in agreement with each other. The kick-off velocities on the keel of the box barge are lower in the LS-DYNA 50cm and 25cm cases but the 15cm LS-DYNA case predicts a very similar keel kick-off velocity as USA. This result is supported by the findings of Wood [11] for his box like ship UNDEX problem. Therefore, using USA as the benchmark for comparison, LS-DYNA gives accurate kick-ff velocities when a small mesh size is used.

At the off keel bottom hull location USA and LS-DYNA results do not compare well. Like the on keel location, LS-DYNA gives lower kick-off velocities for the 50cm and 25cm meshes. USA gives a result that is closer to the LS-DYNA result with cavitation considered but USA is not accounting for cavitation. The off keel comparisons show the response at this location is greatly affected by the size of the mesh used in the analysis as none of the different LS-DYNA models give similar results.

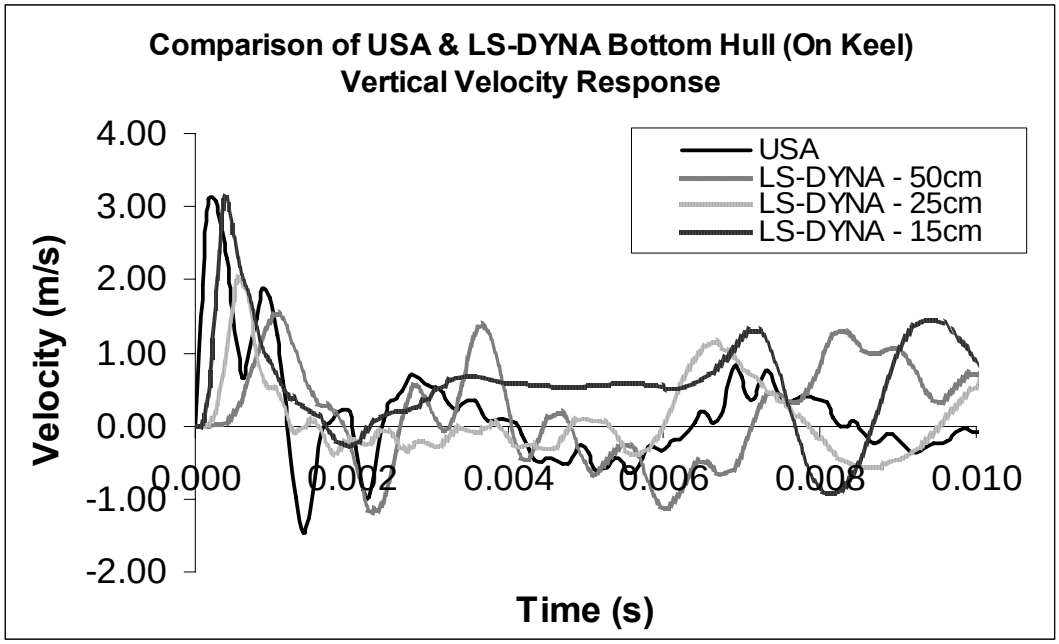

Figure 3.63 USA & LS-DYNA result comparison for on keel velocity response

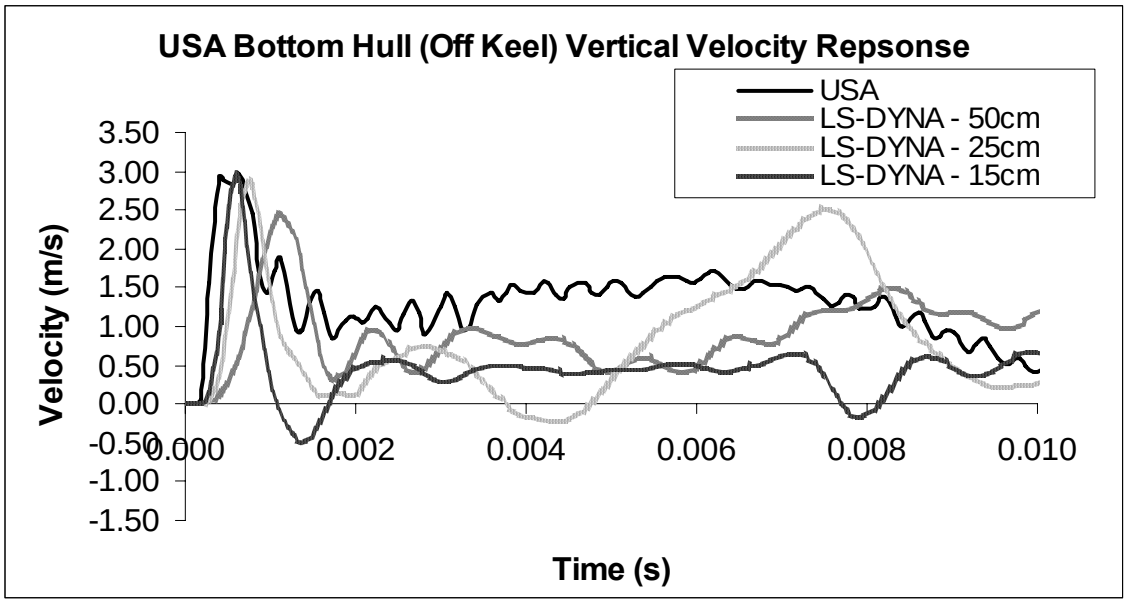

Figure 3.64 USA & LS-DYNA result comparison for off keel velocity response

Both bottom hull responses in USA and LS-DYNA (without cavitation) follow expected UNDEX physics for the early time initial response as the results give a kick-off velocity in response to the shock wave loading followed by decay to a negative velocity as seen in Wood's results for similar models [11].

Overall it can be concluded that USA and LS-DYNA give similar results when modeling the box barge problem without cavitation as long as the LS-DYNA mesh is sufficiently refined. If USA is assumed to be an adequate benchmark for comparison without cavitation, then when cavitation is neglected the LS-DYNA 15cm model gives the best results for the bottom hull response.

When cavitation is considered there are slight differences in the bottom hull velocities of the 50cm and 25cm models suggesting that cavitation might be important to consider. In the 15cm LS-DYNA model the bottom hull velocity response is significantly different when cavitation is considered. The slight differences seen in the 50cm and 25cm models when cavitation is considered compare well with Wood's results

for similar models. The significant changes seen in the 15cm mesh results do not compare well with Wood. This discrepancy between the velocity responses of two larger meshes and the 15cm mesh occurs because of differences in the pressure results. It is expected that the model with the most accurate fluid model is also the model with the most accurate structure results. The critical parameter for the accuracy of the fluid mesh was determined in the results of Section 3.3. In this section it was shown the fluid element on the fluid-structure interface is the critical parameter for fluid mesh accuracy (if the cavitation region is contained within the fluid model). This element is critical for two reasons. First, because it is responsible for propagating the shock wave to the structure. Second, because the cavitation region is determined by the magnitude of the reflected shock wave (Section 1.2.2), it is critical that the fluid first accurately capture the peak pressure of the incident shock wave for an accurate prediction of cavitation.

Figure 3.66 shows that the 15cm mesh captures the peak pressure of shock wave better than the 50cm and 25cm models at the critical element. Notice that none of the meshes capture the discontinuity or exponential decay of the shock wave. The error comparison in Figure 3.67 shows the 15cm mesh captures the shock wave better than Wood's model as well. Because the 15cm model captures the peak pressure the best it also captures cavitation more accurately than the other models. This is shown in Figure 3.65 where the 15cm mesh captures a velocity spike when the cavitation region closes and the structure is re-loaded. The velocity spike in Figure 3.65 could also occur from a wave reflecting from the bottom boundary but as Section 3.4.4 will show, the spike occurs regardless of the bottom boundary condition. Clearly, the 15cm mesh gives the best results in the fluid. This finding is supported by Sprague and Geers [33] who point

out the need for refined meshes to accurately consider cavitation in far-filed UNDEX models using the CAFE approach. However, none of the models studied in this section can be validated by experiment or an analytical solution. Therefore the question becomes which model is correct, the 50cm and 25cm models that compares well with Wood or the 15cm model that has the most accurate fluid results?

To answer this question the 50cm, 25cm, and 15cm models are compared to a UNDEX problem done by Felippa and DeRuntz [31] (Figures 3.68 and 3.69) which was validated with an analytical solution. Although their problem is not a box barge problem, when cavitation is considered the vertical velocity results of the Felippa and DeRuntz model are similar to the results in the 25cm and 15cm model, as shown in Figure 3.69. This figure also shows the 15cm mesh gives a more accurate kick-off velocity (based on USA comparison) than the 25cm mesh. Therefore it is concluded that the 15cm LS-DYNA model is the most correct model because it has the most accurate fluid mesh and compares well to a UNDEX problem that has been validated by an analytical solution. Furthermore, as the 15cm model has shown, an accurate cavitation model changes the response of the bottom hull drastically proving that a good UNDEX finite element model must include cavitation effects.

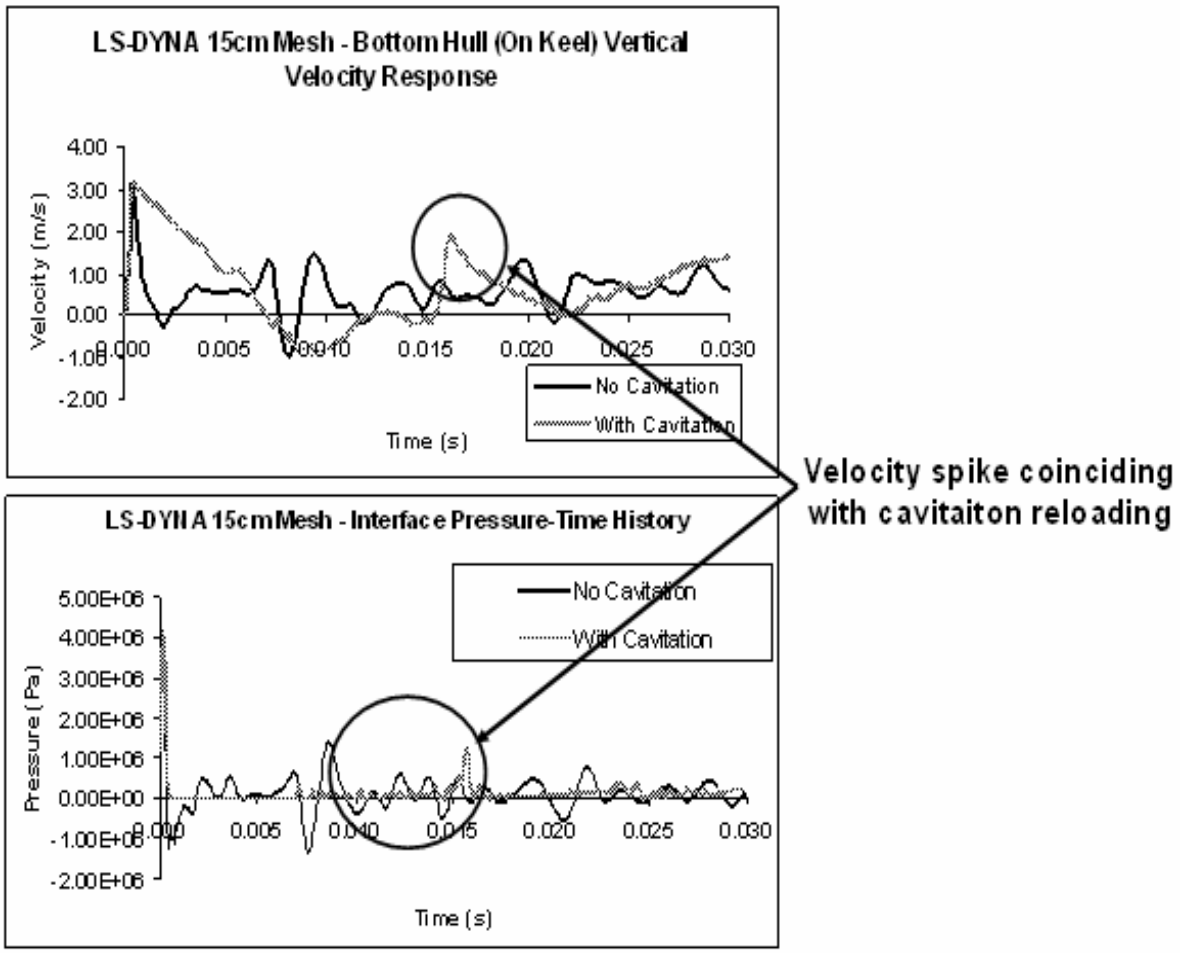

Figure 3.65 Velocity Spike due to cavitation reloading seen in the 15cm LS-DYNA model results

In the previous paragraphs a conclusion reached was that capturing the peak pressure of the shock wave accurately is critical for an accurate fluid model. This conclusion contradicts previous thinking on shock wave modeling in the UNDEX problem. Past works have assumed that it is sufficient for models to capture the correct impulse of the shock wave. Because the impulse is correct, capturing the exact magnitude of the shock wave was not considered important because it was assumed that the structural response was driven by impulse and not peak pressure [5]. Although the initial structural response due to the shock wave may be driven by impulse, the 15cm

model has shown the peak pressure of the shock wave must be captured correctly for an accurate model of cavitation. Therefore when the structure response due to cavitation is considered, accurately capturing the peak pressure becomes critical.

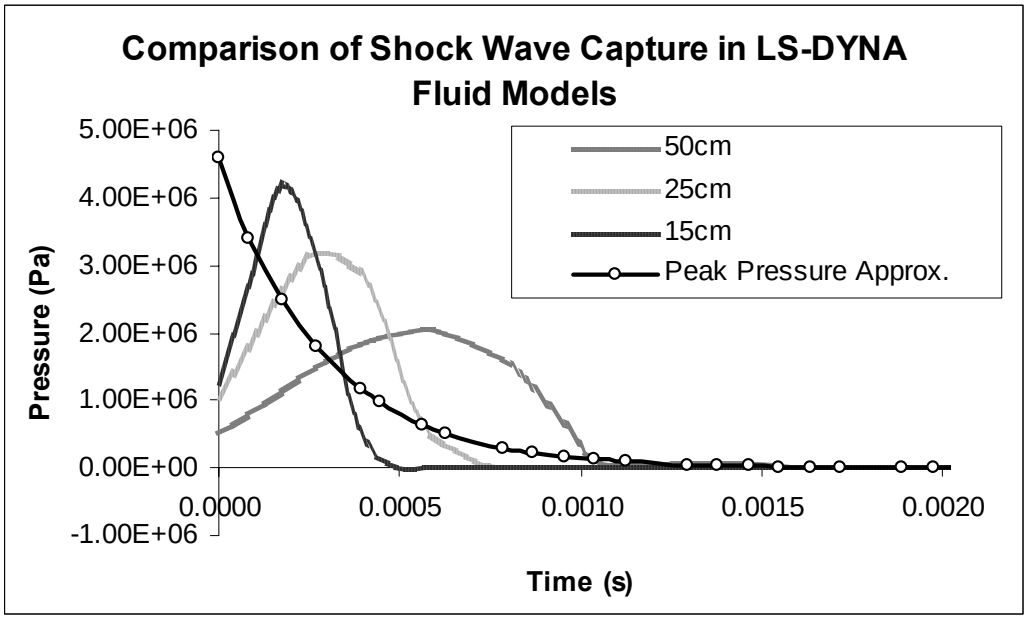

Figure 3.66 Comparison of pressure-time histories for different LS-DYNA fluid models showing ability to capture shock wave

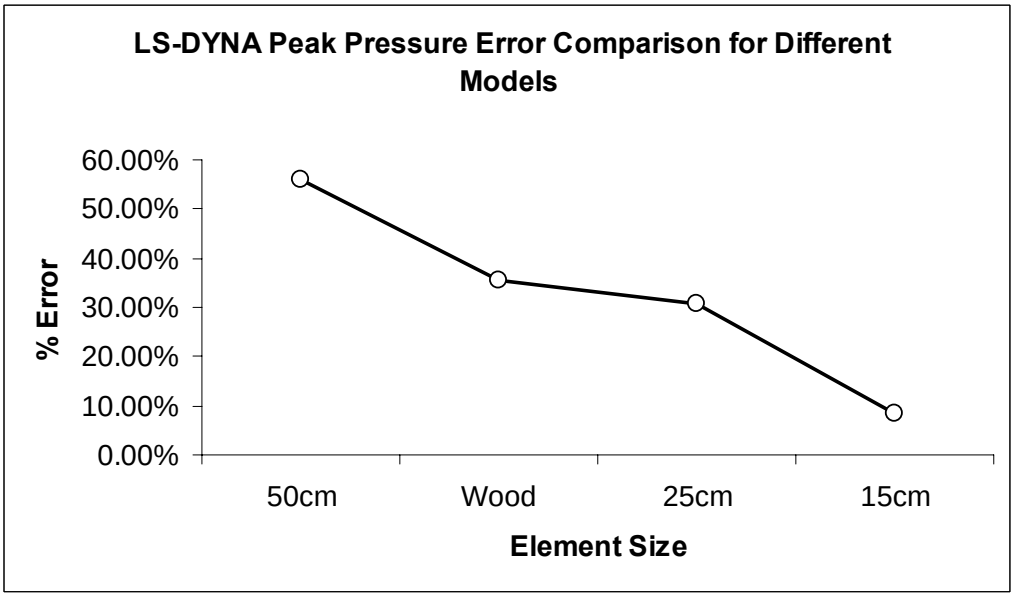

Figure 3.67 Peak pressure error comparison the for four different models

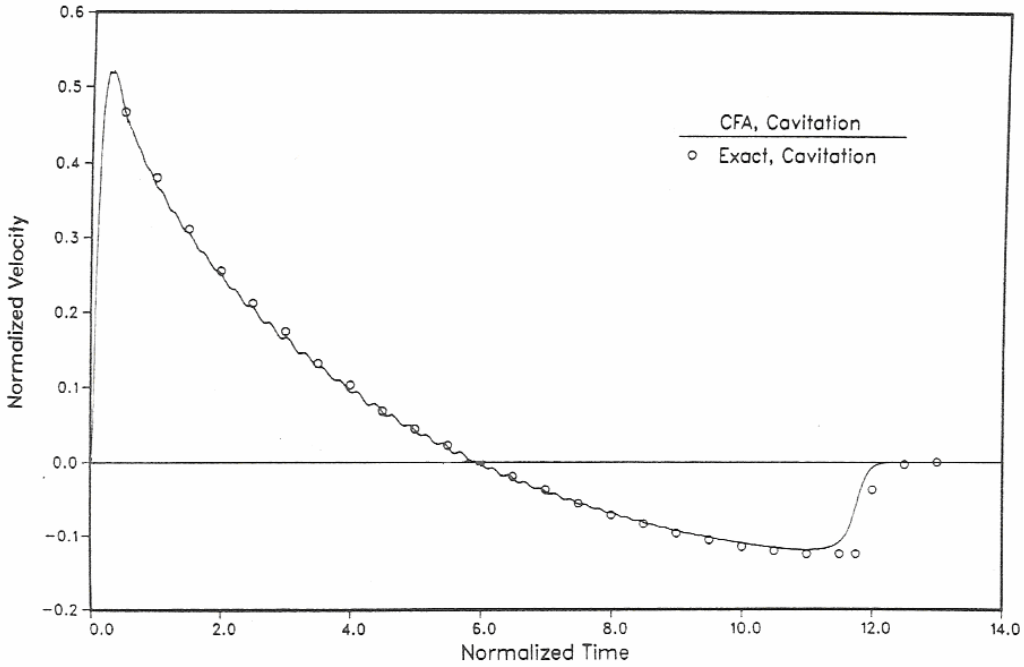

Figure 3.68 Felippa and DeRuntz UNDEX model results [31]

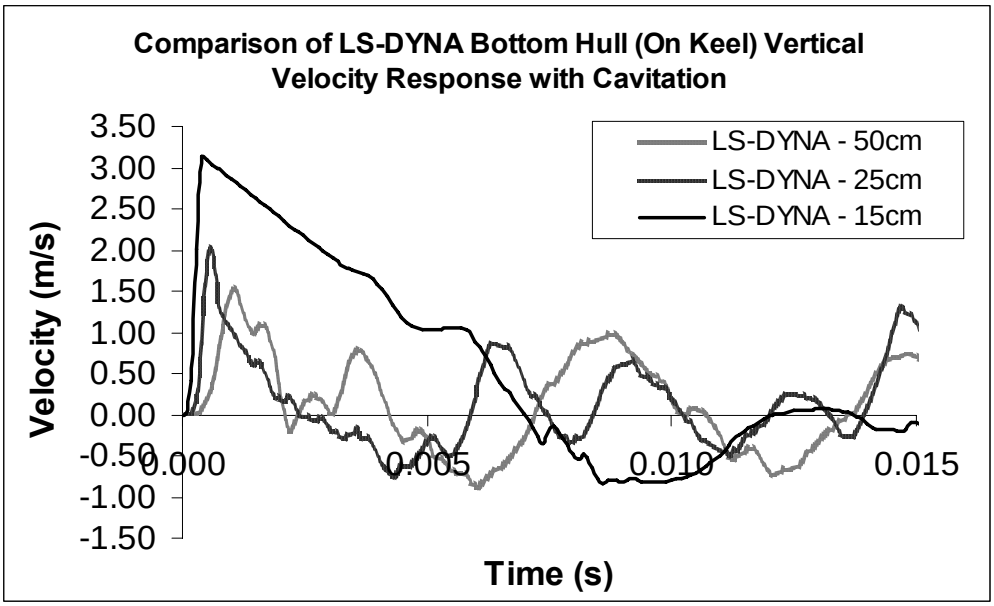

Figure 3.69 Comparison of LS-DYNA on keel velocity responses with cavitation

3.4.2 Acoustic Pressure Elements

In the previous section it was shown that accurately capturing the shock wave in the fluid model plays a critical role in the accuracy of the UNDEX model. It was also shown that although the LS-DYNA 15cm model gives somewhat more accurate results, none of the LS-DYNA fluid models correctly capture the behavior of the shock wave. In this section the fluid models are examined to understand why they do not capture the shock wave.

Recall from Section 2.1.1 that in LS-DYNA the fluid mesh is modeled using acoustic pressure elements. The mathematical formulation for the traditional acoustic pressure element is presented by Zienkiewicz and Bettess [34] and further descriptions can be found in [35, 36]. In LS-DYNA the acoustic pressure elements are formulated using the displacement potential formulation, which is the formulation used in the CAFE method. Traditionally, this formulation uses only the displacement potential to describe the state of the fluid, requiring only one unknown per node. However, in the CAFE approach a condensation variable is introduced to the formulation to account for cavitation [39]. Thus, the CAFE approach is a mixed formulation requiring two unknowns per node. It is not known for sure why LS-DYNA refers to its acoustic elements as pressure elements or why its states only one unknown per node is required. The most logical reasons are that in the CAFE approach only pressure is exchanged between the fluid and structure elements. Also, the coupled governing equations are integrated in time in a manner that treats them as a single degree of freedom system.

Acoustic displacement potential elements for the CAFE approach are formulated by Felippa and DeRuntz [31,32]. To begin, it is assumed the fluid domain can be modeled as a Navier-Stokes fluid (Equation 3.1).

$$\rho\left(\frac{\partial v}{\partial t}+v_j\frac{\partial v_i}{\partial x_j}\right)=\rho b-\frac{\partial \sigma_{ij}}{\partial x_j} \tag{3.1}$$

In Equation 3.1, v is the fluid velocity, p the fluid pressure, b the body forces in the fluid, ρ the fluid density and μ is the viscosity. Acoustic elements assume gravity is the only body force applied to the domain and that it is implied in the pressure term of Equation 3.1. The flow is also assumed to be inviscid, have small compresability ($\Delta\rho << \rho o$), and the convective acceleration term (3rd term in Equation 3.1) is neglected. These assumptions reduce Equation 3.1 to the equation of motion for an acoustic fluid (Equation 3.2).

$$\ddot{d}=-\frac{1}{\rho}\nabla p \tag{3.2}$$

When the continuity equation (Equation 3.3) is combined with the linear equation of state (Equation 3.4), the constitutive equation for pressure and displacement is obtained (Equation 3.5). In these equations K is the bulk modulus of the fluid and c is the speed of sound in the fluid.

$$\frac{\partial \rho}{\partial t}=-\rho\frac{\partial \dot{d}}{\partial x} \tag{3.3}$$

$$p=c^2\rho \tag{3.4}$$

$$\nabla d=-\frac{1}{K}p \tag{3.5}$$

Equations 3.2 and 3.5 can be combined to yield Equation 3.6. If the displacement vector in 3.6 is replaced by the displacement potential defined in Equation 3.7, then the governing equation for a displacement potential element (Equation 3.8) is yielded.

$$\nabla^2 d - \frac{1}{c^2}\ddot{d} = 0 \tag{3.6}$$

$$\rho d = -\nabla \psi \tag{3.7}$$

$$\nabla^2 \psi - \frac{1}{c^2}\ddot{\psi} = 0 \tag{3.8}$$

To account for cavitation the condensation, *s*, defined in Equation 3.9 is used to modify the linear equation of state (Equation 3.10). Equation 3.10 is the bilinear equation of state, it creates a check for cavitation at each node that sets the pressure in the fluid equal to zero if cavitation is present. Using the bilinear equation of state the governing equation for a displacement potential element (Equation 3.8) is modified to its final form shown in Equation 3.11.

$$s = \nabla^2 \psi \tag{3.9}$$

$$p = \begin{cases} p_{hydrostatic} + c^2 s, & s > -p_{hydrostatic}/c^2 \\ 0, & otherwise \end{cases} \tag{3.10}$$

$$\ddot{\psi} = \begin{cases} p - p_{hydrostatic}, & s > -p_{hydrostatic}/c^2 \\ -p_{hydrostatic}, & otherwise \end{cases} \tag{3.11}$$

The assumptions made in the fluid to derive the displacement potential formulation have some potential implications on the box barge model results. Recall that in the box barge model it was assumed that (on the fluid-structure interface) the nodes of the finite element fluid and structure models have one-to-one contact and remain merged through the simulation. This assumption is common in similar prior work [3,11,26]. In effect, the fluid-structure interface assumption acts as a no-slip condition imposed on the fluid. Because the acoustic pressure element neglects viscous terms in the Navier-Stokes equations the no-slip condition imposed on the fluid in the modeling procedure is

violated. This means a no-slip condition is being enforced in the finite element model but is not being accounted for in the mathematical formulation of the problem. This does not affect the initial loading of the structure due to the impact of the shock wave, if modeled properly. However, it does affect the fluid-structure interaction when local cavitation and global ship motion are considered. Recall from Section 1.2.2, that local cavitation is created when the fluid surrounding the ship can no longer keep up with the vertical acceleration of the ship. When the no-slip condition is violated local cavitaiton region is not captured correctly because the boundary layer formed by the no-slip condition is not modeled properly. The inability to model the boundary layer also means that global ship motions, such as heave, pitch, and roll can not be accounted for adequately. Because the no-slip assumption is violated it is concluded the box barge model does not properly model the fluid-structure interaction after the initial structural loading.

To determine why the shock is not adequately captured in LS-DYNA several possibilities are examined. First, the time step used in the time integration scheme is considered to determine the stability of the results. In a one dimensional problem with linear elements, the critical time step for the central difference method is:

$$\Delta t_{critical} \leq \frac{2}{\omega_{\max}^{model}} \tag{3.12}$$

It has been shown [29] that when using a lumped mass matrix the maximum frequency of the acoustic pressure model is equivalent to twice the time it takes a wave traveling at speed c to traverse the length of an element, h_e. Therefore, for stability of the results using acoustic pressure elements Equation 3.6 must be satisfied.

$$\omega_{\max}^{model} = \frac{2c}{h_e} \tag{3.13}$$

Although Equation 3.6 is derived for a one dimensional problem the same methodology for finding the critical time step can be applied in two and three dimensions. In a two dimensional problem dilatational and shear waves occur in the domain. Each wave type travels at a different speed depending on the properties of the domain. The wave that travels at the fastest speed in the model determines the critical time step because according to Equation 3.6 a larger c will cause a smaller Δt. In the fluid, the shock wave has the highest wave velocity because it travels at the speed of sound in water. Therefore, to maintain stability the box barge model must adhere to Equation 3.6 where c is the speed of sound in water (1514 m/s).

A comparison of the time step used in LS-DYNA and the critical time step for each model is made in Table 3.4. Recall that in the LS-DYNA models, the critical time step for the box barge model is controlled by the shell elements of the structural domain. LS-DYNA also computes a new Δt every time step. At the beginning of the simulation all models use a time step on the order of 0.01ms which is more than adequate to capture the shock. After the first few time steps a larger time step is used depending on the mesh size of the model. As Table 3.4 shows, in each LS-DYNA model the time step used is lower than the fluid critical time step. Therefore the time integration scheme used in LS-DYNA is stable for the box barge fluid domain.

Table 3.5 Comparison of critical fluid time steps from Equation 3.7 and LS-DYNA

Model	$\Delta t_{critical}$ (ms)	LS-DYNA Δt (ms)
50cm	0.3300	0.0430
25cm	0.1651	0.0419
15cm	0.0991	0.0262

There are several other known sources of error that arise when modeling shock waves in a finite element model. It is known [37] that in cases where discontinuities, such as a shock, occur in the finite element model, the time integration scheme causes oscillations to occur at the discontinuity. This is true even for the very best of integration schemes [37]. A standard Galerkin finite element approximation, like the one used in LS-DYNA, will also smear a discontinuity, such as a shock, over a number of elements. The dissipation of the peak pressure is further increased in LS-DYNA because first order polynomial basis functions are used for the acoustic elements, a problem which Sprauge and Geers attempt to overcome with spectral element methods [38].

Using more elements in the fluid domain will improve the shock profile, but this will require more computer power. The box barge model results show a substantial improvement of results as the mesh is refined from 50cm to 15cm. However, as Sprague and Geers [38] mention, the refinement needed for accuracy in three-dimensional models is often too computational expensive. Furthermore, UNDEX models that use one-to-one contact on the fluid-structure interface require that any mesh refinement made in the fluid also be made in the structure [38]. In most far-filed UNDEX models a very refined structural is not needed therefore the refining the structural mesh to match the fluid increase computational time without any benefit to the structural solution [38].

A more complex approach, that would solve the refinement and basis function issues is the use of traditional CFD upwinding techniques to prevent smearing [37,40] and damp oscillations that occur near discontinuities. Upwinding effects can be accomplished by using a Petrov-Galerkin formulation of the acoustic pressure equation (3.4), the

discontinuous Galerkin method [41] which has been used to model shock waves [42,43,44], Flux Corrected Transport (FCT) algorithms, or artificial diffusivity [45].

3.4.3 Barge Global Motion

In Section 3.4.2 the inviscid assumption made in the formulation of the acoustic pressure elements was shown to violate the no-slip condition enforced in the LS-DYNA UNDEX model. Because this causes the boundary layer to be modeled incorrectly, it is theorized the global motion of the box barge captured in the LS-DYAN models is incorrect. Global motion refers to traditional ship dynamic phenomena such as heave, pitch, and roll. To test this theory, the box barge is modeled in LS-DYNA without the occurrence of an UNDEX. Instead, the VCG (vertical center of gravity) is initially vertically displaced into the fluid by 0.5 meters to model the heave response of the box barge in LS-DYNA. Figure 3.70 shows the analytical heave response of the box barge's VCG to the initial 0.5 meter displacement. When the same problem is solved using acoustic pressure elements in LS-DYNA, the results (Figure 3.71) are significantly different. Figure 3.71 shows that when acoustic pressure elements are used, the box barge sinks into the fluid after being displaced instead of exhibiting the damped sinusoidal response seen in the analytical solution. This shows that the fluid-structure interaction in the LS-DYNA UNDEX model is not adequately accounted for because of the inviscid assumption made in the formulation of the acoustic pressure element.

By assuming the fluid is inviscid, the effects of the structure on the surrounding fluid such as changes in stress in the fluid created as the box barge heaves cannot be modeled. Other effects such as changes in density are also not accounted for in the fluid model because although it is assumed the fluid is compressible, density is taken to be a constant

by the LS-DYNA acoustic pressure elements. Because of these assumptions the buoyancy of the box barge is not adequately accounted for in the LS-DYNA models. It is concluded that because of the assumptions made, acoustic pressure elements model a medium for the transmission of pressure waves and not a true fluid.

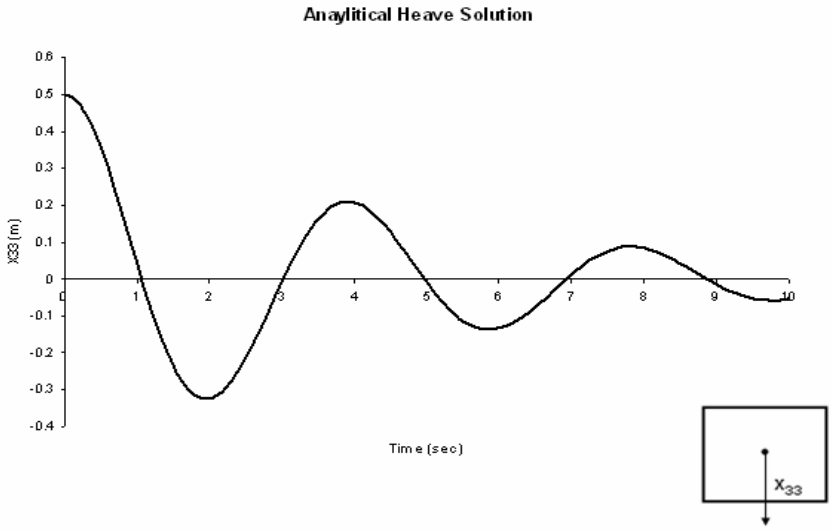

Figure 3.70 Analytical solution to the box barge heave problem in Section 3.4.3

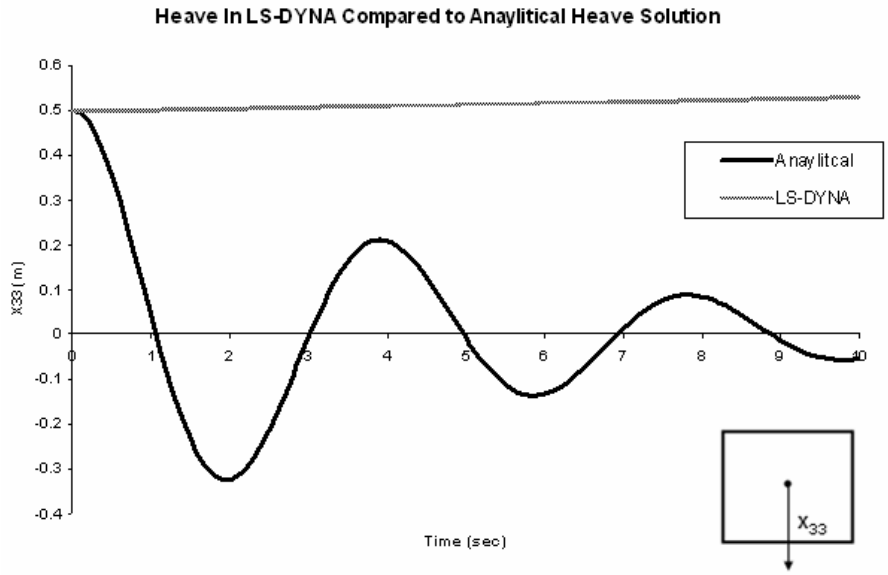

Figure 3.71 LS-DYNA heave result compared to analytical solution to the box barge heave problem

3.4.4 Boundary Conditions

As discussed in Section 2.1.3, when the INITIAL_DETONATION option in LS-DYNA is used to model the shock wave LS-DYNA automatically applies a transmitting or non-reflecting boundary (NRBC) to the fluid domain boundary. However, Section 3.3 showed that this transmitting boundary does not work properly in the box barge models. When USA is used with LS-DYNA and the INITIAL_DETONATION option [3,11,26], the DAA (Section 2.2) is also applied to the fluid boundary. Although the original intent of the DAA was application to a fluid-structure boundary, used in this manner, the DAA is an approximate fluid radiation boundary that is exact at high and low frequencies.

Felippa and DeRuntz [31,32] give the rationale behind using the DAA as a transmitting boundary in their work on studying the effects of cavitation modeling in a simple UNDEX problem. In their UNDEX model, acoustic elements are used to discretize the fluid domain and the DAA is applied to the boundary elements of the fluid domain. A numerical scheme is developed to combine three computer codes, STAGS for the structure, CFA for the fluid, and USA for the DAA boundary. These codes interact in a similar manner to LS-DYNA/USA to solve the UNDEX problem. The method created by Felippa and DeRuntz proved to be successful at implementing the DAA as a boundary condition for their UNDEX models.

Despite the success of Felippa and DeRuntz, the use of USA as a transmitting. the accuracy of results obtained by linking USA with CAFE elements can be problem dependent [1]. Furthermore, a boundary interaction term must be computed to relate the displacements output by the DAA, to a force on the fluid because displacements can not be directly input to the fluid domain. Felippa and DeRuntz point out that this requires a change in the DAA formulation (traditionally the DAA outputs pressure) but there is no

mention in either the USA or LS-DYNA user manuals of either program changing the formulation of the DAA for a fluid boundary. In the BOUNDARY_USA_SURFACE option in LS-DYNA only the set of elements on the DAA boundary and the flag to turn on USA coupling are defined. Neither of these options allows the user to define which DAA formulation is used for the boundary. Therefore it is not known whether the coupling between LS-DYNA and USA is for structural DAA boundaries or fluid DAA boundaries.

Due to these uncertainties in using USA to model a DAA fluid boundary in LS-DYNA and the problems encountered with the INITIAL_DETONATION transmitting boundary, a different boundary condition was sought to replace the DAA boundary used in previous UNDEX models. It was found that LS-DYNA utilizes a viscous boundary condition (VBC) as its NRBC. The VBC is a class of transmitting boundary conditions known as numerical dampers. Numerical dampers have the advantage of simplicity and less computational cost over boundary element methods, such as the DAA, that must couple with boundary element codes, like USA [46,47]. Therefore, the LS-DYNA NRBC was used in the box barge analysis instead of the traditional DAA boundary.

The viscous boundary condition is an approximate NRBC that was originally developed by Lysmer and Kuhlemeyer [48] and later studied by Cohen and Jennings [49]. The viscous boundary condition calculates the normal and shear stress at each boundary node for an incident pressure wave. The incident stresses are matched at each node so that the resulting reflected stress is zero. The VBC works well for simple far-field UNDEX problems (see Chapter 4) and more specific information and analysis of the

VBC is given in Chapter 4. In this section comparisons of results made with and without the VBC in LS-DYNA are made.

Figures 3.72 and 3.73 show both the on keel vertical velocity and the interface pressure-time history for the 15cm box barge model are not greatly influenced by the addition of the VBC. There is only a small change in the magnitude of the velocity spike when the cavitation region closes (15 ms) and a small change in the timing of the closure of the cavitation region. This indicates that the VBC is not working optimally in the box barge model because one would expect to see a significant difference between the two results. A potential cause for this is that boundary conditions such as the VBC have been shown [50] to have trouble at the corner nodes of two and three dimensional finite element models with rectangular meshes. Another cause of error could be that the bottom boundary of the fluid mesh is not extended far enough away from the lower bound of the cavitation region. To determine if corner nodes are the cause of error in the 15cm results a comparison between the 25cm model and cylindrical model is made (the 25cm is used because it uses the same structural model as the cylindrical model).

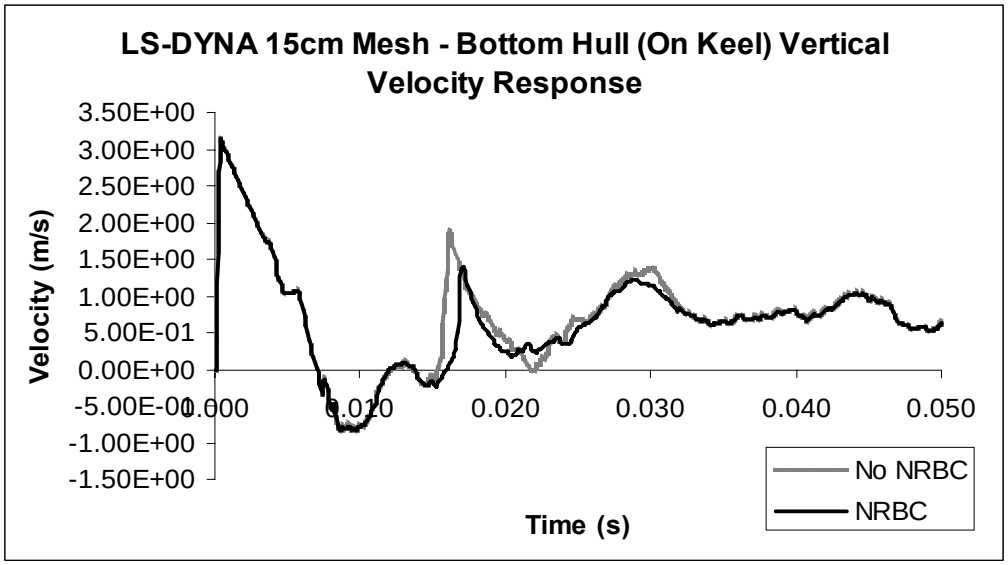

Figure 3.72 LS-DYNA bottom hull velocity with and without added NRBC

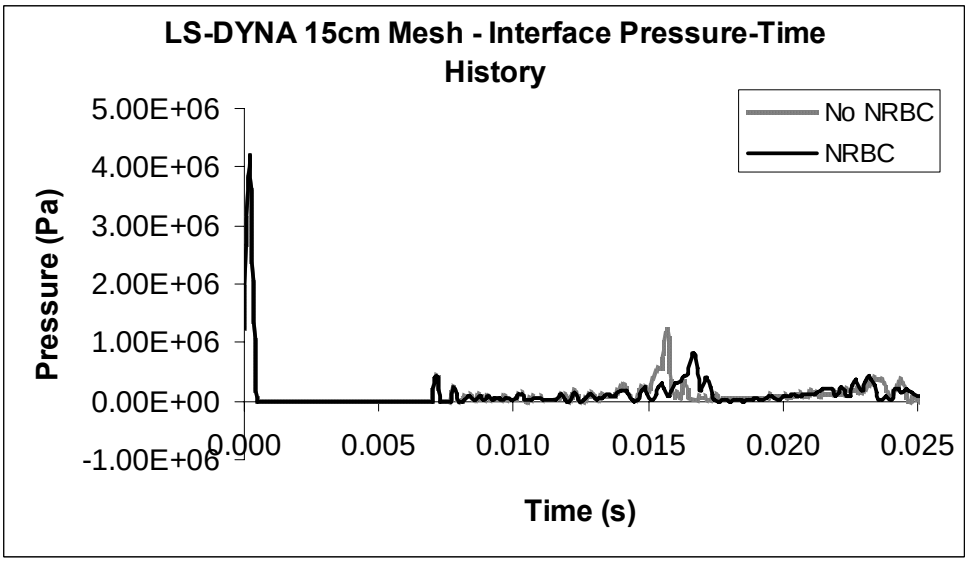

Figure 3.73 LS-DYNA 15cm model pressure-time history at interface with and without added NRBC

In the 25cm and fluid models pressure-time histories (Figures 3.74 – 3.78) the NRBC effects are prominent in the 25cm and cylindrical models at the free surface (Figures 3.74 and 3.76). In these figures the NRBC eliminates a spike in pressure in between 0.015 and 0.020 seconds. In Section 3.3 the middle of the fluid mesh was shown to be an area of concern as the pressure results were inaccurate. Figure 3.75 shows that

when the VBC is added to the 25cm mesh the middle fluid pressure results get worse. When the VBC is added to the cylindrical mesh, the pressure results in the middle of the fluid (Figure 3.77) improve slightly, eliminating a large spike in pressure between 0.0025 and 0.015 seconds. However, there are still large spikes in pressure at later times that should not occur. When compared directly (Figure 3.78), the cylindrical mesh behaves better than the 25cm mesh in the middle of the fluid when the VBC is added, but both meshes still give inaccurate results at this location. These results show that the VBC seems to influence the quality of the fluid results more than the structural response results. But, because there is not a large difference or improvement of the results when a cylindrical mesh is used, it can not be concluded that the use of a rectangular mesh causes the non-optimal behavior of the VBC in the box barge problem.

The results of this section show that there is little change in the results when the VBC is used in the box barge models. These results show that while the VBC does not fail to work, it does not perform optimally in the box barge model. From this three conclusions can be drawn. First, that the VBC has potential to be used as NRBC instead of the DAA in LS-DYNA UNDEX models. The second conclusion is that the bottom boundary of the fluid mesh needs to be extended further from the lower bound of the cavitation region to allow optimum behavior of the VBC. The final conclusion is that perhaps the VBC is not the best numerical damping boundary condition to use in a large scale three dimensional model such as the box barge fluid model. Further investigation of these conclusions are presented in Chapter 4.

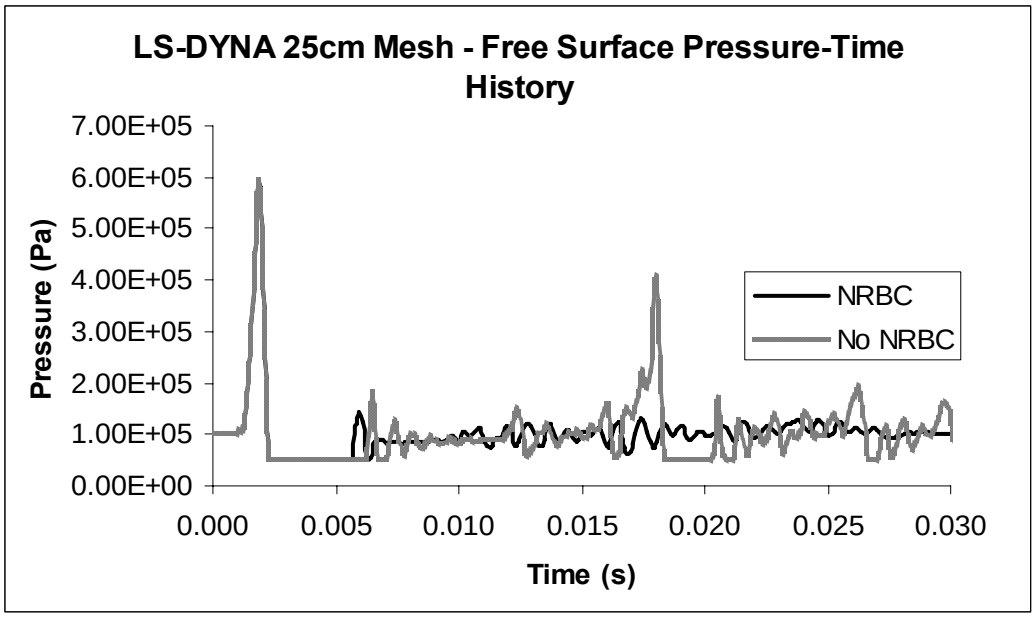

Figure 3.74 LS-DYNA 25cm model pressure-time history at free surface with and without added NRBC

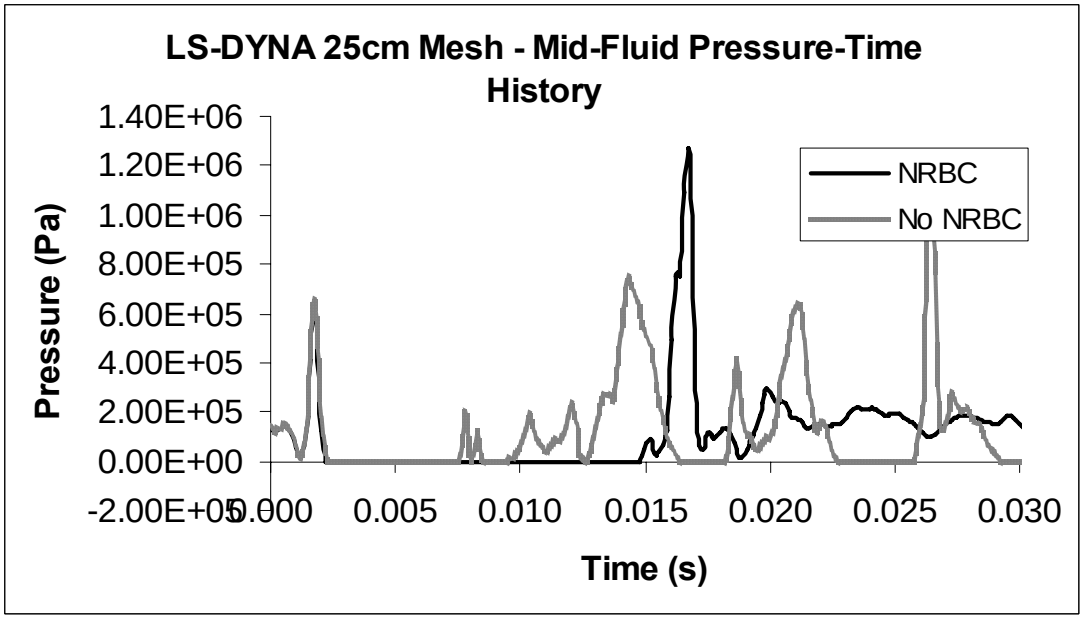

Figure 3.75 LS-DYNA 25cm model pressure-time history at mid-fluid with and without added NRBC

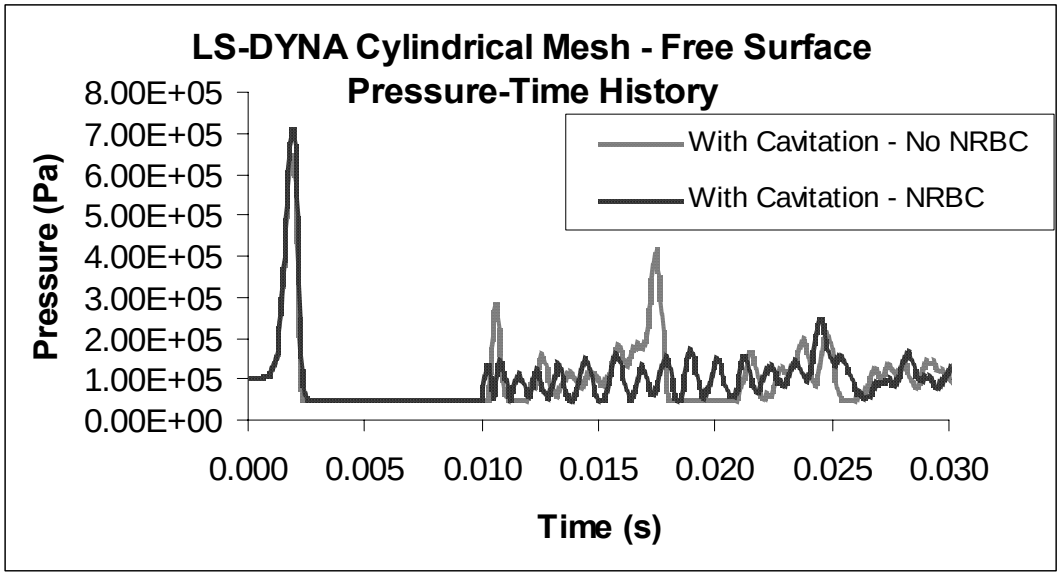

Figure 3.76 LS-DYNA Cylindrical model pressure-time history at free surface with and without added NRBC

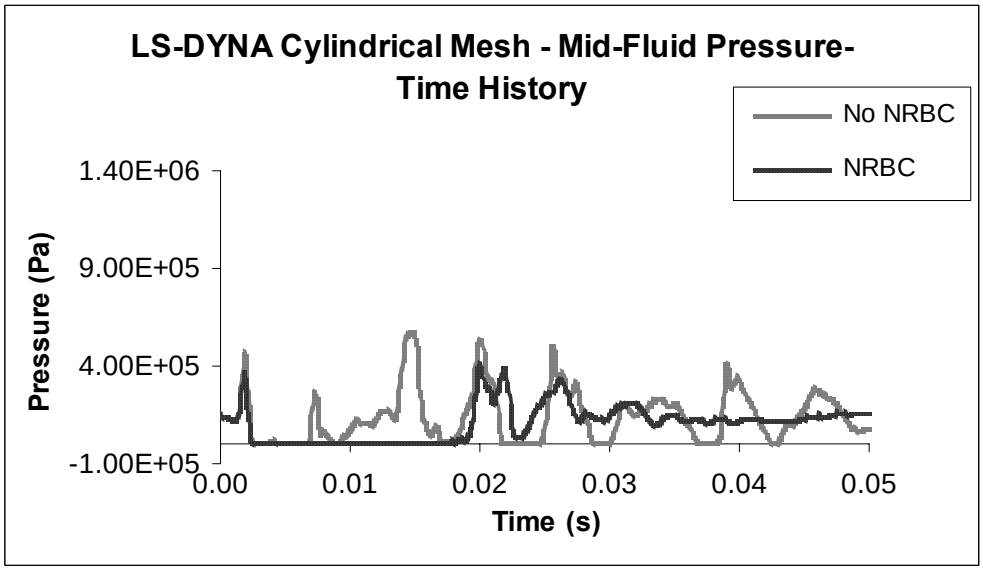

Figure 3.77 LS-DYNA Cylindrical model pressure-time history at mid-fluid with and without added NRBC

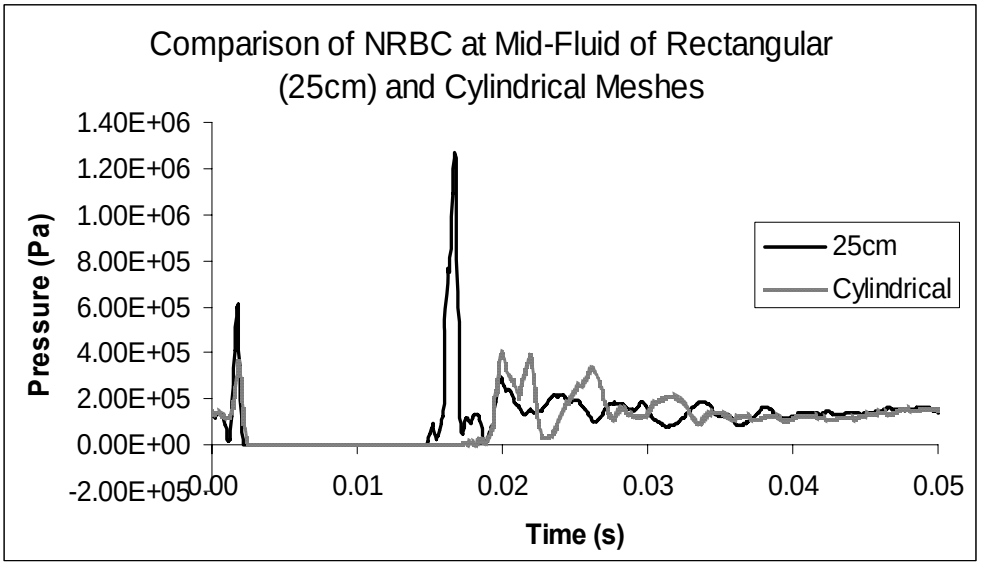

Figure 3.78 Comparison of NRBC effects on LS-DYNA cylindrical and 25cm model pressure-time history at mid-fluid

CHAPTER 4 ASSESSMENT OF BOUNDARY CONITIONS IN LS-DYNA

4.1 Non-Reflecting Boundary

In many physical models the domain of the problem can be considered infinite. A domain is considered to be infinite by a simplifying assumption to a physical problem or when the region of interest is surrounded by a vast medium [50]. In the case of the box barge model, or any far field UNDEX model, the region of interest is a small area of fluid that is part of an entire body of water. Therefore, the fluid region in the mathematical UNDEX model is considered to be an infinite domain.

When a finite element approximation of the UNDEX model is sought a problem arises because every finite model must terminate at a boundary. An obvious solution to

this problem is to create a very large finite model such that the boundary has no effect on the results. However, this is impractical due to large amount of computation needed. A more practical and efficient solution to numerical consideration of infinite domains is the use of non-reflecting boundary conditions.

Non-Reflecting boundaries (NRBCs) are used to model a problem with a physically infinite domain using a finite mathematical model. The term non-reflecting is synonymous with the terms silent, transmitting, absorbing, and radiating. These boundary conditions are artificial boundary conditions, because they do not exist in the physical problem. In general NRBCs allow infinite model behavior by preventing energy radiating toward infinity from being reflected back into the model at an artificial boundary of a finite model. Many types of NRBCs are available; a select few are discussed in the following section.

In Section 3.4.4 the viscous boundary condition (VBC) was introduced as the NRBC used in LS-DYNA. Physically, the VBC can be conceptualized as a viscous damper applied to the boundary nodes of the infinite domain. Numerically, the VBC applies a traction to the boundary in terms of velocities by calculating the normal and shear stress at each boundary node for an incident pressure wave. Then the VBC matches the incident stresses using Equations 4.1 and 4.2, so that the resulting traction on the boundary is zero and therefore the reflection stress is zero.

$$\sigma_{norm} = -\rho c_d v_{norm} \tag{4.1}$$

$$\tau_{shear} = -\rho c_s v_{\tan} \tag{4.2}$$

The VBC has been successfully used in many soil-structure interaction problems where the soil domain is treated as an elastic medium [49,51,52,53]. In these types of problems the VBC performs very effectively absorbing 98.5% of incident compression waves and 95% of incident shear waves [48].

However, the VBC does have certain limitations. Because the VBC is a linear boundary condition, all nonlinear behavior must be contained within the model and interact with the boundary. In the box barge problem this is not an issue because the fluid domain is large enough that the nonlinear cavitation region does not interact with the fluid boundaries.

The effectiveness of the VBC holds for waves of normal incidence but as the angle of incidence becomes more parallel to the boundary, reflections from the boundary begin to increase [49]. This presents a problem in the box barge models with rectangular fluid meshes because in these meshes there are nodes at the bottom corners of the mesh [50]. The corner nodes present a problem because they lie on both the bottom and side boundary of the fluid mesh. At these nodes a wave that has normal incidence at the bottom boundary also has parallel incidence at the side boundary. Therefore they can cause a breakdown in the effectiveness of the VBC at the corners of a rectangular fluid mesh.

Another limitation of the VBC is discussed by Castellani [54] who studied the performance of the VBC in problems with high frequency loadings. Castellani found that the VBC is not able to properly treat problems with high frequency loadings. In a far field UNDEX model where only early time phenomena are accounted for, the only boundary interaction comes when the high frequency shock wave reaches the fluid

domain boundary. The results of Castellani imply that the VBC in LS-DYNA can not properly treat the shock wave and therefore should not be used in models where early time (high frequency) UNDEX phenomena are considered.

Furthermore, although the LS-DYNA manual mentions that the VBC can be used on fluid domains, no mention is made of its applicability to fluid domains that are modeled using acoustic pressure elements. This is a problem because looking at Equations 4.1 and 4.2 the velocity at the boundary nodes must be known to compute the incident tractions. When acoustic elements are used these velocities are not known. Therefore, there are two possibilities as to how LS-DYNA handles the VBC when acoustic elements are used. The first is that a boundary interaction term, like the one need for the DAA, is used to link the fluid nodes to the VBC. This would mean the VBC can not be directly applied to acoustic elements.

The second possibility is that LS-DYNA takes the incident tractions to be the pressures that are already known at the fluid boundary nodes. If this is the case then a possible reason why the results of Section 3.4.4 are uninfluenced by the addition of the VBC is that in LS-DYNA Equations 4.1 and 4.2 are evaluated over segments (element faces) on the boundary instead of at node points on the boundary. This means that LS-DYNA finds the average pressure on the boundary segments and does not take advantage of the fact that in the displacement potential formulation traction can be evaluated at each node point, which would be more accurate than averaging the pressure over a segment.

Another method of imposing a NRBC is the use of infinite elements. Infinite elements are different than the VBC and other numerical damper boundary conditions, in that they use special elements at a boundary rather than a traction applied to boundary

nodes to create the NRBC effect. The concept of infinite elements is to use finite elements to define a semi-infinite domain at the boundary which is desired to be a radiation boundary. These elements are integrated in the model using the same methodology as regular finite elements. The difference is that the infinite elements use special basis functions that are defined over the infinite domain of the element rather than the standard finite element basis functions. Defining the basis functions in this manner allows the infinite element to copy the behavior of the exact solution of the problem at infinity [51]. Infinite elements are an attractive option for the UNDEX problem because they have been successfully applied in fluid-structure interaction problems [55,56,57].

A drawback to infinite elements, is that although infinite elements try to copy the exact solution at infinity, they are evaluated using the finite element method which is a numerical approximation to the exact solution [50]. Therefore, infinite elements like the VBC are approximate boundary conditions and do not behave perfectly for every type of problem. Another drawback to infinite elements is that their application to transient problems has been limited.

Compared to the VBC, infinite elements do not seem to provide any benefit over numerical damping boundary conditions for the far-field UNDEX problem. Furthermore, LS-DYNA does not implement infinite elements as a user option. Due to the fact that only displacements, velocities, traction, or traction expressed as velocity or displacement can be defined as boundary conditions for a fluid it is safe to assume that the transmitting boundary associated with the INITIAL_DETONATION card must be a form of a numerical damping boundary condition. Therefore, NRBCs of the numerical damping

type are investigated further in the remainder of this section and then implemented to show their effectiveness.

Numerical damping boundary conditions, which are referred to as NRBCs in the remainder of this section, can be divided into two categories, local and non-local NRBCs. Non-local NRBCs are complex but provide very good approximations to the infinite domain and can be exact in a number of situations. Examples of nonlocal NRBCs are found in [50,58,59,60]. Givioli [50] presents nonlocal boundary conditions as the better option of NRBCs because of their robustness and accuracy for a wide range of problems. However, the focus of this chapter is on local NRBCs because this is the type of NRBC used in LS-DYNA.

Local NRBCs are computationally simpler than nonlocal NRBCs but only approximate the infinite domain. Their accuracy depends heavily on the type of problem they are used for and the size of the computational domain. Local NRBCs, can provide exact models of infinite domains but only in the most simple of problems. A big advantage to local NRBCs of the numerical damping type is that they are frequency independent [53]. The VBC discussed previously is an example of a local NRBC. Further examples of local NRBCs are found in [50,61-65]. All use the same basic methodology of applying a traction boundary condition in the form of a numerical damper to model the infinite domain. Local NRBCs can be used in time-dependent wave equation problems, but can also be used in time-harmonic problems [50]. One local NRBC worth noting is the Higdon NRBC [66,67], given in Equation 4.3.

$$\prod_{j=1}^{N}\left(\frac{\partial \phi}{\partial t}+C_j\frac{\partial \phi}{\partial n}\right)=0 \tag{4.3}$$

Compared to the VBC, which is an approximate boundary for waves of normal incidence, the Higdon NRBC is an exact boundary for all normal incident waves that propagate at speed c [50]. Theoretically speaking the accuracy of the Higdon NRBC is unlimited, as pointed out by Givol and Neta who expand the Higdon NRBC to higher orders [68]. Therefore, even if the choice of parameter C_j is inaccurate, the accuracy of the NRBC is not affected because taking a higher order of J will correct any error [68]. Another advantage to the Higdon NRBC is that many NRBCs that had been derived previous to his work can be obtained from Equation 4.3 [50]. This makes the Higdon NRBC very robust in the sense that it combines several NRBCs into one equation. The Higdon NRBC is also robust in the sense that it works well for a wide range of wave propagation problems [68]. A final feature of the Higdon NRBC is that the variable φ in Equation 4.3 is a general field variable, meaning that the Higdon NRBC could be applied directly to LS-DYNA acoustic elements without the need for a boundary interaction term as is the case with the DAA. All of these advantages of the Higdon NRBC make it an attractive option for the box barge model.

To study the performance of the Higdon NRBC when used with acoustic elements a simple local NRBC, the Sommerfeld radiation condition (Equation 4.4), is obtained from the Higdon NRBC. Although it was derived on its own previously [69], the Somerfield radiation condition is simply a first order Higdon NRBC [68].

$$\frac{\partial \phi}{\partial t} + c\frac{\partial \phi}{\partial x} = 0 \tag{4.4}$$

The Sommerfeld condition is useful for one-dimensional problems and has been shown [50] to completely absorb incident waves in stress wave propagation problems.

Furthermore it has been previously used successfully with displacement potential elements in multi-dimensional far-field UNDEX problems [39].

In the following section the both the benefits and disadvantages of using the VBC in LS-DYNA are shown. First a one dimensional far-field UNDEX problem is solved to show a case where the VBC works well when compared to the traditional DAA boundary. Next the a case where the inefficiency of the VBC in LS-DYNA greatly affects the results is shown to suggest the use of the Somerfeld radiation for use in future UNDEX models.

4.2 One-Dimensional Model Results

To show a case where the VBC works well in LS-DYNA the Bleich-Sandler problem is solved in LS-DYNA. This is the same problem Felippa and DeRuntz used [31,32] to validate the CAFE method. In the Bleich-Sandler problem a flat plate of unit thickness sitting on the free surface of a column of fluid (Figure 4.1) is subjected to a far-field UNDEX. The properties of the fluid column and plate are given in Table 4.1 and the properties of the UNDEX are given in Table 4.2. In Table 4.2 DP is the distance from the free surface to the charge and both P_{peak} and τ are defined at a node one element away from the structure.

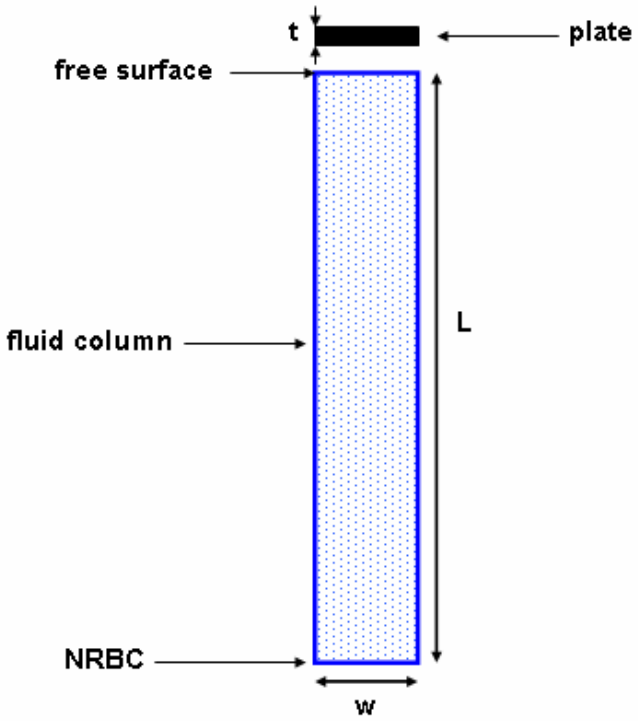

Figure 4.1 Bleich-Sandler problem schematic

Table 4.1 Fluid and structure properties for the Bleich-Sandler problem

Fluid		**Structure**	
L	3.81 m	**l**	3.81 cm
w	3.81 cm	**w**	3.81 cm
t	3.81 cm	**ρ**	5696 kg/m^3
ρ	998 kg/m3	**E**	207 GPa
c	1450 m/s	**υ**	0.3

Table 4.2 UNDEX parameters for the Bleich-Sandler problem

DP	254000 m
P_{peak}	710160 Pa
τ	996 ms

Originally Bleich and Sandler solved this problem analytically in one dimension, however it is not possible to create a true one dimensional model in LS-DYNA. Therefore, when modeled in LS-DYNA the Bleich-Sandler problem becomes quasi-one

dimensional, meaning square elements are used, but the nodes must be consternated to only have one directional degree of freedom.

To model the Bleich-Sandler problem in LS-DYNA the same methodology for far-field UNDEX problems as described in Chapter 3 is used. To model the fluid domain 100 square elements are used and a single shell element is used to model the plate. Initially the DAA (via USA) is applied to the bottom boundary to act as the NRBC. This is done to recreate the results of Felippa and DeRuntz using their exact method. This solution is used as the benchmark solution for the Bleich-Sandler because the results of Felippa and DeRuntz matched the analytical solution to the Bleich-Sandler problem [31,32]. In the second solution, the DAA is replaced by the VBC in LS-DYNA.

Figure 4.2 shows that for the Bliech-Sandler problem a working NRBC is essential for accurate results. Also by looking at the results obtained with no NRBC applied, it is proved that LS-DYNA does not automatically apply a transmitting "acoustic mesh" boundary as the manual implies. Lastly, Figure 4.2 shows that the results obtained with the VBC are similar to the benchmark solution. This proves that the VBC has potential applications to simple far-field UNDEX problems and could be used to replace the DAA as a NRBC. However as the results of section 3.4.4 show, the VBC does not perform well in more complex UNDEX problems. Therefore, in the next section a one dimensional case where the VBC fails to work in LS-DYNA is used to suggest the use of a the Somerfeld NRBC that combines the benefit of computationally efficiency with the added benefit of direct application to acoustic elements.

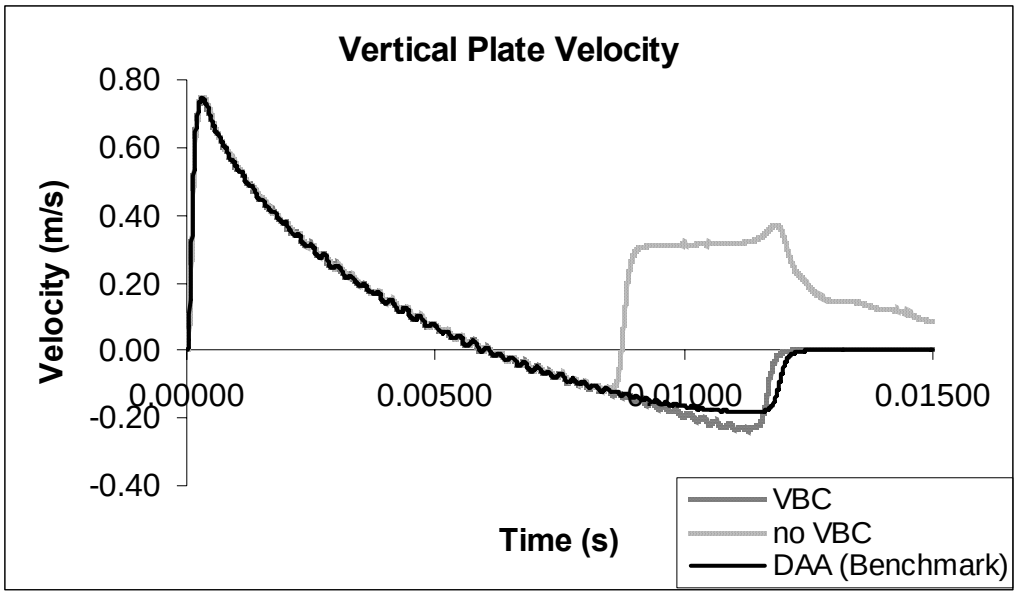

Figure 4.2 Vertical velocity of the Bleich-Sandler plate for three different fluid bottom boundary conditions

To show a case where the VBC fails to work properly in LS-DYNA a one-dimensional acoustic wave propagation problem was setup as shown in Figure 4.3. In this problem a pulse loading, *p(t)* , is applied to the x=0 boundary of an infinite bar. The pulse loading is a discontinuous function, thus it tests the ability of the VBC to handle functions similar to the shock wave in UNDX problems without using the INITIAL_DETONATION card. The infinite domain of the bar is modeled by applying the VBC to the bar at x=L. To show what the LS-DYNA solution should be the problem was also solved using Matlab with the Sommerfeld radiation condition used instead of the VBC at x=L.

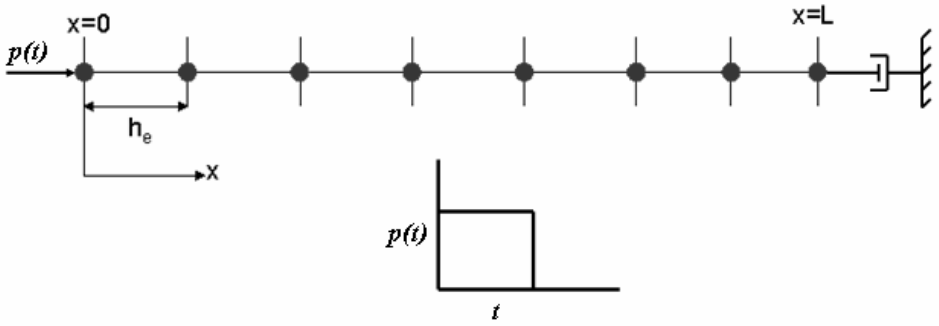

Figure 4.3 Schematic of one-dimensional acoustic wave propagation problem

In Matlab the fluid of the bar is modeled using the acoustic pressure element formulation instead of the displacement potential formulation presented in Section 3.6.2. This choice was made so that the nodal pressure could be computed faster and does not affect the results of the solution. The weak formulation (Equation 4.6) of the governing equation for the acoustic pressure element (Equation 4.5) with the Sommerfeld boundary condition is given in Equation 4.5, where φ is a test function. Note that the addition of the Sommerfeld boundary adds the *dp/dt* term in the weak formulation of the problem.

$$\nabla^2 p - \frac{1}{c^2}\ddot{p} = 0 \tag{4.5}$$

$$\begin{aligned} &\textit{Find} \quad p \in H_0^1[0, L] \quad \textit{such that} \\ &\int_0^L \frac{\partial p}{\partial x}\frac{\partial \phi}{\partial x}dx + \int_0^L \frac{1}{c^2}\frac{\partial^2 p}{\partial t^2}\phi dx - \int_0^L \frac{1}{c}\frac{\partial p}{\partial t}\phi dx = 0 \\ &\textit{for every} \quad \phi \in H_0^1 \quad [0, L] \end{aligned} \tag{4.6}$$

The standard Galerkin approach, Equation 4.7, is used to approximate the solution of Equation 4.5 using piecewise-linear basis functions, ψ, to discretize the domain.

$$\text{Find} \quad p^n \in H_0^1[0,L] \quad \text{such that}$$

$$\int_0^L \frac{\partial p^n}{\partial x}\frac{\partial \phi^n}{\partial x}dx + \int_0^L \frac{1}{c^2}\frac{\partial^2 p^n}{\partial t^2}\phi^n dx - \int_0^L \frac{1}{c}\frac{\partial p^n}{\partial t}\phi^n dx = 0$$

$$\text{for every} \quad \phi^n \in H_0^1 \quad [0,L] \tag{4.7}$$

The semi-discrete equations are given in Equations 4.8 and 4.9, the damping matrix *C* that results from the addition of the Sommerfeld boundary has only one non-zero term at boundary node *n* which in the global system is located at x=L [50].

$$\text{Let} \quad p^n = \sum_{i=1}^{n} p_i \psi_i \qquad \dot{p}^n = \sum_{i=1}^{n} \dot{p}_i \psi_i \quad \ddot{p}^n = \sum_{i=1}^{n} \ddot{p}_i \psi_i \quad \phi^n = \sum_{j=1}^{n} c_j \psi_j$$

$$c_j\left[\int_0^L \frac{\partial \psi_i}{\partial x}\frac{\partial \psi_j}{\partial x}dx\right]p_i + c_j\left[\int_0^L \frac{1}{c^2}\psi_i\psi_j dx\right]\ddot{p}_i - c_j\left[\int_0^L \frac{1}{c}\psi_i\psi_j dx\right]\dot{p}_i = 0 \tag{4.8}$$

$$[K]p_i + [M]\ddot{p}_i - [C]\dot{p}_i = 0 \tag{4.9}$$

$$M_{ij} = \frac{1}{c^2}\int_0^L \psi_i\psi_j dx \qquad C_{nn} = \frac{1}{c}$$

$$K_{ij} = \int_0^L \psi_i'\psi_j' dx$$

The 1-D acoustic wave propagation problem is then solved using both Matlab and LS-DYNA. Both methods use acoustic elements and the input parameters given in Table 4.3. Both methods also used lumped mass matrices and a central difference time integration scheme. The Matlab program is validated (see Appendix C) using a wave propagation problem solved in [70].

Table 4.3 Input for 1-D acoustic wave propagation problem

L	10 m
h_e	1 m
Δt	.049 ms
c	1514 m/s
p(t)	1000 Pa for $t<7\Delta t$

In LS-DYNA solid elements were used to model the bar in the configuration shown in Figure 4.4. On the cross section of the fluid bar the solid elements are 0.5m x 0.5m squares, the x-direction length of the elements are 1m. To make the problem one-dimensional in the LS-DYNA model, the nodes on the fluid bar were constrained so that only motion in the x-direction was allowed.

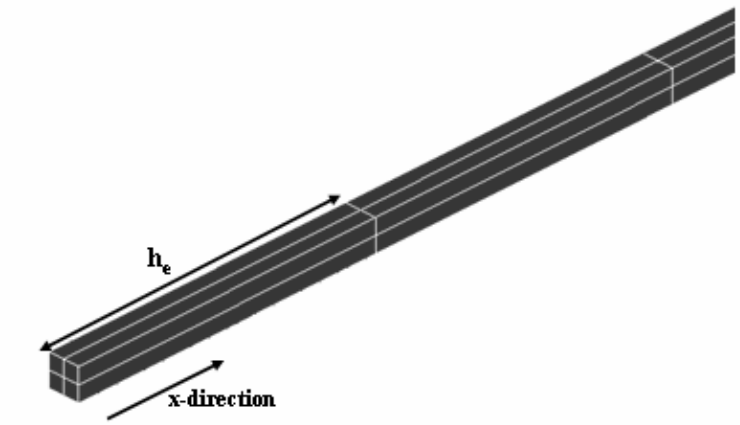

Figure 4.4 Element configuration for the LS-DYNA 1-D acoustic wave model

The Matlab and LS-DYNA results for the 1-D acoustic wave propagation problem are given in Figure 4.5. The results show that the Sommerfeld boundary condition works well with acoustic pressure elements as almost no reflections are seen. A plot of results obtained with a fixed boundary is included for the LS-DYNA model to show that the viscous boundary condition does absorb some of the incident pressure wave. However, the VBC also shows a large amount of the reflected wave re-enters the

model when it should be absorbed. Compared to the Sommerfeld boundary condition, the viscous boundary condition acts more like a fixed boundary than a NRBC in this case. In fact for this problem the VBC behaves more like it did for the box barge problem in Section 3.4.4. The Matlab model results also show that the Sommerfeld and likewise the Higdon NRBCs can be used successfully in pulse wave propagation problems where an acoustic element formulation is used.

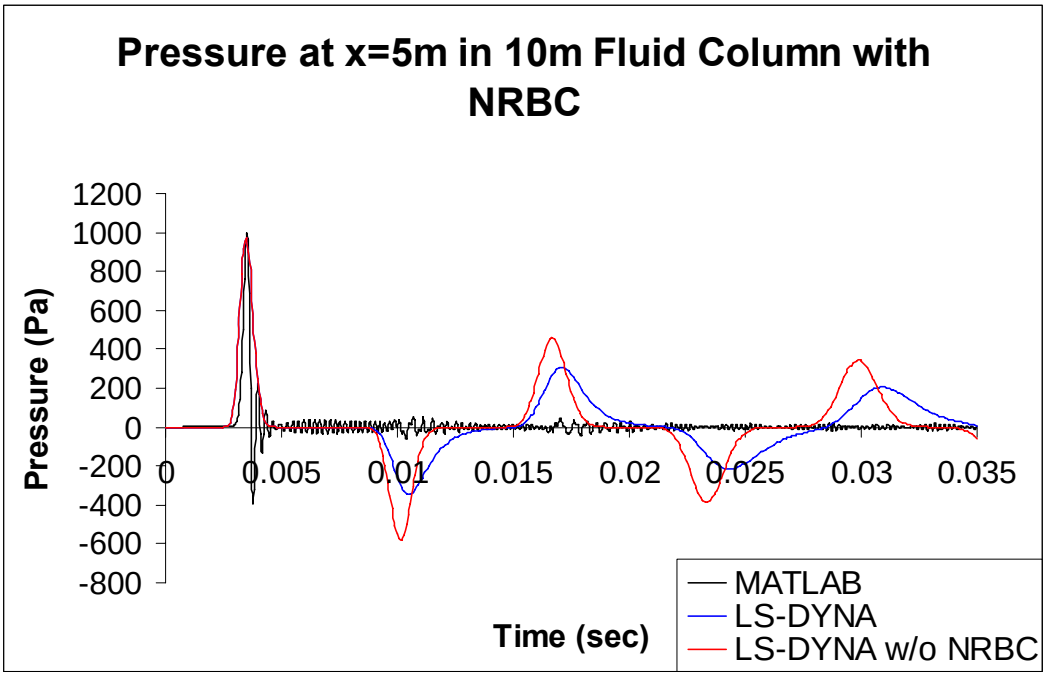

Figure 4.5 Comparison of LS-DYNA and Matlab results for the 1-D acoustic wave propagation problem

The results of the Matlab and Bleich-Sandler model show that while the VBC works well in some cases it fails to work correctly in other cases. The problems encountered with the VBC in LS-DYNA could be a result of any of the limitations that have been described in this chapter, but more investigation is necessary to determine the exact cause. The conclusions of this investigation into NRBCs in LS-DYNA are first that numerical damping NRBCs, such as the Somerfeld condition and the VBC, are easy

to implement and work well with acoustic elements. Secondly, when numerical damping NRBCs are used under the right conditions in simple far-field UNDEX problems they perform almost identically to the traditional DAA NRBC. The major difference between the numerical damping NRBCs and the DAA is that the DAA accounts for added mass effects in the fluid. However in simple problems, like the box barge, added mass effects can be neglected and therefore it is not necessary to use the more complex DAA NRBC in far-field UNDEX problems. Lastly, use of the VBC in multiple dimensions and some one dimension problems is problematic in LS-DYNA and future work should consider the use of the Somerfeld or Higdon NRBCs which are better suited for acoustic formulations and have been proven to work in multiple dimensions [39].

4.3 Special Considerations for UNDEX Boundaries

Thus far the discussion of NRBCs has been limited to boundary conditions that assume that the incident wave propagates to infinity once it leaves the finite domain. In other words the NRBCs in 4.1 do not account for the effects of the infinite domain on the modeled domain. This assumption is valid for far field UNDEX problem of type 1 where only the shock wave and cavitation effects are considered because in these types of problems the cavitation region can be contained within the finite model domain, and the shock wave does not need to interact with fluid in the infinite domain. An aspect of the UNDEX problem that the NRBCs discussed in 4.1 do not include is the changes in the fluid domain due to the interaction between the fluid and structure. Specific NRBCs of the numerical damping type have been developed for fluid-structure interaction problems [47,71,72] but not the general UNDEX case.

The general UNDEX case presents a unique challenge in the development of NRBCs because of the presence of the gas bubble in the fluid domain. The gas bubble is a low frequency phenomena, in contrast to the shock wave which is a high frequency phenomena. Models that account for gas bubble dynamics that have been run at Virginia Tech [73] have shown that the use of a traditional NRBC in the fluid model does not allow the dynamics of the gas bubble to be properly captured in the UNDEX model.

Therefore, a NRBC for the general UNDEX case must be able to explicitly model an infinite fluid and not just an infinite space. This means, the UNDEX boundary condition must account for phenomena such as hydrostatic pressure and density changes which occur in the infinite fluid but affect the fluid in the finite domain. The development of such a boundary condition is left for future work in UNDEX modeling.

CHAPTER 5 CONCLUSIONS AND FUTURE WORK

In this thesis a simple box like ship was subjected to an underwater explosion using the numerical modeling tools USA and LS-DYNA. The box barge model consisted of the box barge mesh in the structural domain and the fluid mesh in the fluid domain. The results obtained from the USA and LS-DYNA simulations were analyzed and compared against the general physics of underwater explosions and results from previous work.

USA was found to be an adequate method of modeling the box barge response to the shock wave loading resulting from an UNDEX, but it cannot be used in problems with cavitaiton.

The LS-DYNA models show that LS-DYNA can model the response due to the initial shock wave loading but the accuracy of these results is very dependent on the fluid mesh. The size of the fluid mesh controls the accuracy of the box barge response to the shock loading because the fluid mesh size determines how well the peak pressure of the shock wave is captured. Through a comparison of results taken from various fluid mesh sizes it was found that failure of LS-DYNA to accurately capture the peak pressure of the shock wave greatly reduces the accuracy of cavitation capture which is critical to the structural response after the initial shock loading. The LS-DYNA models also show that LS-DYNA cannot capture the discontinuity of the shock wave. An assessment of the assumptions made in current LS-DYNA far-field UNDEX models is given in Table 5.1.

An investigation of the fluid element formulation in LS-DYNA showed that the acoustic displacement potential/CAFE element can theoretically be used to capture shock waves but in reality the pressure of the shock wave is smeared over multiple elements

because LS-DYNA uses the standard Galerkin formulation of the governing equations. The inviscid assumption made in the acoustic element derivation was shown to cause inaccuracies in the no-slip condition used in most LS-DYNA UNDEX models for the fluid-structure boundary. These inaccuracies cause the global motion of the box barge to be inadequately modeled.

Table 5.1 Assessment of assumptions made in current LS-DYNA UNDEX models

Assumption	Accept	Review	Reject
UNDEX Phenomena Assumptions			
Plane wave shock			X
No bubble pulses		X	
No bubble migration	X		
No bottom effects	X		
Global structure loading			X
Elastic deformation of hull	X		
UNDEX Modeling Assumptions			
Captured peak pressure of shock does not important			X
Cavitation effects are important	X		
Acoustic element adequate for UNDEX		X	
Inviscid fluid			X
NRBC for fluid models	X		
DAA NRBC for fluid models		X	

The affect of boundary conditions on the box barge model was also studied. In previous models USA was used to provide a DAA radiation boundary on the fluid. In the box barge model this was not done because the use of USA is computationally expensive, the results can be problem dependent [1], and the LS-DYNA and USA manuals do not address modifications to the USA model necessary to use the DAA fluid boundary with acoustic elements. In addition to this it was found that LS-DYNA automatically applies a similar boundary to the fluid model when the INITIAL_DETONATION option is used with acoustic pressure elements to model an UNDEX. The boundary is also inadequate.

In order to compare the box barge model with previous UNDEX models that used the DAA boundary condition, a different radiation boundary condition, the viscous boundary condition, was applied to the box barge fluid model. It was found that the viscous boundary condition works much like the traditional DAA boundary in simple one dimensional far-field UNDEX problems but is not adequate with multiple dimension fluid models when the standard fluid modeling rules are followed. These findings are particularly important because many researchers use these boundary conditions and the LS-DYNA literature provides not discussion or limitations on their use.

A one-dimensional acoustic wave propagation problem demonstrated that the Higdon NRBC, a boundary condition similar to the viscous boundary condition, can be used with acoustic elements and has several features that make it attractive for use in UNDEX models similar to the box barge model, but it cannot be implemented in the current version of LS-DYNA. The need for an UNDEX infinite boundary that can model an infinite fluid by accounting for hydrostatic and density changes was also discussed.

From these findings it is concluded that LS-DYNA's applicability to the general UNDEX problem is limited because of the issues surrounding the inaccuracy of shock capture, the basic assumptions of the fluid model, and the inadequate or computationally expensive boundary conditions. LS-DYNA is only adequate to model the initial shock loading of a ship subjected to an UNDEX. It cannot be used to model mid and late-time phenomena such as cavitation reloading and bubble pulses.

However, LS-DYNA provides many capabilities and solvers that are extremely useful.

To improve the accuracy and extend the application of LS-DYNA to mid and late-time UNDEX and to near-field UNDEX models which have similar problems that have not been addressed explicitly in this thesis the following future work is recommended.

- Increase the computing power and use more elements in the LS-DYNA fluid mesh to assess the improvement in capturing the shock wave.
- Create a non-uniform fluid mesh in LS-DYNA where smaller elements are concentrated near the fluid-structure boundary to improve the capture of the shock wave.
- Further test the use of the VBC in the box barge models to optimize its preformance
- Develop a 2-D code for model and boundary condition development including:
    - Use Discontinuous Galerkin or Petrov-Galerkin methods to see if they improve shock capture.
    - Include viscosity in the fluid element formulation so that the no-slip boundary condition is not violated at the fluid-structure boundary.
    - Develop a fluid model that models the global motion of the ship
    - Incorporate a working NRBC, such as the Higdon, into an UNDEX model to determine the effect it has on the UNDEX model.
    - Develop a NRBC specifically for the UNDEX problem that models the infinite domain as an infinite fluid.

- Extend the UNDEX finite element model in LS-DYNA to include Type 2 far-field problems.
- Present new models and BC for incorporation in LS-DYNA

REFERENCES

1) Baron, M.L. and Daddazio, R. "Underwater Explosions," in *Shock and Vibration Computer Programs*, 1995.

2) OPNAV Instruction 9070.1, "Shock Hardening of Surface Ships," 12 January 1987.

3) Shin, Y. and Schneider, N. "Ship Shock Trial Simulation of USS Winston S. Churchill (DDG 81): Modeling and Simulation Strategy and Surrounding Fluid Volume Effects," *74th Shock and Vibration Symposium*, San Diego CA, Oct. 26-31 2003.

4) Reid, W.D., *The Response of Surface Ships to Underwater Explosions*, Department of Defense, 1994.

5) Mair, H.U., et al., "Lagrangian Hydrocode Modeling of Underwater Explosive/Target Interaction," *61st Shock and Vibration Symposium*, Vol. 5, pp. 79-89.

6) Schittke, H.J., et. al "The Program DYSMAS/ELC and its Application on Underwater Shock Loading of Vessels". *60th Shock and Vibration Symposium*, Vol.1, pp. 55-78, 1989.

7) Misovec, A.P., *Explosion Phenomena*, David W. Taylor Naval Ship Research and Development Center, 1976.

8) Cole, R.H., *Underwater Explosions*, Princeton University Press, 1948.

9) Reid, W.D., *The Response of Surface Ships to Underwater Explosions*, Department of Defense, 1994

10) Keil, A.H., *The Response of Ships to Underwater Explosions*, Department of the Navy, 1961.

11) Wood, S.L., "Cavitation Effects on a Ship-Like Box Structure Subjected to an Underwater Explosion," Master's Thesis, Naval Postgraduate School, Monterey, CA., 1998.

12) Makinen, K., "Cavitation Models for Structures Excited by a Plane Shock Wave," *Journal of Fluids and Structures*, Vol. 12, pp. 85-101, 1998.

13) Swisdak, M. "Explosion Effects and Properties: Part II.– Explosion Effects in Water," NSWC/WOR TR 76-166, 1978.

14) Arons, A.B. "Secondary Pressure Pulses Due to Gas Globe Oscillation in Underwater Explosions. II. Selection of Adiabatic Parameters in the Theory of Oscillation". *Journal of the Acoustical Society of America*, Vol. 20, pp.277, 1948.

15) Rogers, P.H. "Weak-shock Solution for Underwater Explosive Shock Waves," *Journal of the Acoustical Society of America*, Vol. 62, pp.1412, 1977.

16) Mair, H.U. "Review: Hydrocodes for Structural Response to Underwater Explosions," *Shock and Vibration* Vol. 6(2), pp.81-96, 1999.

17) Swegle, J.W., and Attaway, S.W. "On the Feasibility of Using Smoothed Particle Hydrodynamics for Underwater Explosion Calculations," *Computational Mechanics*, Vol. 17, pp.151-168, 1995.

18) Pangilinan, G.I., et. al "Time-Resolved Pressure Measurements From and Underwater Explosion," *PVP-Vol. 431*, pp.185-191, 2001.

19) Chisum, J.E.., "Multimaterial Eulerian and Coupled Lagrangian-Eulerian Finite Element Analysis of Underwater Shock Problems," Master's Thesis, Naval Postgraduate School, Monterey, CA., 1995.

20) Andelfinger, U. "Simulations of Underwater Explosions against Submerged Structures using the DYSMAS/ELC Code-Part A," *65th Shock and Vibration Symposium*, pp.243-251, 1994.

21) DeRuntz, J.A. "The Underwater Shock Analysis Code and its Applications," *60th Shock and Vibration Symposium*, Vol.1, pp.89-107, 1989.

22) DeRuntz, J.A., "The Underwater Shock Analysis (USA) Manual," Unique Software Applications, Colorado Spring, CO, May, 1996.

23) Fox, S.L., "Nonlinear Response of Cylindrical Shells to Underwater Explosion: Testing and Numerical Prediction Using USA/DYNA3D," Naval Postgraduate School, Monterey, CA., 1992.

24) Beiter, K.A., "The Effect of Stiffener Smearing in a Ship-Like Box Structure Subjected to an Underwater Explosion, in Mechanical Engineering," Naval Postgraduate School, Monterey, CA., 1998.

25) Liu, M.B., et. al "Smoothed Particle Hydrodynamics for Numerical Simulation of Underwater Explosion," *Computational Mechanics*, Vol. 30, pp.106-118, 2003.

26) Shin, Y., "Total Ship Shock Modeling and Simulation using LS-DYNA/USA". *LS-DYNA User Conference*, Osaka, Japan October, 2000.

27) Hallquist, J.O., "LS-DYNA Theoretical Manual" Livermore Software Technology Corporation, Livermore, CA, 1998.

28) LSTC, "LS-DYNA Keyword Users Manual" Version 970, Livermore Software Technology Corporation, Livermore, CA, 2003.

29) Hughes, T.J.R., *The Finite Element Method: Linear Static and Dynamic Finite Element Analysis*, Dover Publications, 2000.

30) Deruntz, J.A. "Application of the USA Code to Underwater Shock Problems," *73rd Shock and Vibration Symposium*, 2002.

31) Felippa, C.A. and DeRuntz, J.A., "Finite Element Analysis of Shock Induced Hull Cavitaiton," *Computational Methods in Applied Mechanical Engineering* Vol. 44, pp.297-337, 1984.

32) Felippa, C.A. and DeRuntz, J.A., "Acoustic Fluid Modeling by the Displacement Potential Formulation, with Emphasis on the Wedge Element," *Computers and* Structures, Vol. 41(4), pp.669-686, 1991.

33) Sprague, M.A., and Geers, T.L. "Computational Treatments of Cavitation Effects in Near-Free-Surface Underwater Shock Analysis," *Shock and Vibration* Vol.7, pp.105-122, 2001.

34) Zienkiewicz, O.C. and Bettess, P. "Fluid-Structure Dynamic Interaction and Wave Forces. An Introduction to Numerical Treatment," *International Journal for Numerical Methods in Engineering*, Vol. 13, pp.1-16, 1978.

35) Morand, H. and Ohayon, R. "Substructure Variational Analysis of Vibrations of Coupled Fluid-Structure Systems. Finite Element Results," *International Journal for Numerical Methods in Engineering*, Vol. 14, pp.741-755, 1979.

36) Muller, C. "Simplified Analysis of Linear Fluid-Structure Interaction," *International Journal for Numerical Methods in Engineering*, Vol.17, pp.113-121, 1981.

37) Zienkiewicz, O.C., Taylor, R.L., and Nitharasu, P., *The Finite Element Method for Fluid Dynamics 6th Edition*, Elsevier, 2005.

38) Sprague, M.A., and Geers, T.L., "A Spectral-Element Method for Modeling Cavitation in Transient Fluid-Structure Interaction," *International Journal for Numerical Methods in Engineering*, Vol. 60, pp. 2467-2499, 2004.

39) Newton, R.E. "Finite Element Analysis of Shock-Induced Cavitation," *ASCE Spring Convention*, Portland, OR., 1980.

40) Casey, G.F. and Oden, J.T., *Finite Elements: Fluid Mechanics Vol. VI*, Prentice Hall, 1986.

41) Cockburn, B., Karniadakis, G.E., and Shu, C. (Eds.), *Discontinuous Galerkin Methods*, Springer, 2000.

42) Atkins, H.C., "Local Analysis of Shock Capturing Using Discontinuous Galerkin Methodology," AIAA paper no. 97-2032, 1997.

43) Atkins, H.C. and Shu, C.W., "Continual Development of the Discontinuous Galerkin Method for Areoacoustic Applications," AIAA paper no. 97-1581, 1997.

44) Shu, C.W. and Osher, S. "Efficient Implementation of Essentially non-Oscillatory Shock Capturing Schemes," *Journal of Computational Physics,* Vol. 77, pp.361-383, 1988.

45) Lapidus, A. "A Detached Shock Calculation by Second Order Finite Differences," *Journal of Computational Physics*, Vol.2, pp.54-177, 1967.

46) Sharan, S.K. "Analysis of Unbounded Field Problems using Dampers," *Communications in Applied Numerical Methods*, Vol. 4, pp.761-766, 1988.

47) Pinsky, P.M. and Abboud, N.N. "Two Mixed Variation Principles for Exterior Fluid-Structure Interaction Problems," *Computers & Structures* Vol. 33(3), pp.621-635, 1989.

48) Lysmer, J. and Kuhlemeyer, R.L. "Finite Dynamic Model for Infinite Media," *Journal of Engineering Mechanics*, ASCE, pp.857-877, 1969.

49) Choen M. and Jennings, P.C. "Silent Boundary Methods for Transient Analysis," in *Computational Methods for Transient Analysis*, North Holland, pp. 301-360, 1983.

50) Givoli, D. *Numerical Method for Problems in Infinite Domains*, Elsevier, 1992.

51) Kunar, R.R. and Rodriguez-Ovejero, L. "A Model with Non-Reflecting Boundaries for use in Explicit Soil-Structure Interaction Analyses," *Earthquake Engineering and Structural Dynamics*, Vol. 8, pp.361-374, 1980.

52) Shakib, H. "Evaluation of dynamic eccentricity by Considering Soil-Structure Interaction; A Proposal for Seismic Design Codes," *Soil Dynamics and Earthquake Engineering*, Vol. 24, pp.369-378, 2004.

53) Dieterman, H.A. and Gajewski, R.R. "An Improved Viscous Boundary for Dynamic Soil-Structure Interaction," *Computer Assisted Mechanics and Engineering Sciences*, Vol. 3, pp.55-64, 1996.

54) Castellani, A. "Boundary Conditions to Simulate an Infinite Space," *Meccanica*, Vol. 9(3), pp.199-205, 1974.

55) Zienkiewicz, O.C. and Bettess, P. "Infinite Elements in the Study of Fluid-Structure Interaction Problems," *Lecture Notes in Physics*, No.58, 133-172, Springer, 1976.

56) Bettess, P. and Zienkiewicz, O.C. "Diffraction and Refraction of Surface Waves Using Finite and Infinite Elements," *International Journal of Numerical Methods in Engineering*, Vol. 11, pp.1271-1290, 1977.

57) Zienkiewicz, O.C. and Bettess, P., Chiam, T.C., and Emson, C. "Numerical Methods for Unbounded Field Problems and a New Infinite Element Formulation," *Computational Methods for Infinite Domain Media-Structure Interaction*, AMD Vol. 46, pp.115-148, ASME, 1981.

58) Thompson, L.L. and Huan, R. "Finite Element Formulation of Exact Non-Reflecting Boundary Conditions for the Time-Dependent Wave Equation," *International Journal for Numerical Methods in Engineering*, Vol. 45, pp.1607-1630, 1999.

59) Grote, M.J. and Keller, J.B. "Exact Nonreflecting Boundary Conditions for the Time Dependent Wave Equation," *SIAM Journal of Applied Mathematic,* Vol. 55(2), pp.280-297, 1995.

60) Grote, M.J. and Keller, J.B. "Exact Nonreflecting Boundary Conditions for Elastic Waves," *SIAM Journal on Applied Mathematic,* Vol.60(3), pp.803-819, 2000.

61) Engqist B. and Majda, A. "Absorbing Boundary Conditions for the Numerical Simulation of Waves," *Mathematics of Computation*, Vol. 31, pp.629-652, 1977.

62) Robinson, A.R., "The Transmitting Boundary – Again," in *Structural and Geotechnical Mechanics*, Prentice Hall, 1977.

63) Givoli, D. and Platashenko, I. "Optimal Local Non-Reflecting Boundary Conditions," *Applied Numerical Mathematics*, Vol. 27, pp.367-384, 1998.

64) Barry, A., Bielak, J. and MacCamy, R.C., "On Absorbing Boundary Conditions for Wave Propagation," *Journal of Computational Physics*, Vol. 79, pp.449-468 1988.

65) Halpern, L. "Absorbing Boundary Conditions for Discretization Schemes of the One-Dimensional Wave Equation," *Mathematics of Computation*, Vol. 38, pp.415-429, 1982.

66) Higdon, R.L., "Numerical Absorbing Boundary Conditions for the Wave Equation," *Mathematics of Computation*, Vol. 49, pp.65-90, 1987.

67) Higdon, R.L., "Absorbing Boundary Conditions for Acoustic Elastic Waves in Stratified Media," *Journal of Computational Physics,* Vol. 101, pp.386-418, 1992.

68) Givoli, D. and Neta, B. "High-order Non-Reflecting Boundary Scheme for Time-Dependent Waves," *Journal of Computational Physics*, Vol. 186, pp.24-46, 2003.

69) Sommerfeld, A., "Lectures on Theoretical Physics," Vol. VI(28), in the series: *Partial Differential Equations in Physics*, Academic Press, 1964.

70) Yamada, Y. and Nagai, Y. “Analysis of One-Dimensional Stress Wave by the Finite Element Method,” *Seisan-Kenkyu*, Vol. 23(5), pp.186-189, 1971.

71) Sharan, S.K. “A Non-Reflecting Boundary in Fluid-Structure Interaction,” *Computers & Structures*, Vol. 26(5), pp.841-846, 1987.

72) Kreigsmann, G.A. and Scandrett, C.L. “Assessment of a New Radiation Damping Model for Structural Acoustics Interaction,” *Journal of the Acoustical Society of America*, Vol. 79, pp.9-17, 1986.

73) Webster, K., “Investigation of Close-in/Proximity Underwater Explosion Effects on Ship-Like Plates Using the Multi-Material Arbitrary Lagrangian Eulerian Finite Element Method,” Unpublished Master’s Thesis, Virginia Tech, Blacksburg, VA.

74) Sprague, M.A. and Geers, T.L., “A Spectral-element/finite-element Analysis of a Ship-Like Structure Subjected to an Underwater Explosion,” *Computer Methods in Applied Mechanics and Engineering*, Vol. 195, pp.2149-2167, 2006.

APPENDICIES

Appendix A
Example USA and LS-DYNA Inputs

USA FLUMAS input file example:

```
*fluid_density = 0.9389E-4
*fluid_sound_speed = 59606.3
*symmetry_free_surface
78.74 0., 0., 1., 14.7, 386.4,
```

The flumas input file is used to define the external fluid properties in the USA model. The *fluid_density command defines the fluid mass density in standard U.S. units. The *fluid_sound_speed command is used to define the speed of sound in the fluid. Lastly, the *symmetry free surface is used to define the free surface of the fluid using the x, y, and z coordinates and the directional cosines of a point on the free surface. This command also defines the atmospheric pressure and gravitational acceleration constant in the last two entries of the command.

USA AUGMAT input file example:

```
*daa_formulation, daa1
```

The *daa_formulation command selects the PWA, DAA 1 or DAA 2 to be used in the USA simulation. In this example DAA 1 is used.

USA TIMTIN input file example:

```
*integration,
0, 1.0E-5

*incident_pressure, type=expo
118.11,98.425,-216,118.11,98.425,0
5575, 1.866E-4, 8.754E-6, 201
```

The *integration command in the timtin file controls the start time and time step for the USA simulation. The *incident_pressure command defines the shock wave pressure loading on the ship structure. Defining the type as "expo" tells USA that the shock wave is an exponentially decaying function defined at the standoff point. The first three entries in the second line of the *incedent_pressure command define the position of the explosive charge, the following three lines define the standoff point, taken to be on the wet surface of the structure in this example, of the model. In the third line the first entry is the incident pressure at the standoff point and the second entry is the time constant of the shock wave, which is calculated by similitude. The final two entries are default values that set parameters for the time-history output files in LS-DYNA.

USA/LS-DYNA coupling option: BOUNDARY_USA_SURFACE input

```
$---+----1----+----2----+----3----+----4----+----5----+----6----+----7----+----8
$                                                                              $
$                          BOUNDARY USA SURFACE CARDS                          $
$                                                                              $
$---+----1----+----2----+----3----+----4----+----5----+----6----+----7----+----8
*BOUNDARY_USA_SURFACE
$^USA SURFACE CARD 1
$      SSID    WETDRY      NBEAM
       401         1          0
```

SSID – defines the set of elements that makes up the DAA wet surface in the LS-DYNA model

WETDRY – this turns the coupling between USA and LS-DYNA on or off

LS-DYNA MAT_ACOUSTIC input

```
$---+----1----+----2----+----3----+----4----+----5----+----6----+----7----+----8
$                                                                             $
$                              MATERIAL CARDS                                 $
$                                                                             $
$---+----1----+----2----+----3----+----4----+----5----+----6----+----7----+----8
*MAT_ACOUSTIC
$^M-202
$       MID        RO         C      BETA        CF     ATMOS      GRAV
        202    1025.0    1514.0       0.50       0.0  101300.0      9.81
$        XP        YP        ZP        XN        YN        ZN
        0.0       2.5       2.0       0.0       0.0       1.0
```

MID – Material ID number

RO – Fluid density

C – speed of sound in fluid

BETA – numerical damping factor

CF – flag for consideration of cavitation

ATMOS- atmospheric pressure

GRAV – gravitational acceleration constant

XP,YP,ZP – coordinates of a point on the free surface of the fluid model

XN,YN,ZN – directional cosines of the free surface normal vector

LS-DYNA MAT_ELASTIC input

```
$---+----1----+----2----+----3----+----4----+----5----+----6----+----7----+----8
$                                                                             $
$                              MATERIAL CARDS                                 $
$                                                                             $
$---+----1----+----2----+----3----+----4----+----5----+----6----+----7----+----8
*MAT_ELASTIC
$^STEEL
$       MID        RO         E        PR        DA        DB
        201  7779.9541.9000E+11     0.281       0.0       0.0
```

MID – material ID number

RO – material density

E – Young's modulus

PR – Possion's ratio

LCSS – load curve ID for stress-strain curve

LS-DYNA INITIAL_DET input

```
$---+----1----+----2----+----3----+----4----+----5----+----6----+----7----+----8
$                                                                              $
$                          INITIAL DETONATION CARDS                            $
$                                                                              $
$---+----1----+----2----+----3----+----4----+----5----+----6----+----7----+----8
*INITIAL_DETONATION
$^DETONATION CARD 1
$       PID         X         Y         Z        LT
         -1       4.5       2.5     -18.0       0.0
$      PEAK     DECAY        XS        YS        ZS       NID
 4661000.0 0.0002867       4.5       2.5      -0.5      1583
```

PID – option to define how initial detonation card is applied, here it is selected to be applied to acoustic elements

X,Y,Z – coordinates of charge location

LT – time that the charge ignites in simulation

PEAK – shock wave peak pressure at the initialization point in the fluid model

DECAY – time constant of the shock wave

XS,YS,ZS – coordinates of standoff point

NID – node number of a node that is one element away from the fluid-structure boundary

Appendix B
Example of Similitude Calculations for LS-DYNA input

For an example of how similitude is used to calculate the shock wave parameters for input into LS-DYNA and USA take the example problem of a 10kg TNT charge that detonations 20 meters below the water surface. First, the necessary constants, material data, and point of interest, *R*, where the shock wave parameters will be calculated are defined.

Charge Parameters

Charge Type: TNT

$Z := 20m$ — **Depth of Explosion (surface to charge center)**

$Z_o := Z + 10.05 \cdot m$ — **Hydrostatic depth at inital charge location**

$W := 10kg$ — **Mass of explosive charge**

$R := 17.75m$ — **Distance from charge of point P, our point of intrest**

$\rho := 1.6 \cdot \frac{gm}{cm^3}$ — **Density of charge**

$P_{static} := 1 \cdot atm + 1025 \cdot \frac{kg}{m^3} \cdot g \cdot Z$ — **Hydrostatic pressure at inital charge location (taken at center of charge)**

$P_{atmos} := 101.3 \cdot 10^3 Pa$ — **Atmospheric pressure**

$c := 1514 \cdot \frac{m}{s}$ — **Speed of sound in water**

Next, the peak pressure approximation is used to determine the peak pressure and the total pressure at the point of interest, *R*. These calculations require the use of the similitude constants K_p and α_p.

Shock Wave Calaculations

$K_p := 52.4 \qquad \alpha_p := 1.13$ — **Shock wave similitude constants**

$$P_{peak} := K_p \cdot \left[\frac{\left(\frac{W}{kg}\right)^{\left(\frac{1}{3}\right)}}{\frac{R}{m}} \right]^{\alpha_p} \cdot 10^6 \cdot Pa$$

Peak pressure approximation

$P_{peak} = 4.835 \times 10^6 Pa$ — **Peak pressure at point P**

$P_{total} := P_{static} + P_{peak} + P_{atmos}$ — **Total pressure at point P**

$P_{total} = 5.239 \times 10^6 Pa$

The final step is to calculate the time or decay constant for the shockwave. In this calculation the similitude constants are changed to K_τ and α_τ. Once the time constant is calculated the arrival time of the shock wave at the point of interest is found assuming the shock wave travels at the speed of sound, c, and the pressure-time history of the point of interest, R, is plotted.

$$t_{peak} := \frac{R}{c}$$ **Time that peak pressure occurs**

Pressure-Time history of point R

$$P(t) := \begin{cases} \left[P_{total} \cdot e^{-\left(\frac{t - t_{peak}}{\tau}\right)} \right] & \text{if } t \geq t_{peak} \\ P_{static} & \text{otherwise} \end{cases}$$

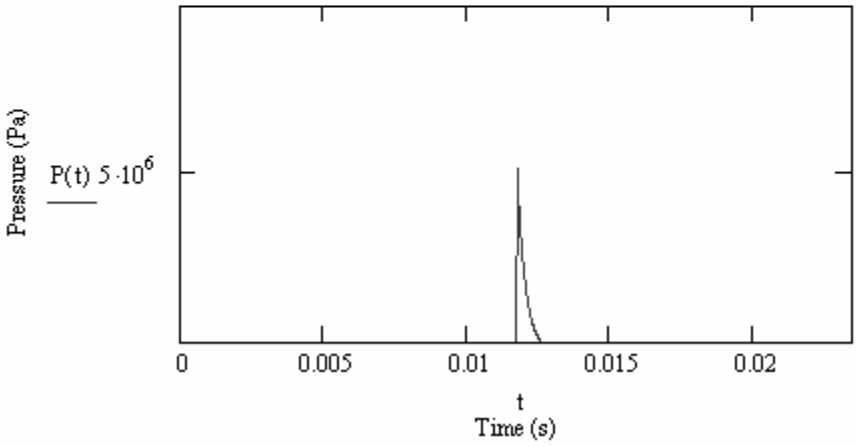

Appendix C
Matlab code validation

To validate the Matlab program used in Section 4.2 a similar one-dimensional problem solved in [70] was used. The validation problem was for stress wave propagation in a cantilever elastic bar. To model this problem in the Matlab code the

$$\nabla^2 p - \frac{1}{c^2} \ddot{p} = 0$$

element formulation in the code was changed slightly. In the Section 4.2 problem acoustic pressure elements, governed by the following equation, were used.

(B.1)

To model the stress wave in elastic bar, the elements equations are governed by a similar relationship (B.2), only displacement, u, is the nodal unknown, and the constants, E and ρ replace c.

$$E\frac{\partial^2 u}{\partial x^2} = \rho\frac{\partial^2 u}{\partial t^2} \tag{B.2}$$

Therefore in the Matlab code the nodal variables and material constants must be changed slightly so that equation B.2 becomes the governing equation. Because these changes do not affect the structure of the code and equations B.1 and B.2 are essentially the same equations, it is assumed that if that Matlab code is validated by the stress wave propagation problem in [70], then it is also validated for the acoustic pressure wave problem of Section 4.2.

In [70] the elastic bar (Figure B.1) is 500 mm long and is modeled using 50 linear elements. The material properties of the bar are given in Table B.1. The bar is fixed at the left end (x=0) and a constant tensile velocity, *v(t)*, is applied to the free end (x=L). The velocity boundary condition can also be expressed as a displacement, *u(t)*, by multiplying the velocity function, *v(t)*, by the current time.

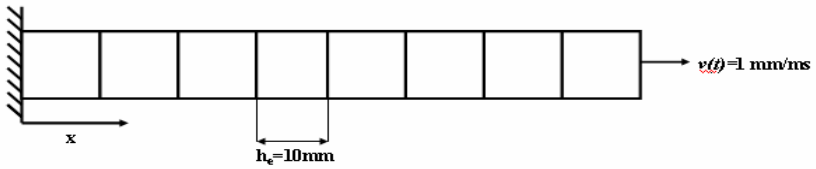

Figure B.1 Setup of one-dimensional stress wave propagation problem

Table B.1 Material properties for elastic bar wave propagation problem

Property	Value
E	20000 kg/mm^2
ρ	0.0008 kg/ms^2/mm^4
c	5000 mm/ms

The problem is solved using both a consistent and lumped mass matrix using a time step of,

$$\Delta t = \frac{h_e}{2c} \tag{B.3}$$

which is less than the critical time step for both the lumped and consistent mass matrices.

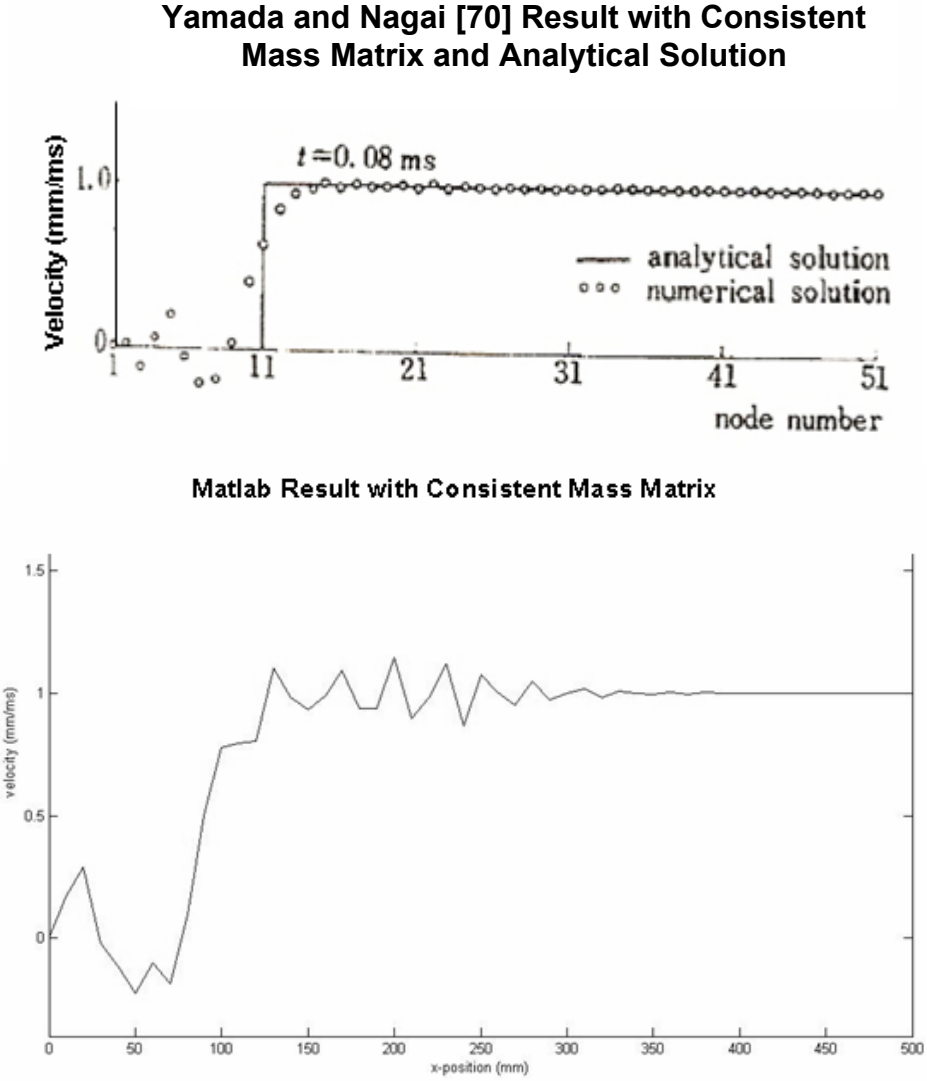

Figure B.2 Comparison of Yamada and Nagai [70] result and Matlab result for consistent mass matrix

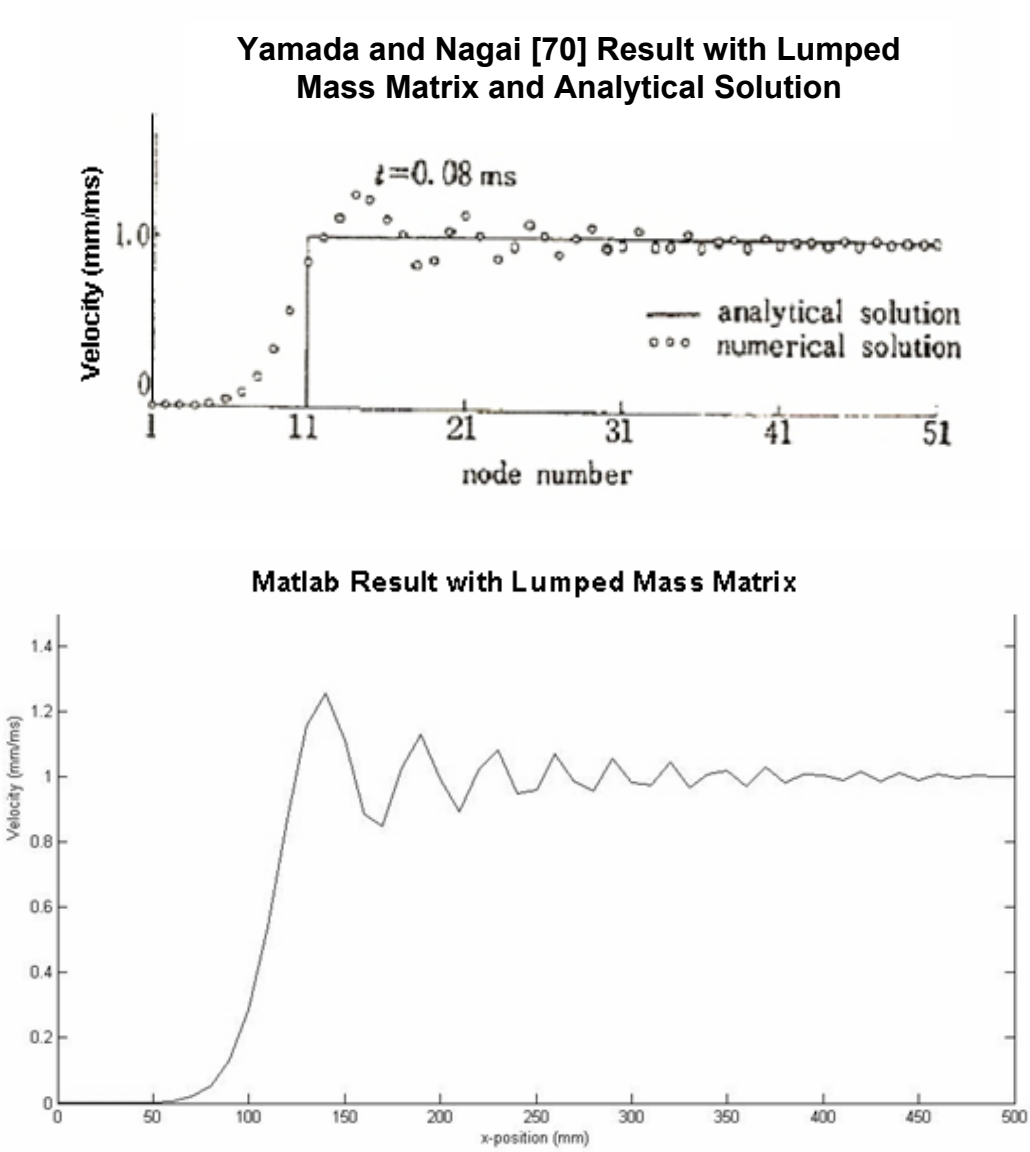

Figure B.3 Comparison of Yamada and Nagai [70] result and Matlab result for lumped mass matrix

The results using the lumped and consistent mass matrices in the Matlab code are compared to the results found in [70] in Figures B.2 and B.3. As the plots show the Matlab code accurately reproduces the results found in [70] which gave comparable results to the analytical solution of the problem. Therefore, it is concluded that the

Matlab code is a valid solution for both the one-dimensional elastic wave and acoustic wave propagation problems.